NOTIONAL SYSTEM REPORT

Technical Report

Submitted to:
The Office of Naval Research

Contract Number: N0014-08-1-0080

Submitted by:
Mike Andrus, Florida State University
Matthew Bosworth, Florida State University
Jonathan Crider, Purdue University
Hamid Ouroua, University of Texas at Austin
Enrico Santi, University of South Carolina
Scott Sudhoff, Purdue University

June 30, 2014

ELECTRIC SHIP RESEARCH AND DEVELOPMENT CONSORTIUM

ESRDC

MISSION STATEMENT

The Electric Ship Research and Development Consortium brings together in a single entity the combined programs and resources of leading electric power research institutions to advance near- to mid-term electric ship concepts. The consortium is supported through a grant from the United States Office of Naval Research.

Florida State University

Massachusetts Institute of Technology

Mississippi State University

Naval Postgraduate School

Purdue University

University of South Carolina

The University of Texas at Austin

2000 Levy Avenue, Suite 140 | Tallahassee, FL 32310 | www.esrdc.com

TABLE OF CONTENTS

LIST OF FIGURES

LIST OF TABLES

1 EXECUTIVE SUMMARY

The objective of this report is to set forth a group of time-domain models for the early-stage design study of shipboard power systems, and to demonstrate their use on various system architectures. The effort stemmed out of an earlier effort in which waveform-level models of three notional architectures – a Medium Voltage AC System, a High-Frequency AC System, and a Medium Voltage DC System were partially developed. Unfortunately, these codes were extremely computationally intense, limiting their usefulness for early design studies in which large numbers of runs, and a degree of user interactiveness, is required.

This effort again considered three systems - a Medium Voltage AC System, a High-Frequency AC System, and a Medium Voltage DC System. However, this effort was focused on simplified models to serve the needs of interactive early stage design. Within this context, this work focused on two distinct aspects. The first aspect was the development of a set of component models in mathematical form. Such a description is advantageous in that it is language independent. The second aspect of this effort was the use of the component models to study the three aforementioned systems.

With regard to the first aspect of this work, that is the component modeling, fundamental component models (in mathematical form) were defined in sufficient detail to represent a notional system using the three aforementioned architectures. The component models are highly simplified abstractions of shipboard power system components. The motivation for the simplification is two-fold. First, at an early design stage it is doubtful if the parameters needed for a more detailed system representation would be available. A highly detailed simulation would be based on many assumptions leading to results which are no more indicative of actual performance than a highly simplified simulation. The second reason for the creation of highly simplified model is for the sake of computational speed, so that system simulations based on the component models will run at speeds compatible with the needs of exploring the system behavior under a large variety of conditions.

The types of model simplifications used are three-fold. First, throughout this report average-value models are used. In particular, the switching of the power semiconductors is only represented on an average-value basis. Secondly, reduced-order models are typically used. Thus, high-frequency dynamics have been neglected. Simulation based on these models cannot be used to predict behaviors such as the initial response to a fault. In general, temporal predictions of features on a time scale of ~100 ms or less will not be reliable. The third simplification that has been made is that many components are represented in the abstract based on the operation goals of the component rather than on the details of what might physically be present.

The set of models provided herein is fairly extensive and adequate to serve as a basis for studying a variety of power system architectures. The models set forth include: turbines, turbine governors, wound-rotor synchronous machine based ac generators, generator paralleling controls, rectified wound-rotor synchronous machine based dc generation systems, ac input permanent magnet synchronous machine based propulsion drives, dc input permanent magnet synchronous machine based propulsion drives, hydrodynamic models, ac and dc pulsed load models, isolated dc/dc conversion models, dc loads, non-isolated dc/ac inverter modules, ac loads, active zonal rectifiers, circuit breakers and controls, as well as a variety of supporting components.

For the purposes of brevity and because of the resources available, model validation results are not presented herein. However, comments on model maturity have been included with

each component to provide the reader with a sense of the degree of model confidence for each component.

The component models developed under this effort were set forth in a previous report, "Notional System Report," but are included again herein in Appendix A. The remainder of this effort focused on applying the component models in Appendix A to MVAC, HFAC, and MVDC instantiations of a notional architecture. Unfortunately, this aspect of the effort was only partially successful. It is demonstrated herein that the models developed are computationally effective; however, in the case of all three systems either only partial system models are used or there are remaining simulation issues to be resolved.

The primary reason for this failure to completely model the systems was related to the choice of simulation engine. In particular, Simscape was used. This proved to be rather trying on the part of the simulationists involved in this effort. The reason that Simscape was chosen were the results of a study of a small notional system also considered by the group, and set forth in [1]. Therein, it was shown that Simscape yielded superior performance over a number of simulation implementations. Unfortunately, as the system scope grew, this language proved problematic. In retrospect, it is recommended that Simulink be used instead, preferably with a user defined solver of the network interconnection equations, also as described in [1]. Such an approach should be much more robust, and more open to modification if needed.

2 INTRODUCTION

The organization of this report is as follows. In Section 3, a Notional System is introduced, and Medium Voltage AC (MVAC), High-Frequency AC (HFAC), and Medium Voltage DC (MVDC) instantiations of this system are introduced. Then more detailed system descriptions of these three systems, along with system studies, are carried out in Section 4, Section 5, and Section 6, respectively. In each of these sections, descriptions of the system response to ship startup, a pulsed load, and a loss of generation are considered. General conclusions on the effort are given in Section 7. Section 8, the first appendix, sets forth a collection of system models used in the studies. Finally, Section 9 lists the parameters of the component models used in the studies described herein.

3 NOTIONAL SYSTEM

3.1 Description of Notional System

The component models and studies discussed herein were motivated by the desire to study a variety of shipboard power systems including a Medium Voltage AC (MVAC) system, a High-Frequency AC (HFAC) system, and a Medium Voltage DC (MVDC) system. All of these systems utilize the notional system arrangement depicted in Fig. 3.1.1. The MVAC system utilizes 4160 V (l-l, rms) 3-phase, 60 Hz power distribution for the main busses. In the HFAC system, the main bus is 4160 V (l-l, rms), 3-phase, and 240 Hz. Finally, in the MVDC system, the bus voltage is 5000 V.

There are two main and two auxiliary power generation modules (main PGM1, main PGM2, auxiliary PGM1, and auxiliary PGM2). These power generation modules feed starboard and port side busses that form a ring bus through the bow and stern cross-hull disconnects. The generation systems consist of wound rotor synchronous machines (WRSM) driven by gas

turbines. This distribution bus feeds four types of loads. There is a starboard and a port side propulsion motor as well as a high power pulsed load. The propulsion motors include a variable speed drive (VSD) that represents the power converters between the motor and the bus. The last load type is a zonal load that represents the ship service electrical components throughout the ship. Each zonal load center is in itself a small network. These zonal load centers differ based on the architecture of the notional system.

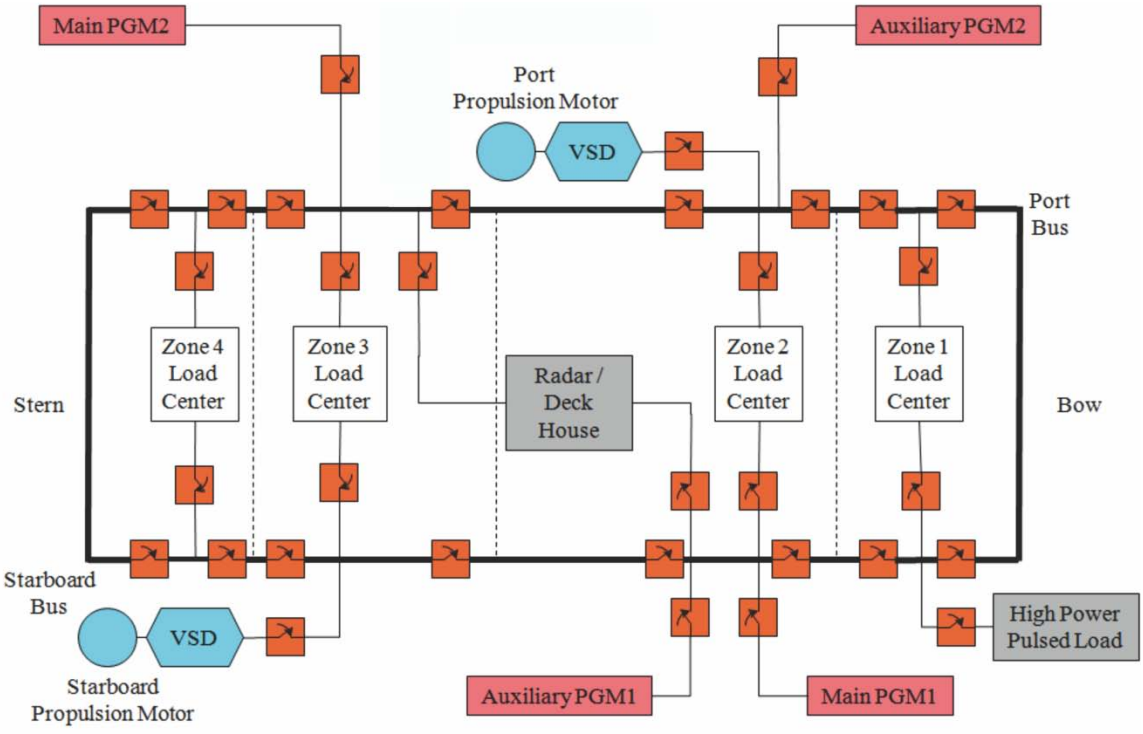

Fig. 3.1.1: Notional Power System.

4 MEDIUM VOLTAGE AC SYSTEM

4.1 System Description

As mentioned in Section 3, there are three instantiations of the notional power system shown in Fig. 3.1.1. The first is a Medium Voltage AC (MVAC) power system. As a result of solver convergence issues within the simulation environment used to implement the system model (Simscape), the system studied was reduced to represent the generation and load components present on the port bus side only, as shown in Fig. 4.1.1. Thus, the event scenarios considered herein focus on split-plant operation. In the case of the medium voltage ac system two generators of equal power ratings supply the port-side bus, each interfaced through separate circuit breakers. This is unlike the MVDC and HFAC systems wherein the main and auxiliary generators have unequal ratings. The port-side bus feeds four zonal load centers, a pulsed load, and the port propulsion motor.

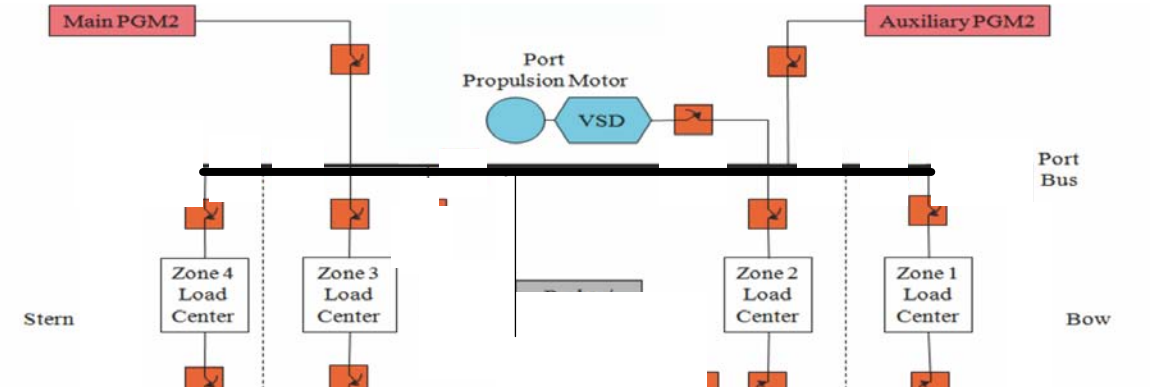

Fig. 4.1.1: Notional Power System Split-plant, Port-side Operation Only

ZONAL LOAD CENTERS

The zonal load center for this system is depicted in Fig. 4.1.2 and consists of ac distribution busses on the starboard and port side. The ac loads can therefore be fed from the ac bus through a transformer (T) while the zonal dc loads are fed through a zonal active rectifier (ZAR). The ZAR will typically include an internal transformer, but this is considered to be within that component.

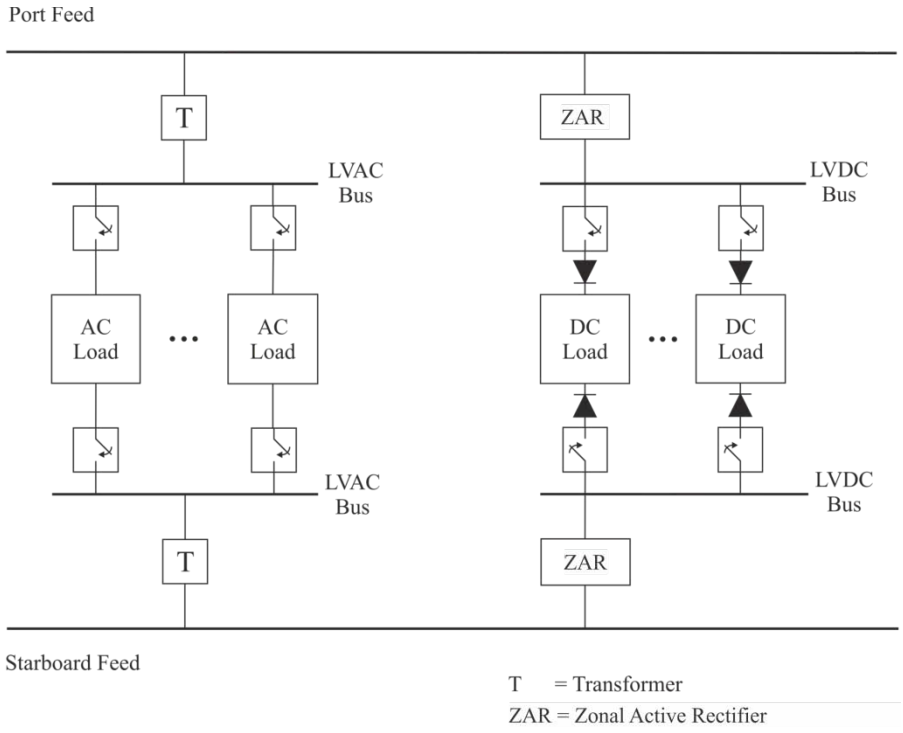

Fig. 4.1.2: Notional MVAC Zone.

An adaptation of the notional MVAC zone is shown in Fig. 4.1.3. Two transformers are utilized to convert the port side bus voltage to levels appropriate for application to the connected

AC loads and a Zonal Active Rectifier (ZAR). In Fig. 4.1.3 the ZAR transformer is shown as a separate component. All AC and DC loads are interfaced to the LVAC bus or LVDC bus via individual circuit breakers.

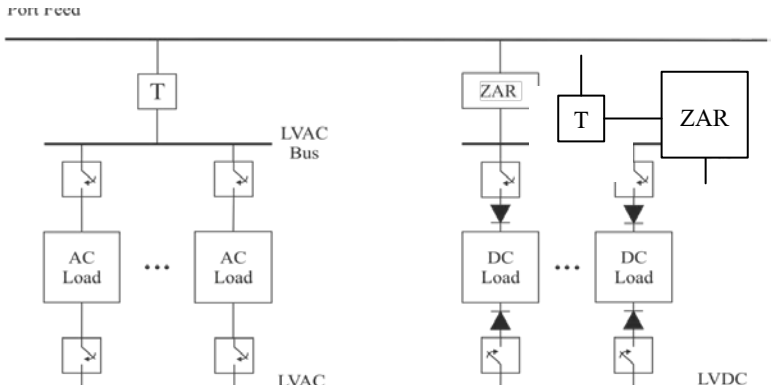

Fig. 4.1.3: Notional MVAC Zone Center Adaptation.

The two transformers and ZAR have been grouped into a Power Conditioning Module (PCM) subsystem that supplies the appropriate voltages to the interfaced loads. The AC and DC loads have been partitioned into subsystem blocks according to type. The PCU subsystem contains two transformers to scale the port side bus voltage to the levels required at the LVAC and LVDC busses. The transformer models are implemented as described in Section 8.2.14 of Appendix A, with parameters listed in Section 9.3 of Appendix B.

The LVDC bus is established via a ZAR as described in Section 8.2.15 of Appendix A using parameters listed in Section 9.8 of Appendix B. The ZAR model contains an internal supervisory controller that monitors the AC voltage present at its input terminals. User adjustable parameters establish high and low level voltage thresholds under which the unit is permitted to start up. Similar threshold parameters control the range of input voltages for which the unit may continue to run. An additional logic input controls the desired status of the component. This input is driven by a timer block, whose behavior is defined in the overall model configuration file. The voltage regulation performance of this rectifier under load, fault characteristics, and efficiency are user adjustable parameters.

Both AC and DC load models have been grouped into separate subsystems. As described in Section 8.2.16 through 8.2.18 of Appendix A, the AC and DC load models have two input voltage busses. Each load has a low voltage input connection for the port side bus and starboard side bus. Since this MVAC system model operates in the split-plant configuration and only includes the port side voltage bus, this component model has been suitably modified for a single input bus. Note that the circuit breakers indicated in the notional MVAC zone have been superseded by appropriate control of the AC and DC load operational status logic inputs. These logic inputs are driven by a timer block that is instantiated in the simulation configuration file to apply the loads at the desired simulation time. Both load types contain internal supervisory control structures that monitor the applied input voltage from either the LVAC or LVDC bus. User adjustable minimum and maximum voltage thresholds determine when the load may start and under what conditions it may continue to operate. For the DC load models, the load resistance may be specified. Both resistance and inductance may be defined for AC load models.

The MVAC system model contains four individual zonal load centers. Zone 1 and Zone 2 each contain a PCM, four AC loads, and two DC loads. Zone 3 and Zone 4 each contain a PCM, four AC loads, and one DC load. The assumed parameters are listed in Section 9.6 of Appendix B.

PULSED LOAD

The pulsed load is based on a modification of the Generic Pulsed Load (GPL) model. In particular, the pulsed load was broken into several parallel pulsed loads which together formed the aggregate pulsed load. As defined in the Section 8.2.10 of Appendix B, each GPL, requires three voltage inputs. A high voltage connection is used for the bulk power. Control and ancillary power is supplied via two low voltage connections. Since this MVAC model operates in split plant configuration and only draws power from the port side bus, the starboard side low voltage connection has been removed from the GPL model.

Timers are configured to enable the GPL to switch between standby and operational modes. An internalized supervisory controller monitors the voltage present at both the low voltage and high voltage connections, allowing the GPL to enter the start and run states when user specified conditions are met.

The standby and operation mode power of each GPL unit was specially configured such that the overall pulsed load behavior would match that of a detailed model previously developed by ESRDC researchers. In the detailed model, the pulsed load is a combination of several individual loads operating in a synchronized fashion for a brief window of time. The detailed model pulsed load power ratings and timing were transposed into the simplified GPL models to preserve the overall system behavior.

TURBO-GENERATORS

Each of the two generators is comprised of a wound-rotor synchronous machine, twin-shaft gas turbine, and exciter. The operation of these components and their associated control algorithms is given in Sections 8.2.2, 8.2.5, and 8.2.3 of Appendix A. Parameters are listed in Sections 9.1, 9.1.1, and 9.1.1 of Appendix B.

The generator model requires the establishment of a common synchronous reference frame. To this end, the angular speed of the synchronous reference frame is a weighted average of the rotor speeds of the two generators connected to the port-side voltage bus. In this model implementation, the weighting factors are equal, since the base power of each generator is the same.

PROPULSION DRIVE

The propulsion drive system consists of an inverter motor (IM) block and transformer rectifier (TR). The TR provides a DC voltage to the IM. The control system consists of a supervisory controller, DC link stabilizing controller, a PI speed controller, and a slew rate limiter. The shaft model is used to model the ship dynamics. The torque is proportional to the square of the motor speed. The details of each block are given in the component models in Sections 8.2.8, and 8.2.9 of Appendix A. Parameter values are listed in Sections 9.5 of Appendix B.

CABLE

Each turbo-generator is connected to the port side bus via cables. Cables are represented by a reduced-order model in which transients are neglected, as described in Section 8.2.12 of Appendix A with parameters listed in Section 9.10 of Appendix B.

CIRCUIT BREAKER

Circuit breakers throughout the MVAC system model control the connection of various components to the port side voltage bus. The switches are native components within the Simscape foundation library. They accept a physical signal input from the timed step source. When this signal is greater than the user specified threshold value, the switch is closed. Otherwise, the switch remains open. The resistance of the switch when closed and conductance of the switch when open are also user controlled parameters.

4.2 Studies

Three system studies were executed to evaluate the capabilities of the average-value reduced-order system model as a design tool. All studies were conducted for the port side bus of the ship only. Thus, the ship is always operating in the split-plant configuration in the scenarios considered. The MVAC system model was evaluated for the following three studies:

Study 1: Ship start-up from zero to full speed
Study 2: Pulsed load response
Study 3: Loss of a generator in split-plant configuration

4.2.1 Ship Startup

In this scenario, the port side propulsion motor is accelerated from zero to full speed. As a result, the port propulsion drive operates at its maximum power of approximately 37 MW. The four zonal loads are also operated, bringing the total system power consumption to approximately 50 MW. Prior to the start of simulation, the ship generators and propulsion motor are at rest with all circuit breakers open. The simulation sequence of events is given in Table 4.2.1. In this simulation scenario, the pulsed load is present in the MVAC system. However, its operation was not under investigation and its respective circuit breaker remained open for the duration of the simulation.

Table 4.2.1: Simulation Sequence of Events for Study 1.

Event Number	Event Start Time (sec.)	Event Description
1	0	Start simulation. Two generators are accelerated to rated speed.
2	150	Close each generator's circuit breaker. Port-side bus is now energized.
3	170	Close all zonal load center circuit breakers. All zonal loads are now active.
4	200	Propulsion breakers closed. DC-Link energized.
5	250	Port-side propulsion motor accelerated to full speed.
6	500	End of simulation. Record computer simulation time.

The load configuration of this simulation is detailed in Table 4.2.2. The power level of all zonal load connections and the propulsion system are given. The load connections are summarized in Table 4.2.3.

Table 4.2.2: Detailed Zonal Load and Propulsion Power Levels.

Loads	Power (kW)
Z1L1	150
Z1L2	615
Z1L3	715
Z1L4	400
Z1L5	910
Z1L6	0
Z2L1	1
Z2L2	75
Z2L3	1400
Z2L4	750
Z2L5	975
Z2L6	40
Z3L1	40
Z3L2	1200
Z3L3	1900
Z3L4	750
Z3L5	0
Z4L1	60
Z4L2	480
Z4L3	1750
Z4L4	675
Z4L5	0
Propulsion Motor	36,500

Table 4.2.3: Summary of MVAC System Loads for Simulation Study 1.

Load Type	Power (kW)	Per Unit on 80 MW Base
Zonal Load Centers 1-4	12,886	0.161
Pulsed Load	0	0
Propulsion Load	36,500	0.456

Total Load	49,386	0.617

This study was performed successfully and generated results consistent with expected power system behavior for the prescribed events. The simulation timing information is as follows:

- Simulation performed on an Intel® Core™ i7 CPU 960 @ 3.20 GHz / 16 GB RAM running Windows 7 Enterprise 64-bit
- Total simulation events time is 500 seconds
- The computer execution time for the simulation is 120 seconds

TURBO-GENERATOR SPEED RESPONSE

The turbo-generator speed of turbo-generator 1 (main generator on the port bus) is shown in Fig. 4.2.1 together with the speed reference in per-unit (P.U.). Initially, the turbo-generator exhibits a large overshoot in regard to the reference speed ramp, as evidenced in Fig. 4.2.1. The speed also contains oscillations around the reference value, shown in Fig. 4.2.1. When the zonal load breakers are closed at 170 sec., the turbo-generator speed falls slightly following a brief oscillation. This behavior occurs again at 200 sec. when the propulsion system breaker is closed and the DC-link is energized, Fig. 4.2.1. The lower generator speed as a result of system loading is expected as a result of the droop control implemented to enforce equal load sharing between the two turbo-generator units present in the system. Propulsion motor startup at 250 sec. causes a further speed droop and oscillation, as depicted in Fig. 4.2.1. The turbo-generator speed response for unit 2 (aux generator on the port bus) is identical to the results for unit 1.

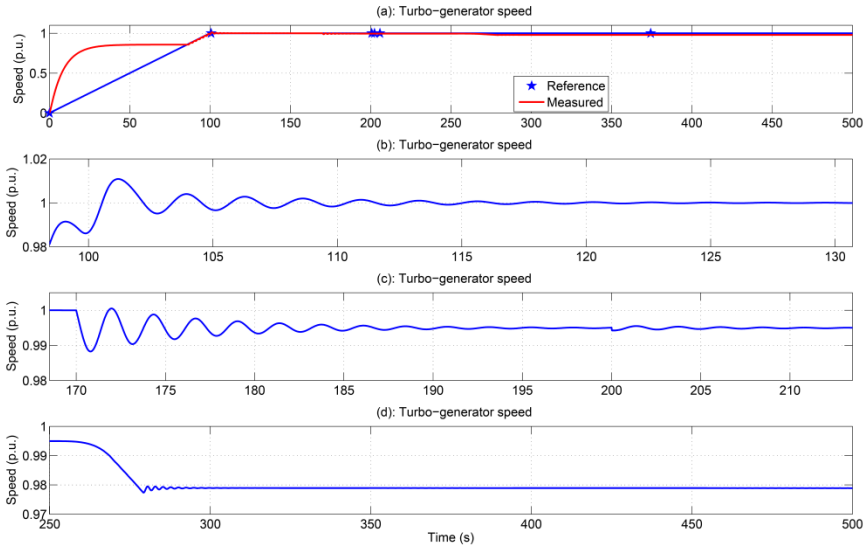

Fig. 4.2.1: Turbo-generator 1 Speed.

TURBO-GENERATOR POWER

The output power of turbo-generator 1 (main) is shown in Fig. 4.2.2. The results show that the expected load power is being provided by the turbo-generator for the prescribed simulation events. At the 170 sec., the output power of turbo-generator 1 increases sharply to approximately 6.4 MW, half of the total zonal load center power. A sharp spike in generator

power occurs at 200 sec. when the propulsion system breaker is closed. This spike, detailed in the bottom plot, is the result of the DC-link capacitor charging. The turbo-generator power then ramps up to a total 25 MW as the propulsion motor is accelerated to full speed at 250 sec. The turbo-generator 2 (aux) output power data is identical to that shown in Fig. 4.2.2, since the total system power is divided evenly between the two units as a result of the droop controller.

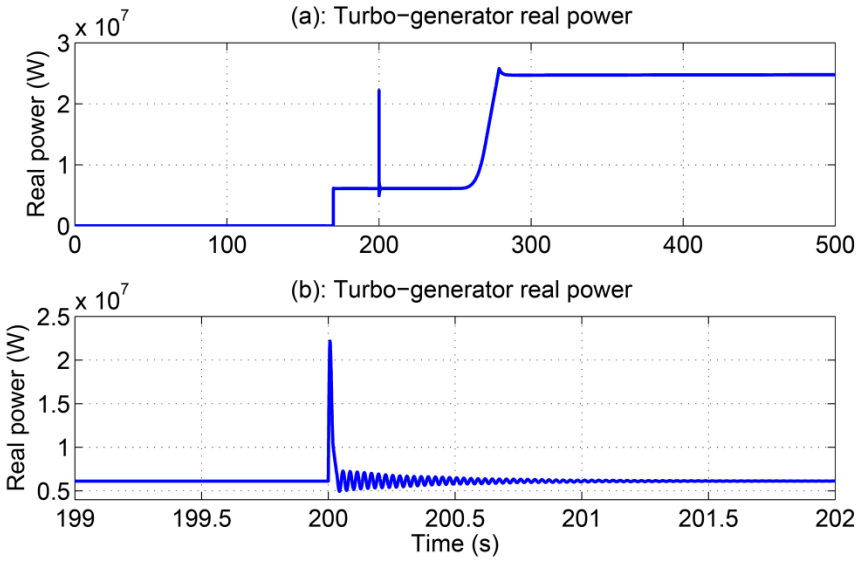

Fig. 4.2.2: Turbo-generator 1 Power.

PORT-SIDE VOLTAGE

The port-side bus voltage during this study is shown in Fig. 4.2.3. The events are more visible in the zoomed data of the bottom plot. Note, however, that the port-side bus voltage recovers after each loading event due to the action of the voltage regulator present in the exciter system, Fig. 4.2.4.

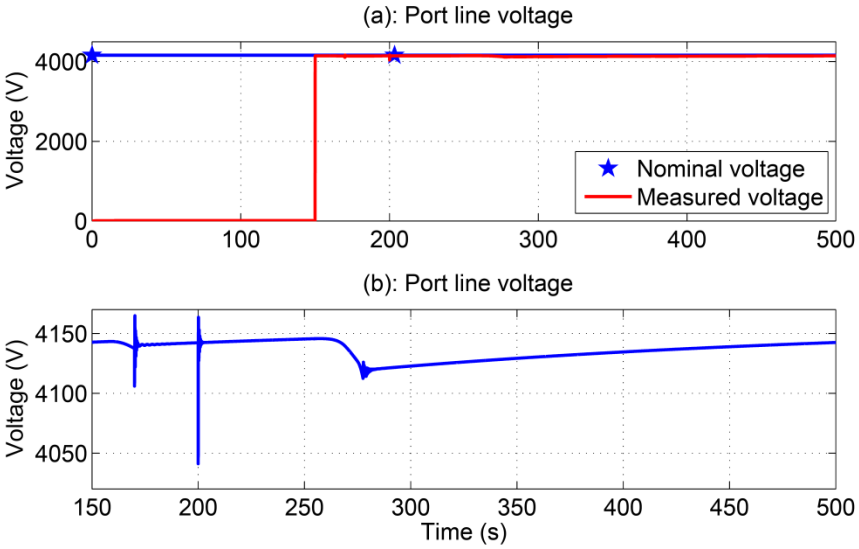

Fig. 4.2.3: Port-side Bus Voltage.

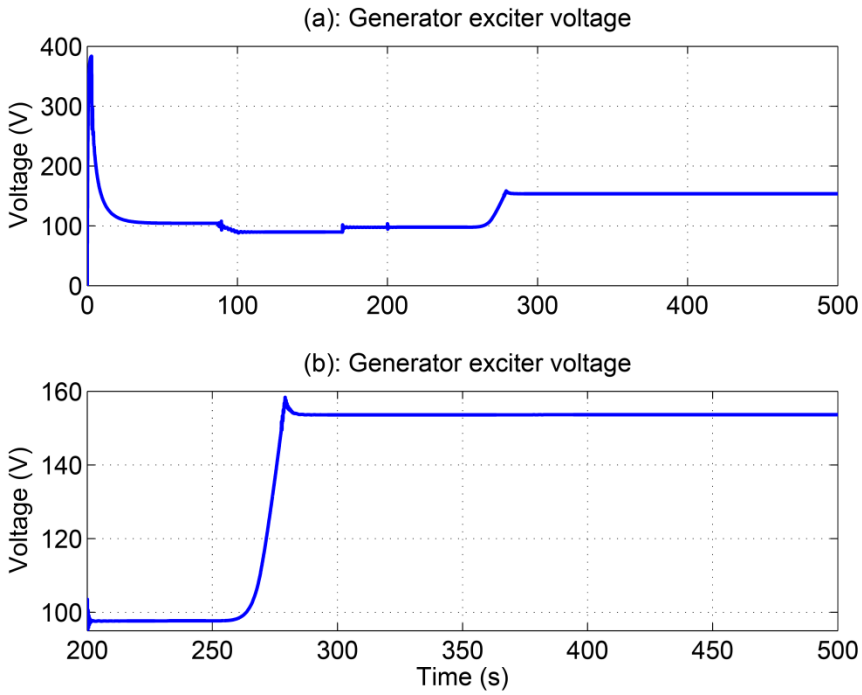

Fig. 4.2.4: Generator Exciter Voltage.

PROPULSION SYSTEM

Fig. 4.2.5 contains three plots detailing the behavior of the propulsion drive system. These plots include the port-side propulsion motor speed, torque, and power. The inverter line voltage and current are shown in Fig. 4.2.6. All of these results are as expected, showing the propulsion motor ramping up starting at time 250 sec. The port motor speed accurately tracks the reference value, exhibiting only a slight overshoot upon reaching the rated value. The motor torque is as expected, again showing only slight overshoot upon reaching the rated value. The port motor power reaches 36.5 MW following a brief overshoot. The inverter output voltage and current waveforms are as expected.

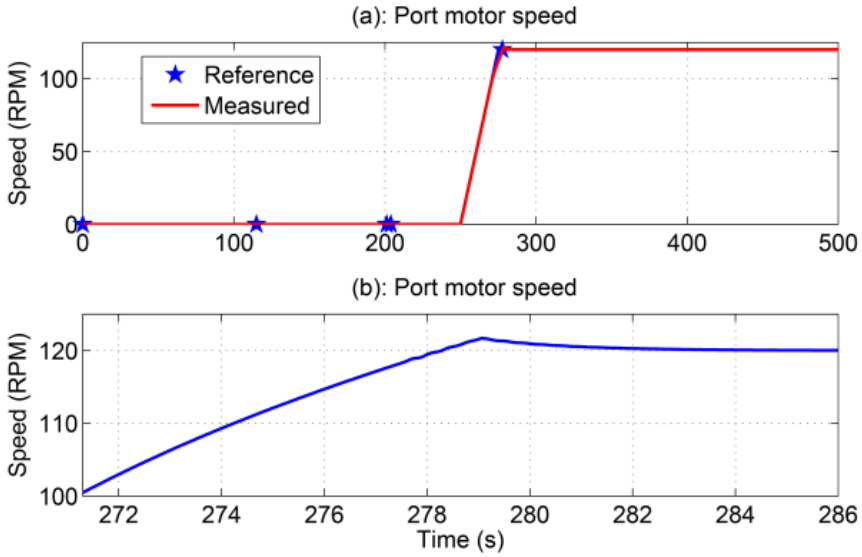

Fig. 4.2.5: Port Motor Speed.

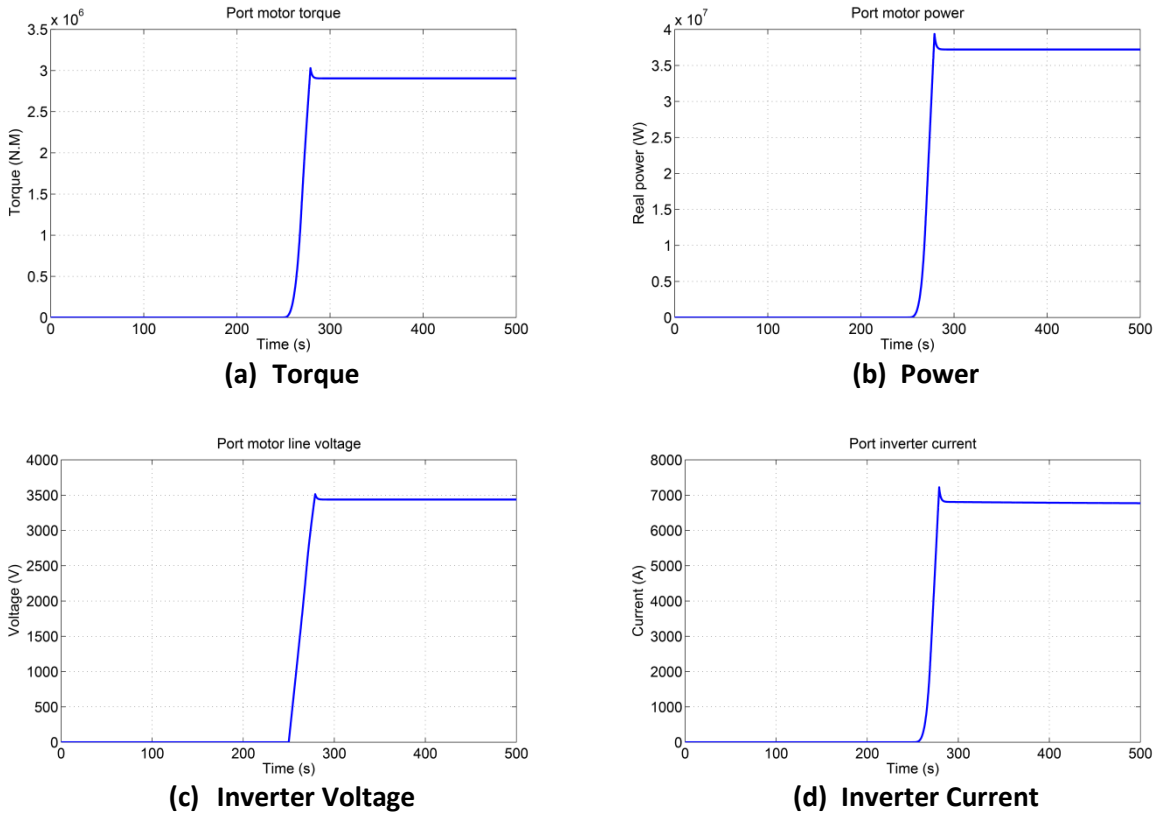

Fig. 4.2.6: Port-side Propulsion Motor Overview.

The port-side DC-link voltage is shown in Fig. 4.2.7. This system is shown to come into operation at 200 sec., exhibiting a brief overshoot in voltage. The middle subplot of Fig. 4.2.7 depicts the zoomed DC-link voltage oscillating briefly after startup. The operation of the braking resistor is shown in the bottom subplot of Fig. 4.2.7. The DC-link voltage changes quickly between the upper and lower braking resistor hysteresis control thresholds. The voltage then settles into a damped oscillation as the braking resistor ceases operation.

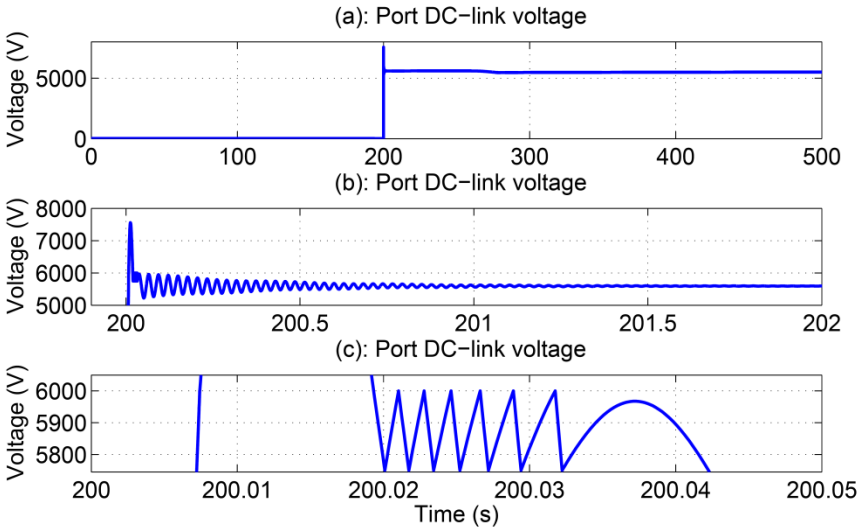

Fig. 4.2.7: Port-side DC-Link Voltage.

ZONAL LOAD CENTERS

The simulation results of all individual zones are depicted in Fig. 4.2.8 through Fig. 4.2.11. The zonal power is computed from the terminal voltage and current for each load present in the system. All results are as expected. Note the presence of a small spike and sag in AC line voltage and AC power for all zones. These features arise due to the closing of the propulsion system breaker at 200 sec. and subsequent acceleration of the propulsion motor beginning at 250 sec. These events do not appear in the DC voltage and DC power plots for each zone since the ZAR model is unaffected by changes of the applied input voltage within a user specified range.

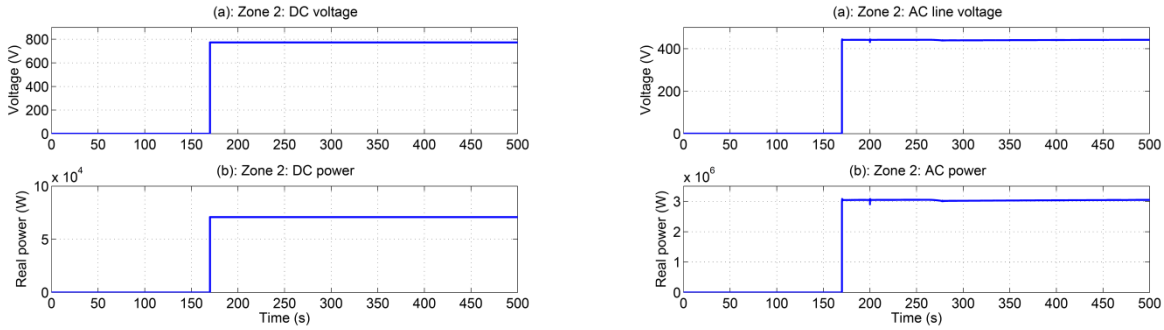

Fig. 4.2.8: Zone 1 Voltage and Power.

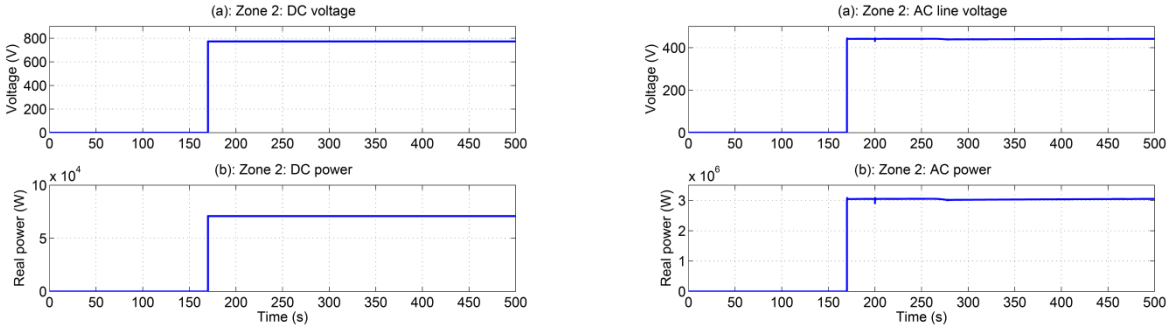

Fig. 4.2.9: Zone 2 Voltage and Power

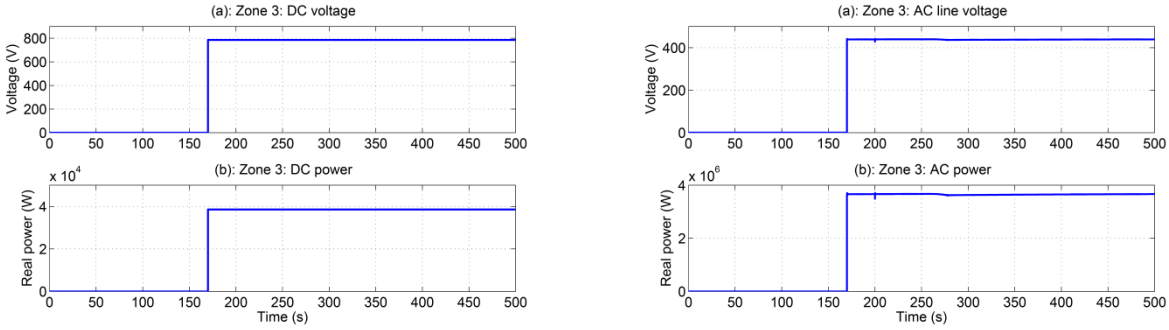

Fig. 4.2.10: Zone 3 Voltage and Power.

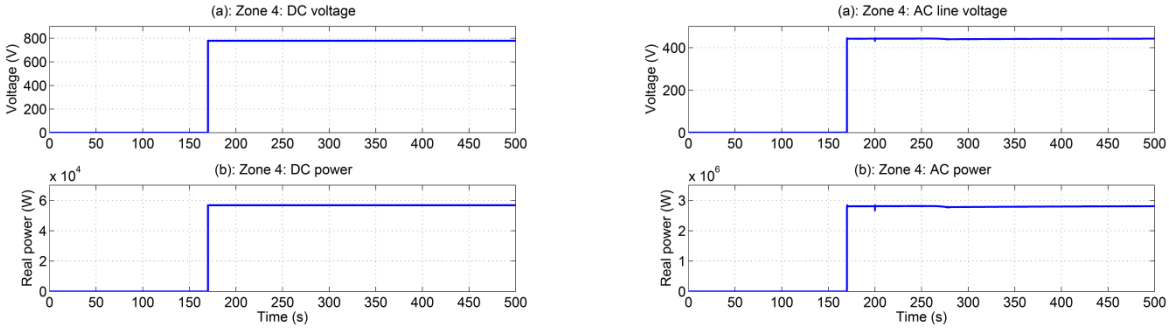

Fig. 4.2.11: Zone 4 Voltage and Power.

SUMMARY

This study confirmed the reduction in simulation time afforded by the averaged-value reduced-order MVAC system model in the SIMSCAPE modeling environment. Simulation of 500 sec. of MVAC system events required 120 sec. of execution time. It is important to note that most of the execution time expires during transient simulation events such as circuit breaker closings. Simulation of steady-state MVAC system behavior is executed very quickly.

The results of this study show that the power system components of the port-side system operate as expected in split plant configuration. Turbo-generator startup, zonal load center operation, and propulsion motor operation were all successfully demonstrated. The turbo-generator results show that the load power was evenly split between the two units present in the system. The change in speed as a result of loading also demonstrated correct operation of the droop controller in the governor system. Addition of the zonal load centers resulted in expected voltage and power waveforms in the system. Startup of the propulsion motor system, including the transformer rectifier and inverter-motor system gave expected results.

4.2.2 Pulsed Load Response

In this scenario, the pulsed load is operated in conjunction with all the zonal loads and propulsion load. The pulsed load is operational for 6 seconds at approximately 18 MW at maximum load. The four zonal loads are also operated, bringing the total system power consumption to approximately 68 MW when the pulse load is at its maximum value. The purpose of this simulation is to analyze the response of the power system to high power AC and DC pulsed loads. The simulation sequence of events is given in Table 4.2.4.

Table 4.2.4: Simulation Sequence of Events for Study 2.

Event Number	Event Start Time (sec.)	Event Description
1	0	Start simulation. Two generators are accelerated to rated speed.
2	150	Close each generator's circuit breaker. Port-side bus is now energized.
3	170	Close all zonal load center circuit breakers. All zonal loads are now active.
4	200	Propulsion breakers closed. DC-Link energized.
5	250	Port-side propulsion motor accelerated to full speed.
6	422	Pulsed Loads in standby mode.

7	423	Pulsed Load operation mode.
8	429	Pulsed Loads disabled.
9	500	End of simulation. Record computer simulation time.

The load configuration of this simulation is detailed in Table 4.2.5 and Table 4.2.6. The power level for all zonal load connections, pulsed load, and the propulsion systems are given. The load connections are summarized in Table 4.2.7.

Table 4.2.5:Detailed Zonal Load and Propulsion Power Levels.

Loads	Power (kW)
Z1L1	150
Z1L2	615
Z1L3	715
Z1L4	400
Z1L5	910
Z1L6	0
Z2L1	1
Z2L2	75
Z2L3	1400
Z2L4	750
Z2L5	975
Z2L6	40
Z3L1	40
Z3L2	1200
Z3L3	1900
Z3L4	750
Z3L5	0
Z4L1	60
Z4L2	480
Z4L3	1750
Z4L4	675
Z4L5	0
Propulsion Motor	36,500

Table 4.2.6: Detailed Pulsed Load Power Levels

Time (s)	LV Power (kW)	LV Mode	HV Power (kW)	HV Mode
422	11	Standby	443.5	Standby
423	11	Standby	8866.5	Operation
424	21	Operation	8946.6	Operation
425.5	21	Operation	17786.6	Operation
427.5	41	Operation	17786.6	Operation
428.5	31	Operation	1866.5	Operation
428.75	11	Standby	8566.5	Operation
429	0	Disabled	0	Disabled

Table 4.2.7: Summary of MVAC System Loads for Simulation Study 2.

Load Type	Power (kW)	Per Unit on 80 MW Base
Zonal Load Centers 1-4	12,886	0.161
Pulsed Load Maximum	17,828	0.222
Propulsion Load	36,500	0.456
Total Load	67,214	0.840

This study was performed successfully and generated results consistent with expected power system behavior for the prescribed events. The simulation timing information is as follows:

- Simulation performed on an Intel® Core™ i7 CPU 960 @ 3.20 GHz / 16 GB RAM running Windows 7 Enterprise 64-bit
- Total simulation events time is 500 seconds
- The computer execution time for the simulation is 153 seconds

PULSED LOAD RESPONSE

The pulsed load profile assumed for this study is shown in Fig. 4.2.12. Detailed load times and power levels are found in Table 4.2.7. The pulsed loads also consume standby power, which is significantly smaller than the pulsed power. The standby mode begins at 422 sec., or 1 sec. before the pulsed loads become operational. The remaining figures for this study show features of interest in the interval 423 sec – 429 sec. when the pulsed loads become operational and cause a perturbation of all other electrical ship systems.

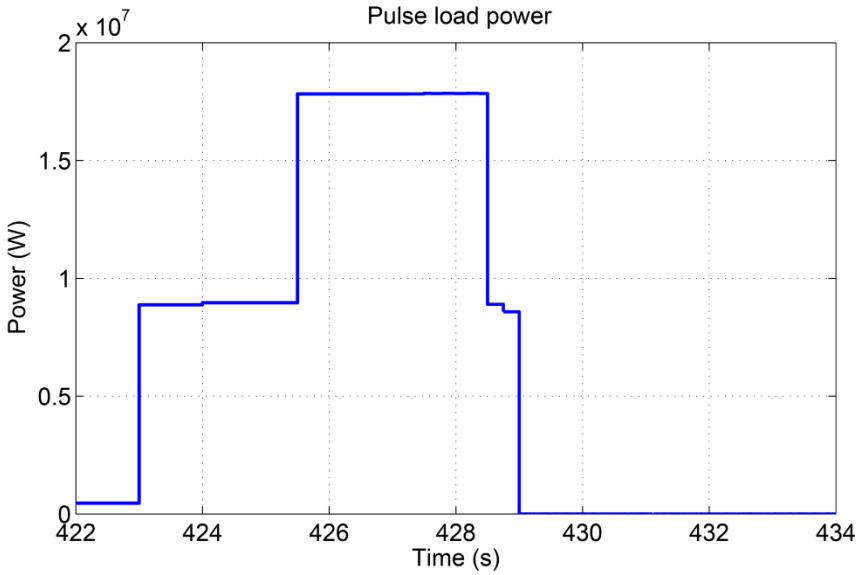

Fig. 4.2.12: Pulsed Load Power.

TURBO-GENERATOR SPEED RESPONSE

The speed response for turbo-generator 1 (main) is shown in Fig. 4.2.13. Initially, this unit exhibits a large overshoot in regard to the reference speed ramp, as evidenced in Fig. 4.2.13. Additional speed oscillations around the reference value are shown in Fig. 4.2.13. When the zonal load breakers are closed at 170 sec., the turbo-generator speed falls slightly following a brief oscillation. This behavior occurs again at 200 sec. when the propulsion system breaker is closed and the DC-link is energized, Fig. 4.2.13. At 422 sec., minor oscillations begin because the pulsed loads enter standby mode. At 423 sec., high frequency oscillations occur when the pulsed loads become operational, Fig. 4.2.13. The speed dampens out after several seconds once the pulsed loads are disabled at 429 sec. The turbo-generator's speed does not deviate more than 1% from its droop value (0.98 p.u.) at any instant during the pulsed load operation, demonstrating satisfactory performance from the control system.

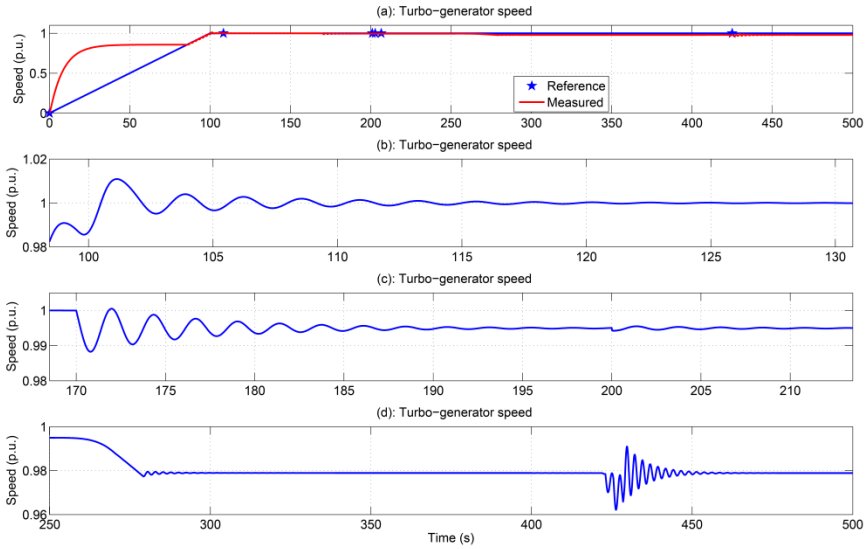

Fig. 4.2.13:Turbo-generator 1 Speed.

TURBO-GENERATOR POWER

The output power of turbo-generator 1 (main) is shown in Fig. 4.2.14. The results show that the expected load power is being provided by the turbo-generator for the prescribed simulation events. At 423 sec., the output power of turbo-generator 1 increases sharply by approximately 4.4 MW to supply power to the pulsed load, and additionally 4.5 MW at 425.5 sec. At 429 sec., turbo-generator 1 decreases sharply by approximately 4 MW back to its steady state value of 25 MW to supply ship power to the remaining systems. The output power of turbo-generator 2 is the same as that of unit 1 since both generators supply equal power during Study 2.

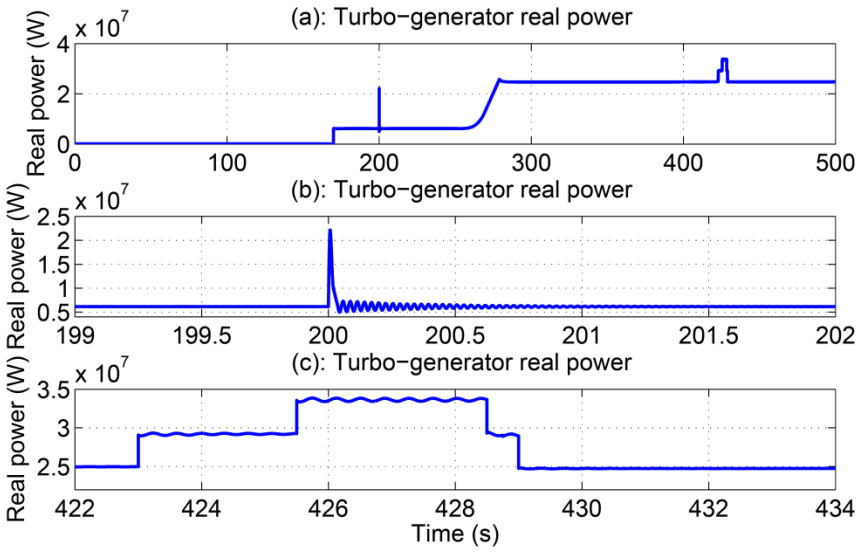

Fig. 4.2.14: Turbo-generator 1 Power.

PORT-SIDE VOLTAGE

The port-side bus voltage during this study is shown in Fig. 4.2.15. As expected, pulsed loading events during the simulation result in corresponding voltage sags on the port-side bus. An oscillation is first induced when the pulsed load enters standby mode at 422 sec., and increases when the pulsed loads are operational at 423 sec. The port-side bus voltage recovers after the pulsed loads are disabled at 429 sec. In Fig. 4.2.16, the exciter voltage of turbo-generator 1 increases sharply at 423 sec. in attempt to maintain the system voltage constant under the loading conditions. High frequency oscillations on the port side voltage occur throughout the pulsed load event, but never go unstable. Also, the bus voltage sag never drops below 5% during the pulsed loads, which is satisfactory performance from the control system.

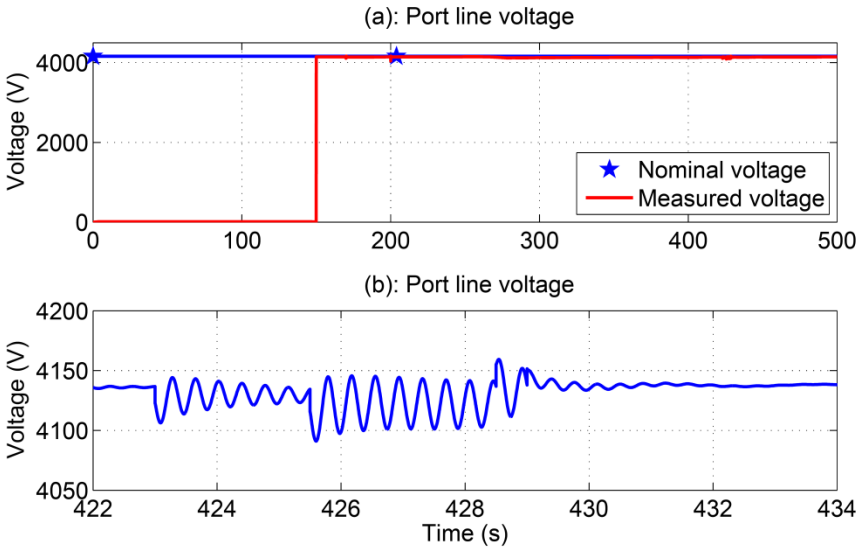

Fig. 4.2.15: Port-side Bus Voltage.

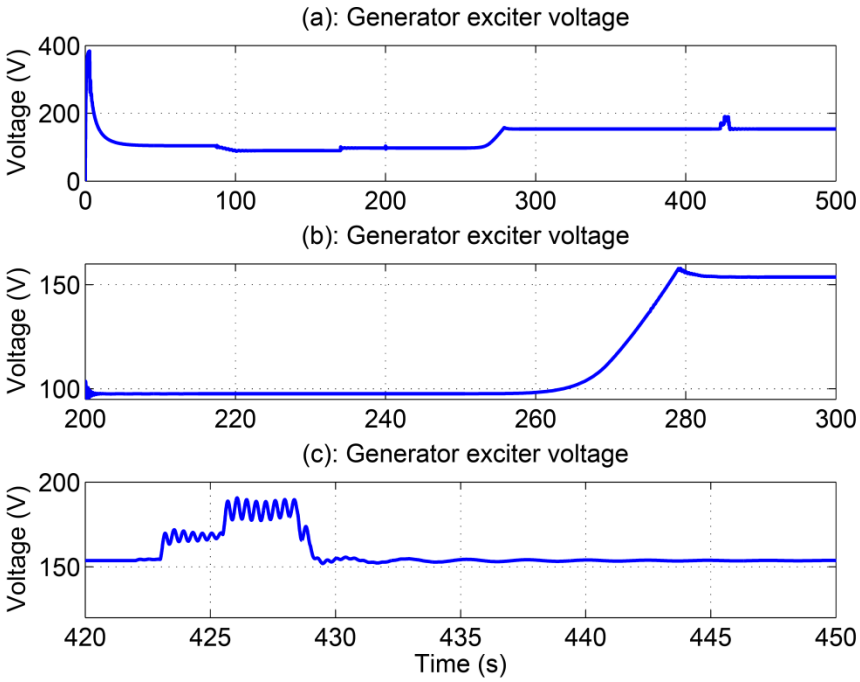

Fig. 4.2.16: Turbo-generator Exciter Voltage.

PROPULSION SYSTEM

Fig. 4.2.17 contains three plots detailing the behavior of the propulsion drive system. These plots include the port-side propulsion motor speed, torque, and power. The inverter line voltage and current are shown in Fig. 4.2.18. Each individual plot includes zoomed depictions of the system behavior at 423 sec. when the pulsed loads become operational. All of these results are as expected. The port motor speed accurately tracks the reference, exhibiting only a slight overshoot upon reaching the rated value. Oscillations are introduced into the system when the pulsed loads enter standby mode and worsen when the pulsed loads become operational at 423 sec. However, the motor speed recovers to the reference value after the pulsed loads are disabled, and never approaches instability. The motor torque is as expected, again showing oscillations during the pulsed loads. The port motor power reaches a peak of 37.5 MW during the pulsed loads event. The inverter output voltage and current appear as expected with oscillations at 423 sec., which do not exceed a 5% deviation due to the corrective action of the control system.

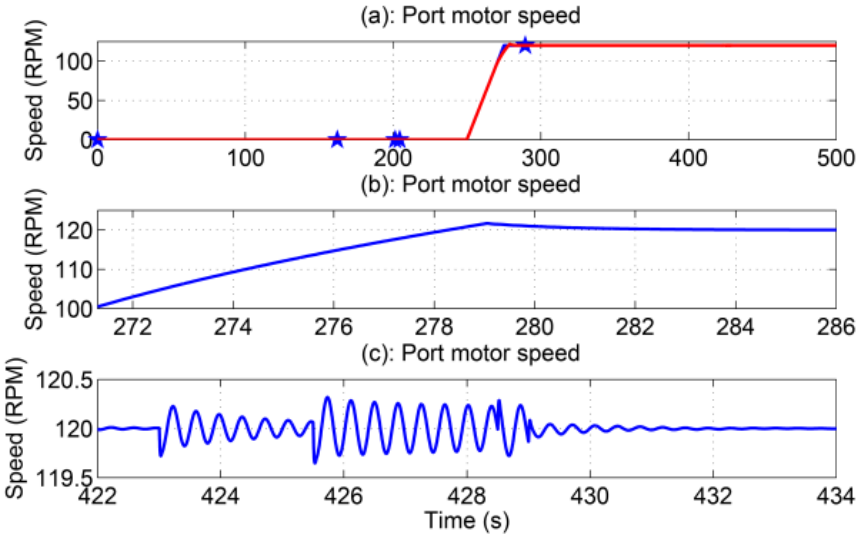

Fig. 4.2.17: Port-side Propulsion Motor Speed.

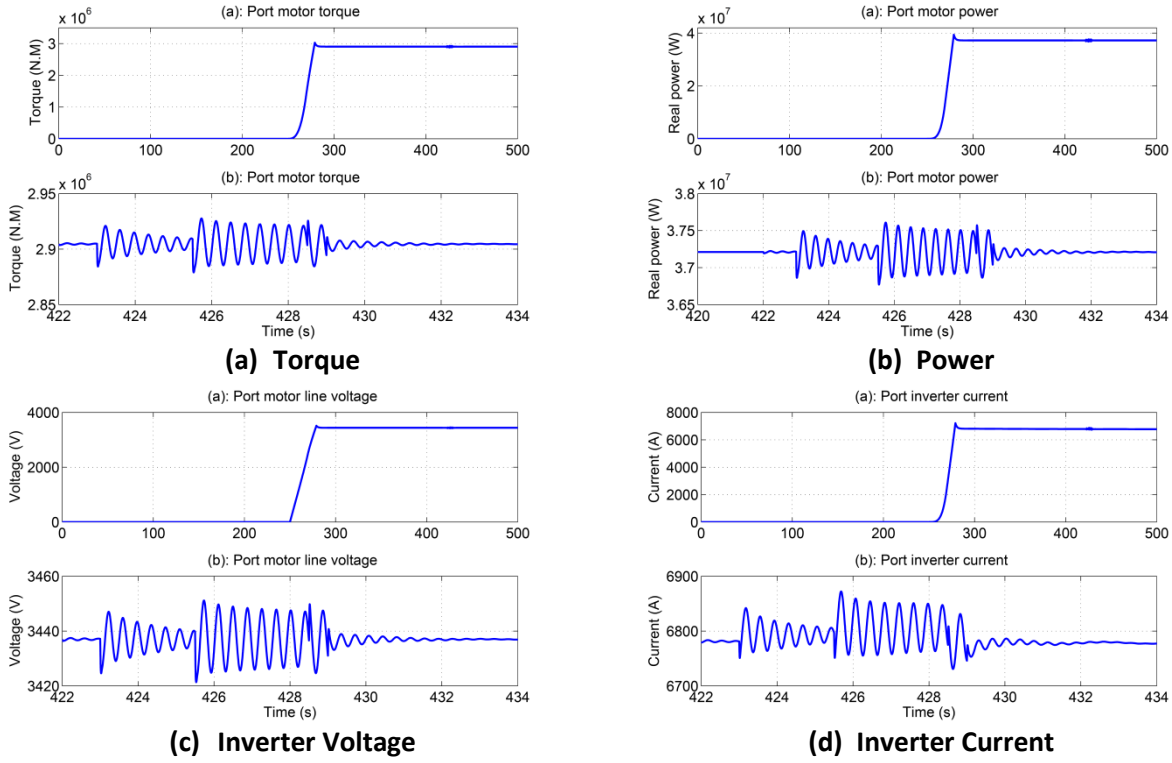

Fig. 4.2.18: Port-side Propulsion Motor Overview.

The port-side DC-link voltage is shown in the top subplot of Fig. 4.2.19. This system is shown to come into operation at 200 sec., exhibiting a brief overshoot in voltage. The second subplot in Fig. 4.2.19 depicts the zoomed DC-link voltage oscillating briefly after startup. The operation of the braking resistor is shown in the third subplot of Fig. 4.2.19. The DC-link voltage changes quickly between the upper and lower braking resistor hysteresis control thresholds. The voltage then settles into a damped oscillation as the braking resistor ceases operation as shown in the lower subplot of Fig. 4.2.19. When the pulsed loads become active at 423 sec., a damped oscillation is introduced. As the pulsed loads become individually disabled, the oscillations decrease, and are eventually damped out after a few seconds. The braking resistor never introduces any instability when the pulsed loads become active or inactive.

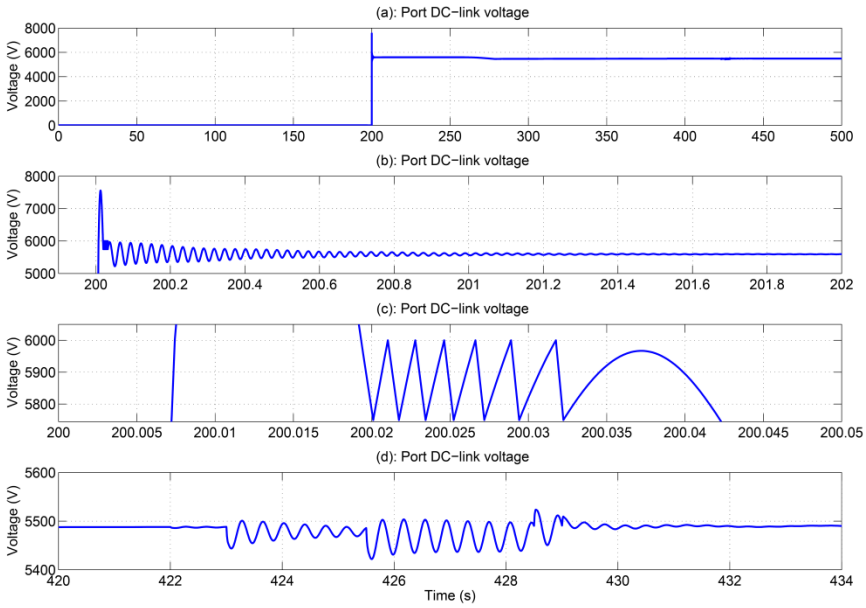

Fig. 4.2.19: Port-side DC-Link Voltage.

ZONAL LOAD CENTERS

The simulation results of all individual zones are depicted in Fig. 4.2.20 through Fig. 4.2.23. The zonal power is computed from the terminal voltage and current for each load present in the system. All results are as expected. Note the presence of a small spike and sag in AC line voltage and AC power for all zones at 200 sec. These features arise due to the closing of the propulsion system breaker at 200 sec. and subsequent acceleration of the propulsion motor beginning at 250 sec. The pulsed loads introduce minor oscillations to the AC line voltages for all zonal loads at 422 sec. when the pulsed loads enter standby, and worsen when the pulsed loads become operational at 423 sec. This behavior in both the line voltage and power is detailed for zone 4 in Fig. 4.2.24. All oscillations in both voltage and power are within operating ranges, and dampen out after the pulsed loads are removed. These events do not appear in the DC voltage and DC power plots for each zone since the ZAR model is unaffected by changes of the applied input voltage within a user specified range.

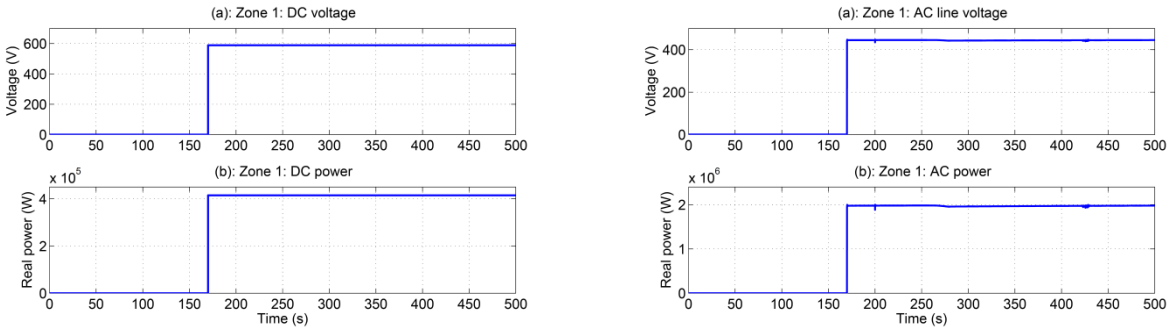

Fig. 4.2.20: Zone 1 Load Voltage and Power.

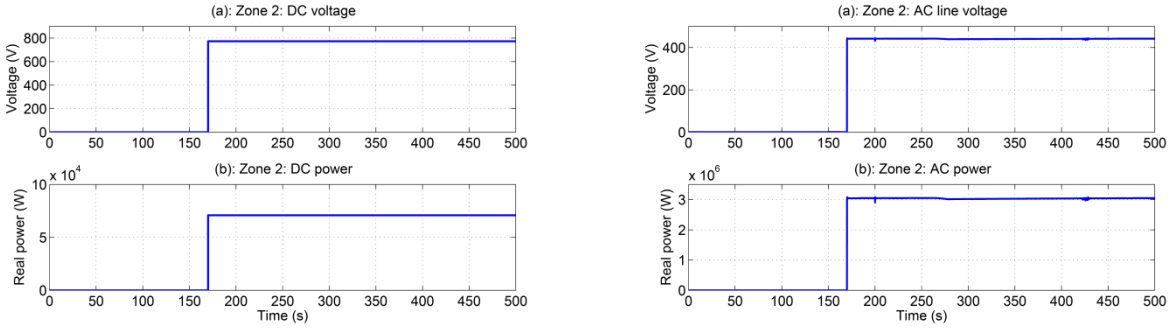

Fig. 4.2.21: Zone 2 Load Voltage and Power.

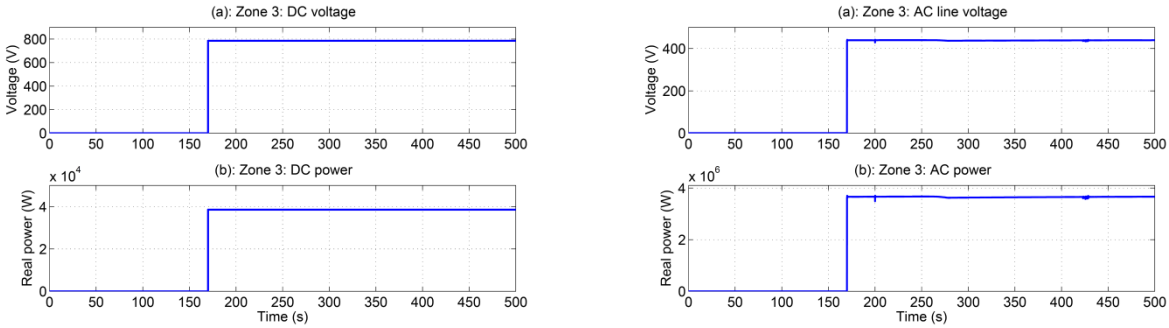

Fig. 4.2.22: Zone 3 Load Voltage and Power.

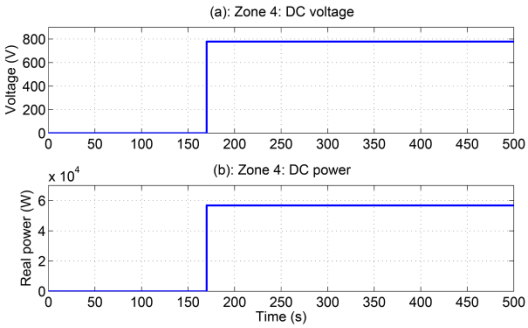

Fig. 4.2.23: Zone 4 DC Load Voltage.

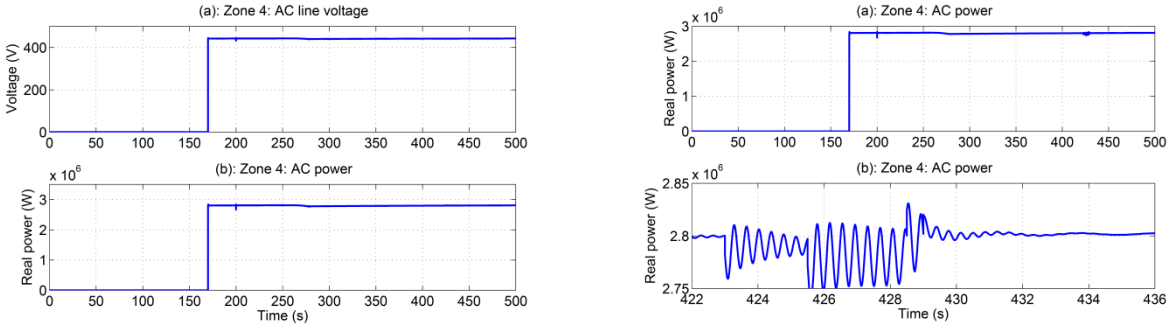

Fig. 4.2.24: Zone 4 Load AC Voltage and Power.

SUMMARY

The simulation results of Study 2 confirm that the averaged-value reduced-order MVAC system model can be used to analyze the effect of pulsed load events in the split-plant

configuration while maintaining a convenient, fast execution time. It was found that the pulsed loads do not significantly affect the system in a negative manner if the available power generation is not exceeded by the load demand. All oscillations in electrical and mechanical systems were operating within their respected ranges, never approached instability, and damped out after the pulsed loads were disabled. To provide for a more realistic scenario, isolated and local energy storage systems may be used to supply pulsed power loads; thus reducing high frequency oscillations and power demand throughout the electrical ship system.

4.2.3 Loss of Generator in Split-Plant Configuration

In this study, both turbo-generators are accelerated to full speed. All zonal load centers are connected to the port-side voltage bus and the propulsion motor is brought into operation. Following this, turbo-generator 2 is disconnected from the port-side bus at 350 sec. by opening its respective circuit breaker. To ensure that turbo-generator 1 is not overloaded during the loss of generation, the overall system load was reduced for this simulation only. The reduction in load power is achieved by lowering the desired final speed of the propulsion motor to approximately 105 rpm. As a result, the port propulsion drive operates at just under 22 MW in comparison to the rated 37.5 MW. Thus, with the four zonal loads also in operation, the total system power consumption is approximately 34 MW. This power level is less than the 40 MW rated maximum of Generation Unit 1, guaranteeing that the system will not become overloaded. Prior to the start of simulation, the ship generators and propulsion motor are at rest with all circuit breakers open. The simulation sequence of events is given in Table 4.2.8. In this simulation scenario, the pulsed load is present in the MVAC system. However, its operation was not under investigation and its respective circuit breaker remained open for the duration of the simulation.

Table 4.2.8: Simulation Sequence of Events for Study 3.

Event Number	Event Start Time (sec.)	Event Description
1	0	Start simulation. Two generators are accelerated to rated speed.
2	150	Close each generator's circuit breaker. Port-side bus is now energized.
3	170	Close all zonal load center circuit breakers. All zonal loads are now active.
4	200	Propulsion breakers closed. DC-Link energized.
5	250	Port-side propulsion motor accelerated to full speed.
6	350	Generation Unit 2 circuit breaker opened.
6	500	End of simulation. Record computer simulation time.

The load configuration of this simulation is detailed in Table 4.2.9. The power level of all zonal load connections and the propulsion system are given. The load connections are summarized in Table 4.2.10.

Table 4.2.9: Detailed Zonal Load and Propulsion Power Levels.

Loads	Power (kW)
Z1L1	150
Z1L2	615
Z1L3	715
Z1L4	400
Z1L5	910
Z1L6	0
Z2L1	1
Z2L2	75
Z2L3	1400
Z2L4	750
Z2L5	975
Z2L6	40
Z3L1	40
Z3L2	1200
Z3L3	1900
Z3L4	750
Z3L5	0
Z4L1	60
Z4L2	480
Z4L3	1750
Z4L4	675
Z4L5	0
Propulsion Motor	21,750

Table 4.2.10: Summary of MVAC System Loads for Simulation Study 3.

Load Type	Power (kW)	Per Unit on 80 MW Base
Zonal Load Centers 1-4	12,886	0.161
Pulsed Load	0	0
Propulsion Load	21,750	0.272
Total Load	34,636	0.433

Since this simulation involved the disconnection of a turbo-generator from the system, the reference frame estimator was disabled. The turbo-generator rotor speed will return to the rated value when its respective circuit breaker is opened. The rotor speed information of from the disconnected unit is no longer of use in the reference frame estimation since the generator is no longer providing power to the system. Due to time constraints, no logic was implemented in the reference frame estimator to account for this scenario. Since the simulation would result in only one generator feeding the system, the reference frame estimator was removed. Reference frame synchronism is assumed at the start of the study because the two turbo-generator models are identical and the impedance between them is small. In retrospect, a better approach would have been to simply assign the synchronous reference frame speed to be that of the remaining unit.

This study was performed successfully and generated acceptable results that matched the expected power system behavior for the prescribed events. The simulation timing information is as follows:

- Simulation performed on an Intel® Core™ i7 CPU 960 @ 3.20 GHz / 16 GB RAM running Windows 7 Enterprise 64-bit
- Total simulation events time is 500 seconds
- The computer execution time for the simulation is 231 seconds

TURBO-GENERATOR SPEED RESPONSE

The speed response for turbo-generator 1 (main) is shown in Fig. 4.2.25. Initially, this unit exhibits a large overshoot in regard to the reference speed ramp, as evidenced in Fig. 4.2.25. Additional speed oscillations around the reference value are shown in Fig. 4.2.25. When the zonal load breakers are closed at 170 sec., the turbo-generator speed falls slightly following a brief oscillation. This behavior occurs again at 200 sec. when the propulsion system breaker is closed and the DC-link is energized, Fig. 4.2.25. At 350 seconds, turbo-generator 2 is removed from the system by opening its circuit breaker. This action results in a transfer of the entire system load to turbo-generator 1, resulting in the additional speed droop exhibited in Fig. 4.2.25.

The speed response for turbo-generator 2 (aux) is shown in Fig. 4.2.26. The simulation results for this unit are that same as that of turbo-generator 1 until 350 sec. At this time, turbo-generator 2 is completely unloaded. Thus, the turbo-generator 2 rotor speed returns to 1 p.u. after some damped oscillation, as shown in Fig. 4.2.26.

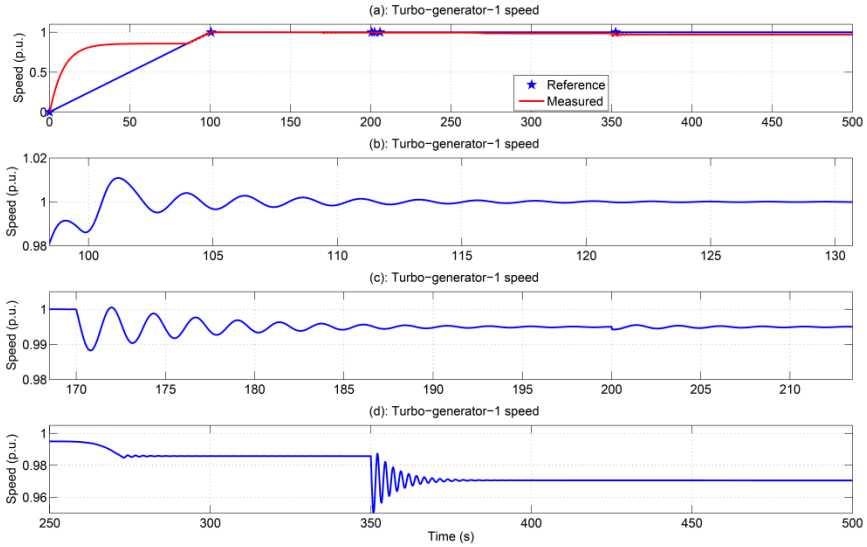

Fig. 4.2.25: Turbo-generator 1 Speed.

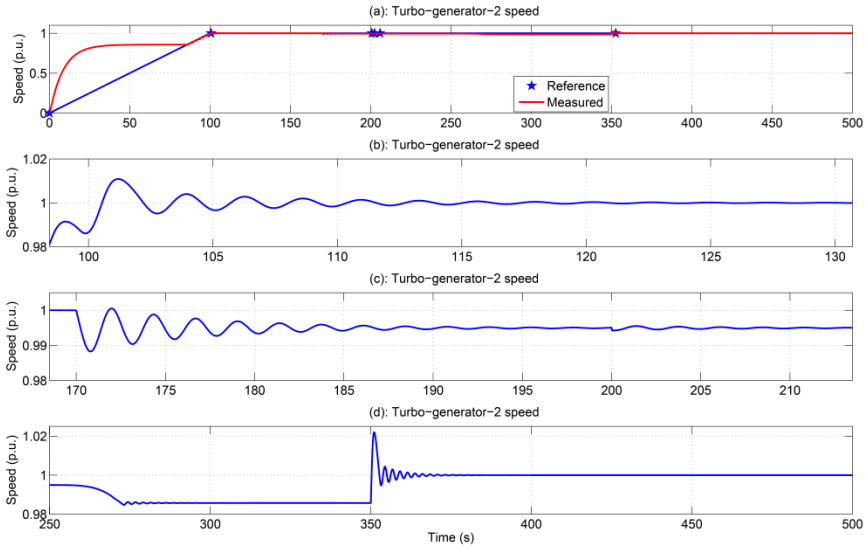

Fig. 4.2.26: Turbo-generator 2 Speed.

TURBO-GENERATOR POWER

The output power of turbo-generator 1 (main) is shown in Fig. 4.2.27. The results show that the expected load power is being provided by the turbo-generator for the prescribed simulation events. At 170 sec., the output power of turbo-generator 1 increases sharply to approximately 6.4 MW, half of the total zonal load center power. A sharp spike in generator power occurs at 200 sec. when the propulsion system breaker is closed. This spike, detailed in Fig. 4.2.27, is the result of the DC-link capacitor charging. The turbo-generator power then ramps up to a total 17.3 MW as the propulsion motor is accelerated to at 250 sec. At 350 sec., turbo-generator 2 (aux) is removed from the system. As a result, the turbo-generator 1 output power quickly rises to approximately 34 MW as it assumes all of the system loads. Fig. 4.2.27 shows that this causes a brief oscillation in the generator output power.

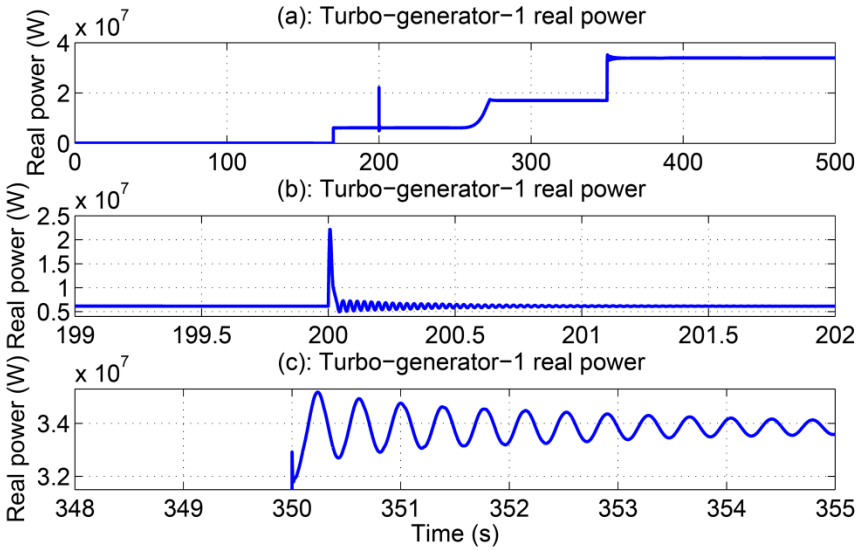

Fig. 4.2.27: Turbo-generator 1 Power.

The output power of turbo-generator 2 is shown in Fig. 4.2.28. The plots show that the generator response is identical to that of turbo-generator 1 for all simulation events prior to 350 sec. This is expected since the two units share the system loads equally. At 350 sec. turbo-generator 2 is removed from the system by opening its circuit breaker. The output power of this unit goes to zero, accordingly.

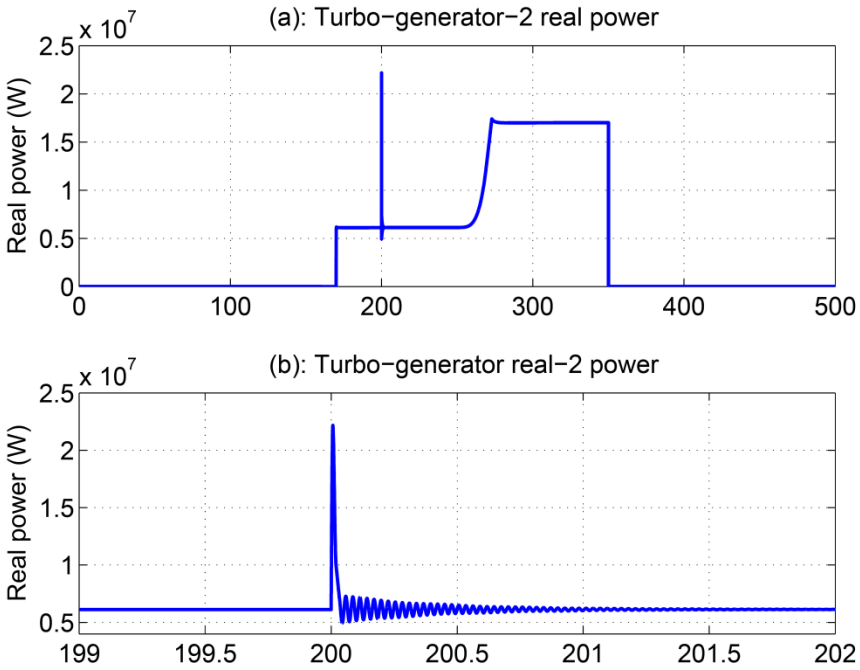

Fig. 4.2.28: Turbo-generator 2 Power.

PORT-SIDE VOLTAGE

The port-side bus voltage during this study is shown in Fig. 4.2.29. As expected, loading events during the simulation result in corresponding voltage sags on the port-side bus. An oscillation is induced in the port line voltage when turbo-generator 2 is removed from the system at 350 sec. The port-side bus voltage recovers after each loading event due to the action of the voltage regulator present in the exciter system. The exciter voltages of turbo-generator 1 and turbo-generator 2 are shown in Fig. 4.2.30 and Fig. 4.2.31, respectively. In Fig. 4.2.30 the exciter voltage of turbo-generator 1 increases sharply at 350 sec. to maintain the system voltage under the heavier loading conditions. The exciter voltage of turbo-generator 2 falls at 350 sec., Fig. 4.2.31, as a result of it being disconnected from the system.

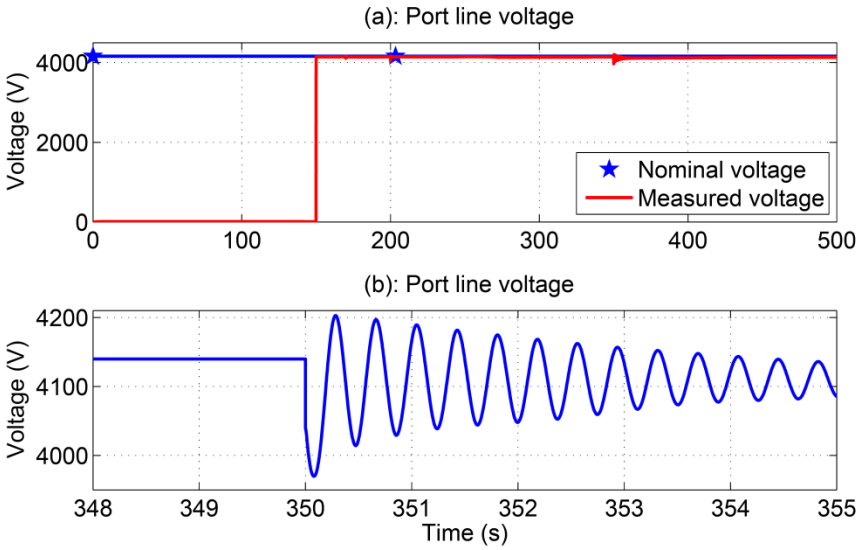

Fig. 4.2.29: Port-side Bus Voltage.

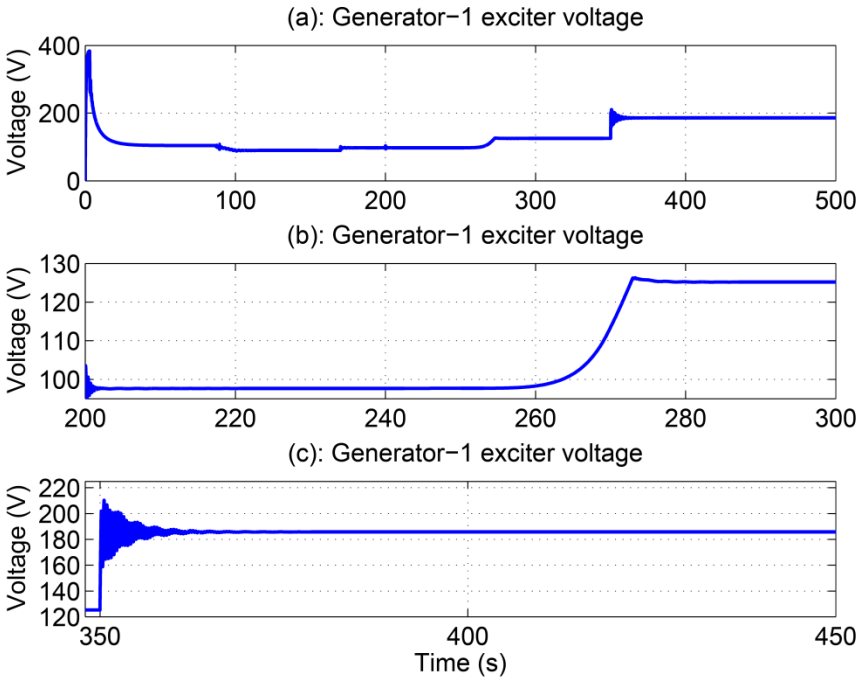

Fig. 4.2.30: Turbo-generator 1 Exciter Voltage.

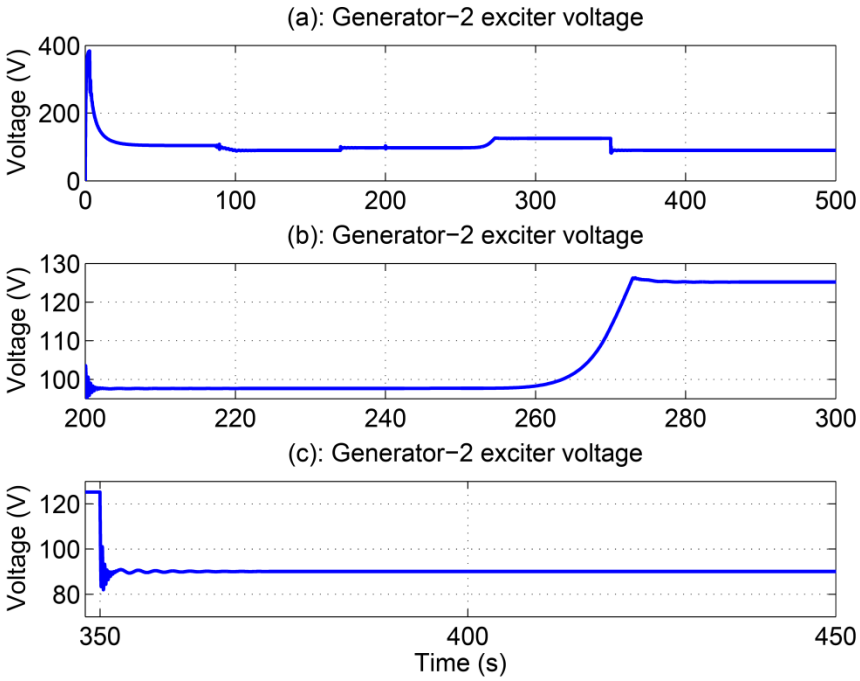

Fig. 4.2.31: Turbo-generator 2 Exciter Voltage.

PROPULSION SYSTEM

Fig. 4.2.32 contains three plots detailing the behavior of the propulsion drive system. These plots include the port-side propulsion motor speed, torque, and power. The inverter line voltage and current are shown in Fig. 4.2.34. Each individual plot includes zoomed depictions of the system behavior at 350 sec. when turbo-generator 2 is removed from the system. All of these results are as expected. The port motor speed accurately tracks the reference, exhibiting only a slight overshoot upon reaching the rated value. An oscillation is introduced into the motor speed upon the removal of turbo-generator 2 from the system. However, the motor speed recovers to the reference value before the end of the simulation. The motor torque is as expected, again showing only slight overshoot upon reaching the rated value. The loss of generation causes a torque oscillation that is fully damped before the end of simulation. The port motor power reaches 21.75 MW following a brief overshoot. Again, an oscillation is present at the loss of generation event. The inverter output voltage and current appear as expected with oscillations at 350 sec. as a result of the loss of generation.

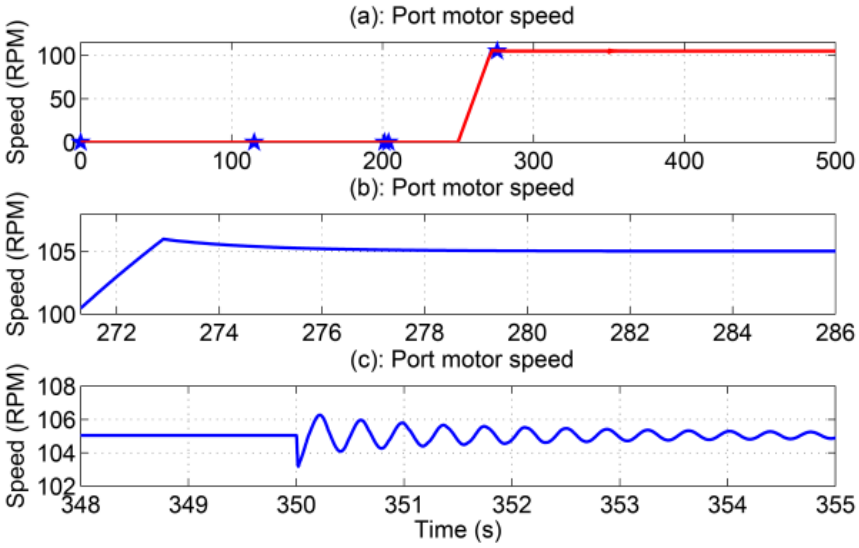

Fig. 4.2.32: Port-side Propulsion Motor Speed.

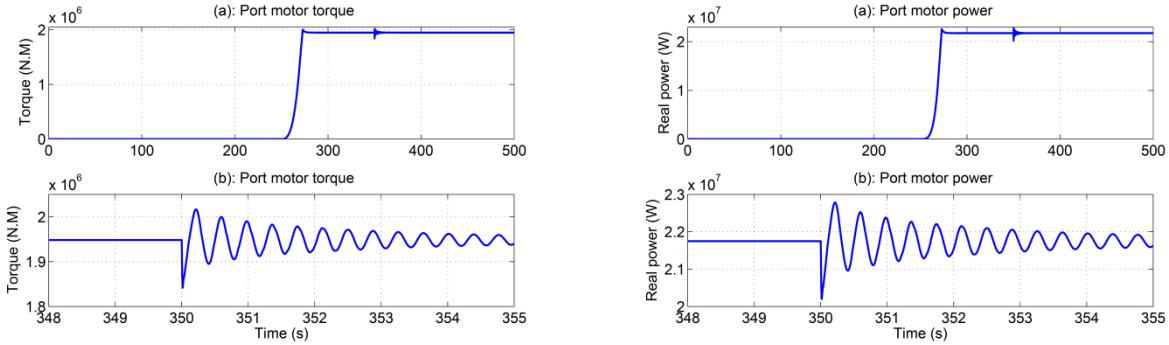

Fig. 4.2.33: Port-side Propulsion Motor Torque and Power.

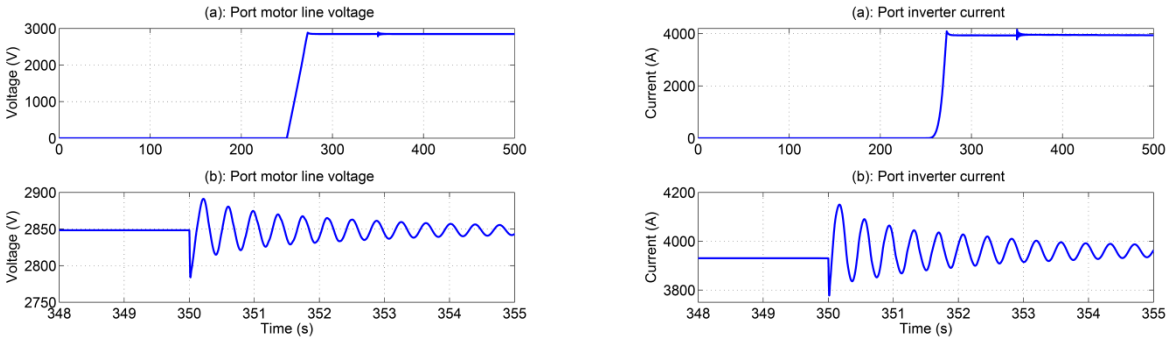

Fig. 4.2.34: Port-side Inverter Voltage and Current.

The port-side DC-link voltage is shown in Fig. 4.2.35. This system is shown to come into operation at 200 sec., exhibiting a brief overshoot in voltage. Fig. 4.2.35depicts the zoomed DC-link voltage oscillating briefly after startup. The operation of the braking resistor is shown in Fig. 4.2.35. The DC-link voltage changes quickly between the upper and lower braking resistor hysteresis control thresholds. The voltage then settles into a damped oscillation as the braking resistor ceases operation. The removal of turbo-generator 2 introduces a damped oscillation into the DC-link voltage at 350 sec.

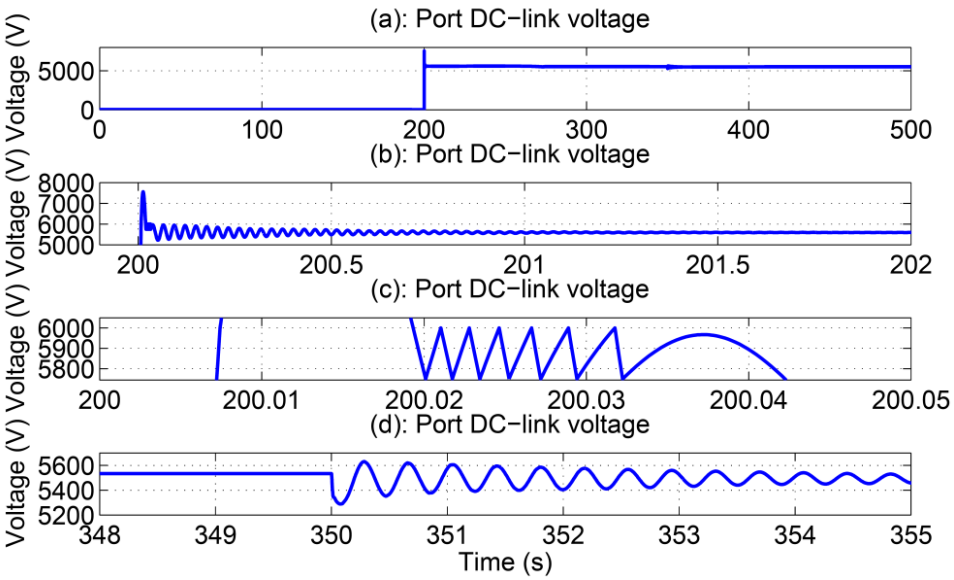

Fig. 4.2.35: Port-side DC-Link Voltage.

ZONAL LOAD CENTERS

The simulation results of all individual zones are depicted in Fig. 4.2.36 through Fig. 4.2.40. The zonal power is computed from the terminal voltage and current for each load present in the system. All results are as expected. Note the presence of a small spike and sag in AC line voltage and AC power for all zones at 200 sec. These features arise due to the closing of the propulsion system breaker at 200 sec. and subsequent acceleration of the propulsion motor beginning at 250 sec. The loss of generation at 350 sec. causes an oscillation in the AC line voltage for all zones. This behavior in both the line voltage and power is detailed for zone 4 in Fig. 4.2.40. The resulting port-side voltage bus sag is also apparent following the removal of turbo-generator 2. These events do not appear in the DC voltage and DC power plots for each zone since the ZAR model is unaffected by changes of the applied input voltage within a user specified range.

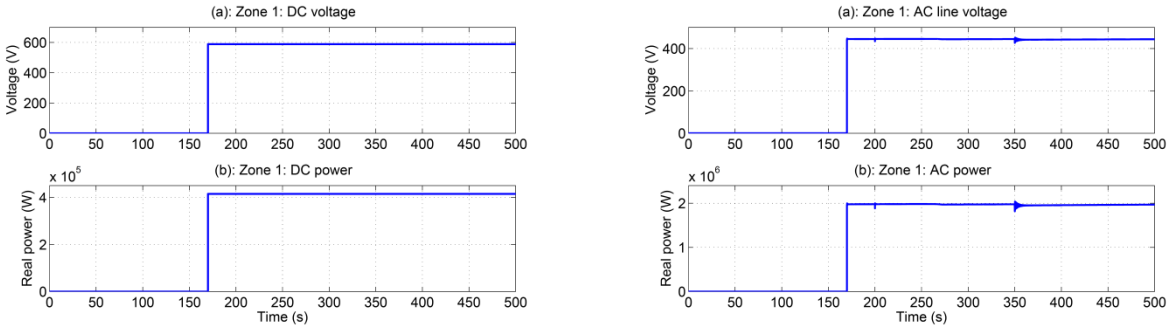

Fig. 4.2.36: Zone 1 Load Voltage and Power.

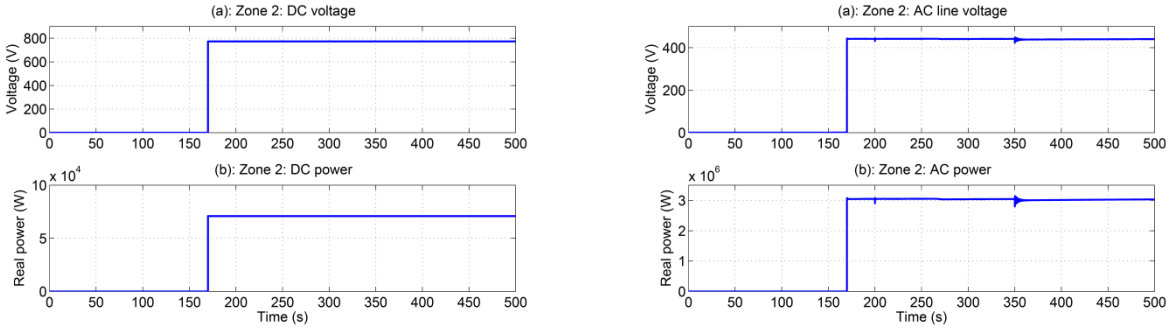

Fig. 4.2.37: Zone 2 Load Voltage and Power.

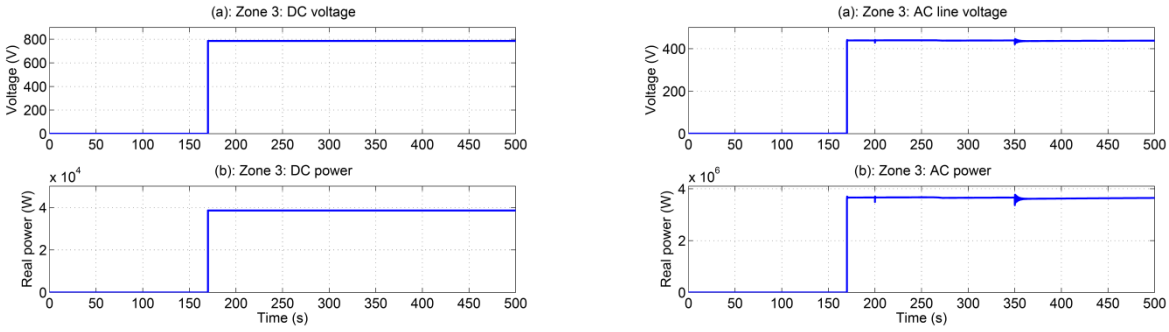

Fig. 4.2.38: Zone 3 Load Voltage and Power.

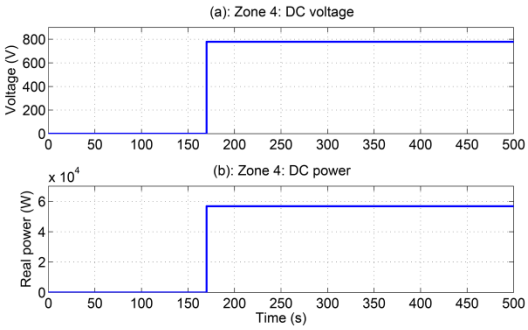

Fig. 4.2.39: Zone 4 DC Voltage.

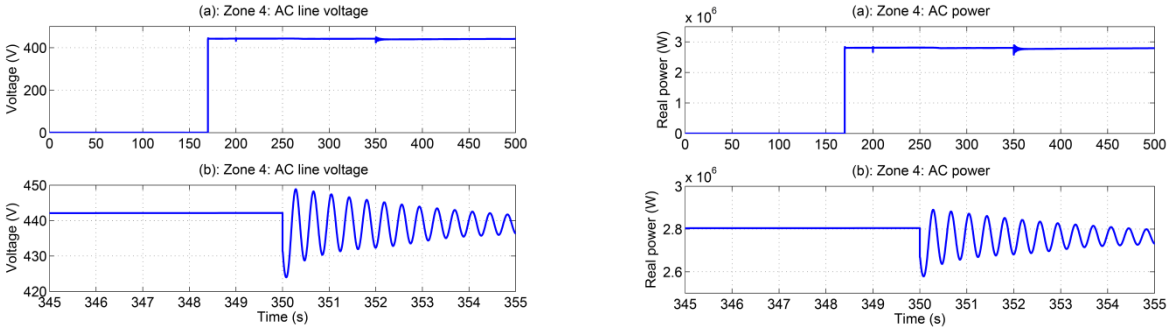

Fig. 4.2.40: Zone 4 Load AC Voltage and Power.

SUMMARY

The simulation results of Study 3 confirm that the averaged-value reduced-order MVAC system model can be used to analyze the effect of a loss of generation in the split-plant configuration while maintaining a convenient, fast execution time. It was found that the loss of a turbo-generator does not significantly affect the system in a negative manner if the available power generation is not exceeded by the load demand. Note that the propulsion motor load in this simulation was manually modified to ensure that the remaining turbo-generator would not be overloaded. To provide for a more realistic scenario, future simulations would incorporate an automatic load shedding scheme to account for a loss of generation.

5 HIGH FREQUENCY AC SYSTEM

5.1 System Description

The second version of the notional power system is a High Frequency AC (HFAC) power system. The zonal load center for this system is depicted in Fig. 5.1.1. Like the MVAC system, the HFAC version has ac distribution busses on the starboard and port side. The high frequency ac loads are fed from the ac bus through transformers (T) while the dc loads are fed through zonal active rectifier (ZAR) modules which may include internal transformers, like in the MVAC system. Low frequency ac loads are fed off of the low voltage dc bus (LVDC) through non-isolated inverter modules (NIMs).

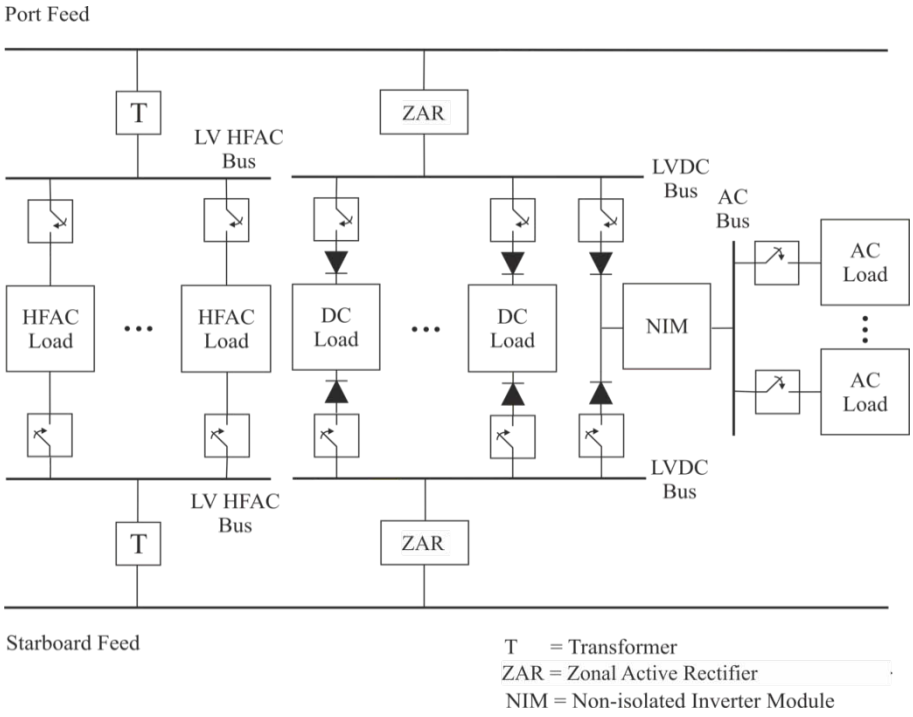

Fig. 5.1.1: Notional HFAC Zone.

In addition to the system depicted in Fig. 3.1.1 and the zonal load depicted in Fig. 5.1.1, the HFAC system model includes a generic hydrodynamic block and a power sharing block. The

hydrodynamic block accounts for the propulsion load and the power sharing block accounts for paralleling of the four turbo-generators to ensure synchronization and proportional load sharing.

A specific attribute of the HAFC power system model is the use of high-frequency transformers which are much smaller in size than their 60 Hz counterparts. Each of the four load zones contains four transformers with the special load using another two transformers giving a total of eighteen 240 Hz transformers. Zone 2 is identical to Zone 1, with the same number and type of loads, power conditioning modules, and breakers, but the load values are different. Zone 3 and Zone 4 are similar to Zone 1 and Zone 2 but have a total of five loads each instead of six.

Another attribute of the HFAC power system model is its ring bus with a 240 Hz distribution frequency. The ring bus includes sixteen ac breakers and eight bus segments modeled as RL ac lines. The two line connections through the breakers and bus segments are the main busses. The average synchronous frequency is calculated in the power sharing block and connected to the components that need it.

The generator model assumes that the synchronous reference frame is the same as the rotor reference frame. This is valid for single generator operation. However, when operating in parallel with other generators, a single synchronous reference frame is needed, as discussed in Section 8.2.1 of the component model documentation (Appendix A) and which was defined by a weighted average of rotor speeds of all active generators. This is left as a future improvement.

The generator real time synchronization controller described in the component model documentation (Appendix A, Section 8.2.4) uses frequency and phase controls to keep the generators synchronized at all times and share power proportionately when operating in parallel. In this initial version of the HFAC power system model only the frequency control was implemented and the results show that this was adequate to maintain the generators synchronized and share power equally. The generators' controller uses power feedback to dynamically calculate reference frequencies which are fed back to the gas turbines' governors. The controller forces the generators speeds (frequencies) to remain very close to the nominal 240 Hz system frequency, or 1 p.u. As will be shown in the study results section later, the controller was able to perform its function successfully. In order to determine the generator frequency, the controller uses the statuses of the four generator breakers and the sixteen ring bus breakers and determine through a combinatory analysis which generators are in parallel.

The two propulsion drives are each composed of a rectifier block, a DC link block, a motor controller-inverter and a PM motor. Slight modifications to the rectifier and DC link models were made to force the DC link current to remain positive and prevent it from returning to the rectifier block during braking operations. The changes consisted of adding an ideal diode between the rectifier and DC link blocks. Several tests simulating braking operations gave the expected results where the DC current remained positive or zero at all times during the braking operation. Additionally, it is important to note that the braking resistor system includes a chopper that was not modeled in terms of average-value representation and if braking operation is simulated with this model of the chopper operation, being a very fast event, will slow the simulation significantly. Consequently, an average-value representation of the braking resistor system needs to be developed in future efforts. However, for demonstrating the operation of braking operation with this model, a very large DC link capacitor can be used to reduce the chopper frequency and allow a fast simulation. This was demonstrated by the developer of this model.

The Generic Pulsed Load (GPL) has three power feeds one high-voltage feed from the starboard bus for extracting high power during pulse operation and two low-voltage feeds taken from Zone 1 and Zone 2 used to power various auxiliary equipment needed by a GPL.

The low-voltage feeds are connected to the transformer output 450 V \ 240 Hz frequency with the assumption that the GPL auxiliaries can function with 240 Hz power. It is also possible to connect the GPL low-voltage feeds to the 450 V – 60 Hz bus that is available in each zone. This 60 Hz bus is provided by the NIMs in each zone to power the 60 Hz RL loads.

Unless otherwise noted, the component models used are as described in Appendix A, with model parameters as set forth in Appendix B.

5.2 Studies

Three system studies were performed using the HFAC average-value reduced-order model to demonstrate its capability as a design tool. The first two studies, a ship start-up study and a pulsed load response study, were completed successfully. The third study, loss of generation, was also set-up with the supervisory controls for all components modeled as defined, since this study represents a stringent test for the proper operation of the supervisory control systems. However, this third scenario was not completed successfully as will be discussed in Section 5.2.3. Finally, it is important to note that for the HFAC power system model, the three studies were analyzed using the full average-value reduced-order power system model as depicted by the top level system model in Fig. 3.1.1, including the supervisory controls, for each component and sub-system, which were modeled as defined and used in the simulations accordingly.

5.2.1 Ship Startup

In this scenario the ship is accelerated from rest to full speed, to about 32 Knots for the component parameters used in the HFAC power system. This translates to operating the propulsion drives at their full combined power of ~ 70 MW. Other ship service loads are also active so that the ship power system is operating at full capacity, ~ 80 MW.

The simulation sequence of events is given in Table 5.2.1. An event number is assigned to each action performed from the start to the end of the simulation, with the corresponding time that action was taken, and the definition of what that action is. When inspecting the power system responses this table helps determine what action caused a given feature, such as a sudden drop in a bus voltage for example, by simply referring to the event in the table that corresponds to the time the feature occurred.

Table 5.2.1: Study 1 Simulation Sequence of Events.

Sequence #	Event start – (end) time	Event Description
0	0	Ship at rest, power off, prop drive caps charged to 5600 V
1	0-(300)	START SIMULATION–Accelerate turbo-gens to rated speed
2	310	Turn excitation field on
3-6	600,610,620,630	Close all 4 generator breakers sequentially (10 sec apart)
7-18	700,710,720,730,740,750, 760,770,780,785,790,795	Close ring bus breakers for split-plant configuration sequentially (12 breakers)
19	800	Close zone distribution breakers simultaneously (8 breakers)
20	850	Close special load distribution breakers (HV breakers)
21	870	Close generic pulsed load breakers
22-25	1000,1100,1200,1300	Close zone 1 through 4 load breakers sequentially
26-28	1410,1415,1420	Enable operation of zone 1 ZAR and NIM
29-31	1425,1430,1435	Enable operation of zone 2 ZAR and NIM
32-34	1440,1445,1450	Enable operation of zone 3 ZAR and NIM
35-37	1455,1460,1465	Enable operation of zone 4 ZAR and NIM
38-43	1500,1510,1520,1530,1540,1550	Operate zone 1 loads sequentially (10 sec apart)
26-29	1560,1570,1580,1590,1600,1610	Operate zone 2 loads sequentially (10 sec apart)
30-34	1620,1630,1640,1650,1660	Operate zone 3 loads sequentially (10 sec apart)
35-39	1670,1680,1690,1700,1710	Operate zone 4 loads sequentially (10 sec apart)
40,41	1800,1810	Close port bus corner breakers (all 4 gens in parallel)
43	2000	Close propulsion breakers
44	2010	Enable propulsion startup (spd* = 1pu)
45	2015	Operate propulsion (Opd* = true)
46	2100	Start ship acceleration from rest to full speed (~32 knots)
47	4000	END SIMULATION – record simulation time

In the simulation sequence of events for study 1 all load breakers are ordered to close prior to starting the ship acceleration even though some of these loads are not activated, such as the special load and the pulsed power load. This is to maximize power system response by setting all distribution and load busses “hot” during the exercise.

The setup of load connections to the port and starboard busses are given in Table 5.2.2 and Table 5.2.3. At the end of the acceleration the power system will be operating at 98.8% capacity.

Table 5.2.2: Study 1 Zonal Load Levels.

Loads	Port Bus (kW)	Starboard Bus (kW)
Z1L1	70	
Z1L2		0
Z1L3	640	
Z1L4	390	
Z1L5		275
Z1L6		7
Z2L1	0	
Z2L2		20
Z2L3		930
Z2L4	300	
Z2L5	400	
Z2L6	35	
Z3L1		20
Z3L2	1200	
Z3L3		550
Z3L4	375	
Z3L5		4
Z4L1		0
Z4L2		200
Z4L3	415	
Z4L4		220
Z4L5	4	
Sub Total	3829	2208
Zone Total	6037	

Table 5.2.3: Study 1Load Summary.

Load Type	Port Bus (kW)	Starboard Bus (kW)
Special Load	0	
Pulsed Load Standby	0	0
Pulsed Load Operation	0	0
Propulsion Load	36500	36500
Zone Total	3829	2208
Sub Total	40329	38708
Total	79037	

Simulation Results:

- The total events time for study 1 is 66 minutes (~ 4000 s)
- The computer execution time for the simulation is 6 minutes (360 s)
- Computer used: Dell Precision T7500 64-bit
- Processor: Intel Xeon® X5680 @ 3.3 GHz / 24 GB RAM

The turbo-generator speeds are shown in Fig. 5.2.1. The minor disturbances on the bottom graphs are due to the loads. The first one is due to the zonal loads being turned on sequentially; the larger ones are due to the fast acceleration period. Consult the simulation event table (Table 5.2.1) to correlate events and features on the graphs. From the bottom graph, with the expanded y-axis, it appears that the real time synchronization controller did an excellent job at keeping the four generators' frequencies close to the 240 Hz system frequency (1 p.u.).

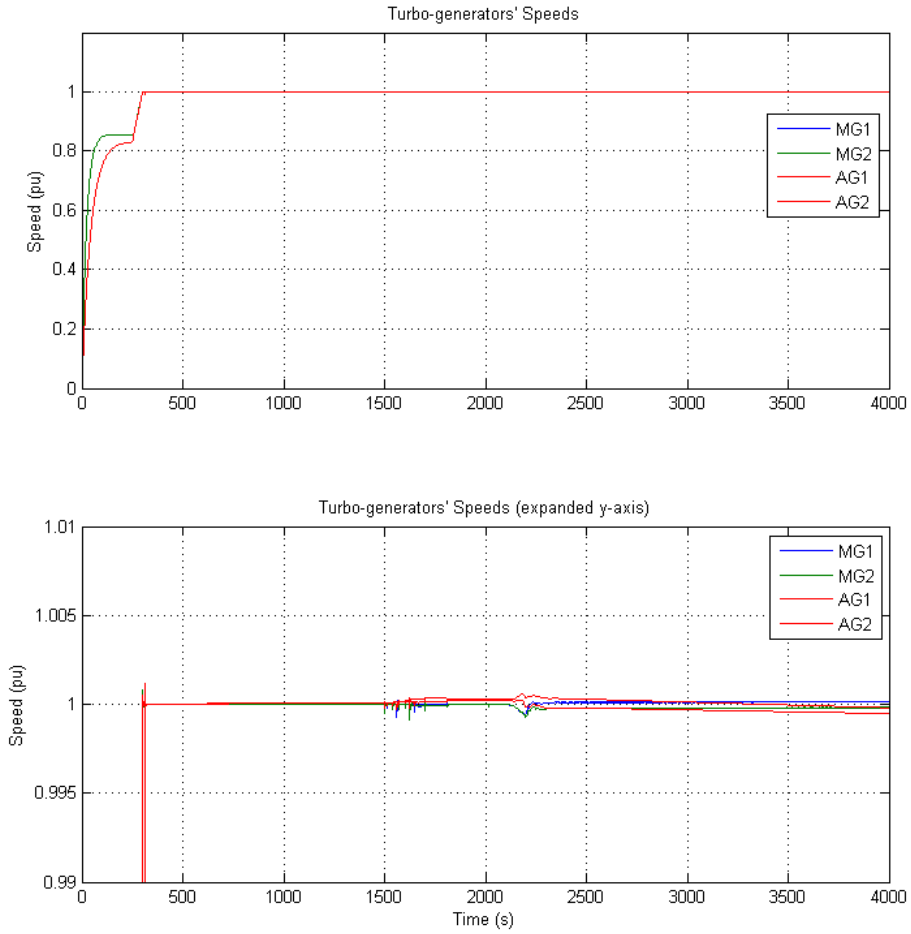

Fig. 5.2.1: Study 1 Turbo-generator Speeds.

The output powers for each generator are shown in Fig. 5.2.2. The results correlate well with the sequence of events. The first sharp spike is due to the start of field excitation (event #2 @ 310 s). The second spike is due to the closing of the propulsion breakers (event #43 @ 2000 s). The features on the graph prior to the closing of the propulsion breakers are due to the zonal loads being added sequentially.

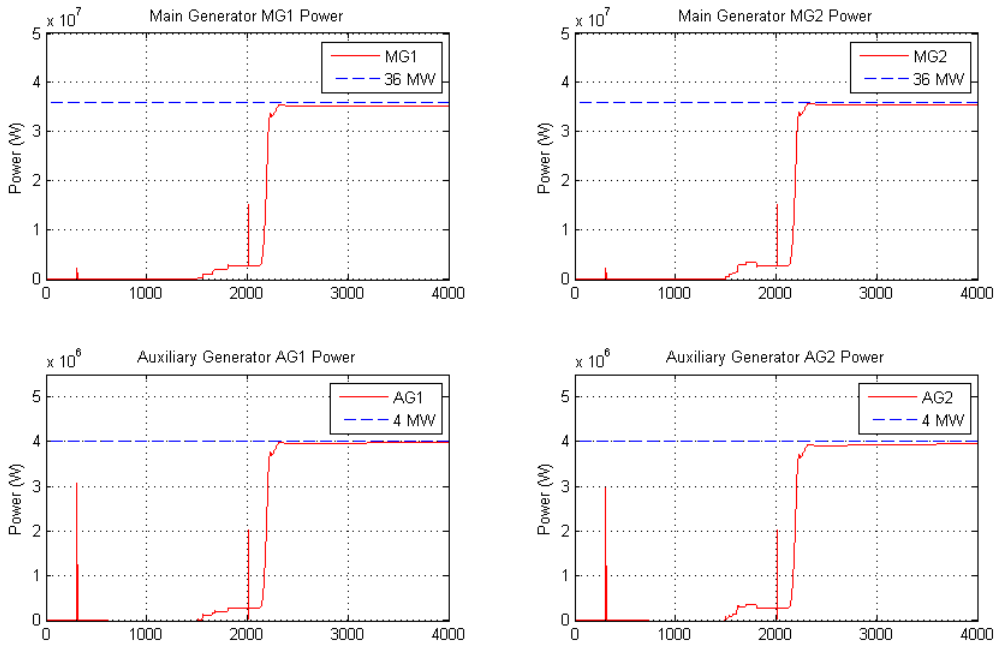

Fig. 5.2.2: Generator Output Powers.

Fig. 5.2.3 depicts the generator output powers plotted on the same axis to check load sharing among the generators. A perfect proportional load sharing would result in the four curves being on top of each other. The results obtained differ due to component parameters such as governors' gains and exciters' parameters needing to be adjusted in future runs. It is to be noted that the exciter KPR parameter for the port auxiliary generator had to be reduced slightly as compared to the corresponding starboard exciter parameter in order to keep its output power under its maximum value when operating close to its power rating. In addition, the point at which the curves join together just before closing the propulsion breakers is when the port and starboard busses are connected in parallel (events #41 and #42 in events table).

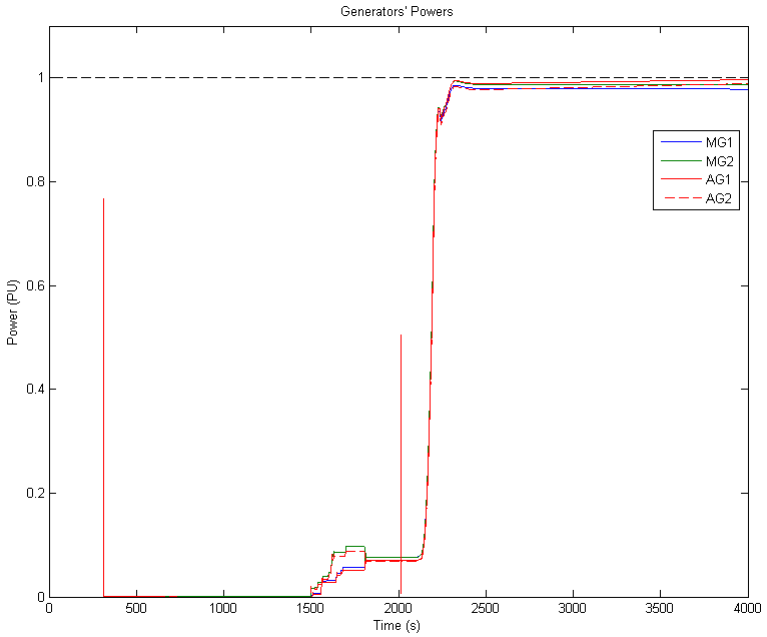

Fig. 5.2.3: Generator Output Powers (Single Axis).

Fig. 5.2.4 shows the port and starboard voltages during the study. A drop in both bus voltages is observed, as expected, since the two busses are connected in parallel.

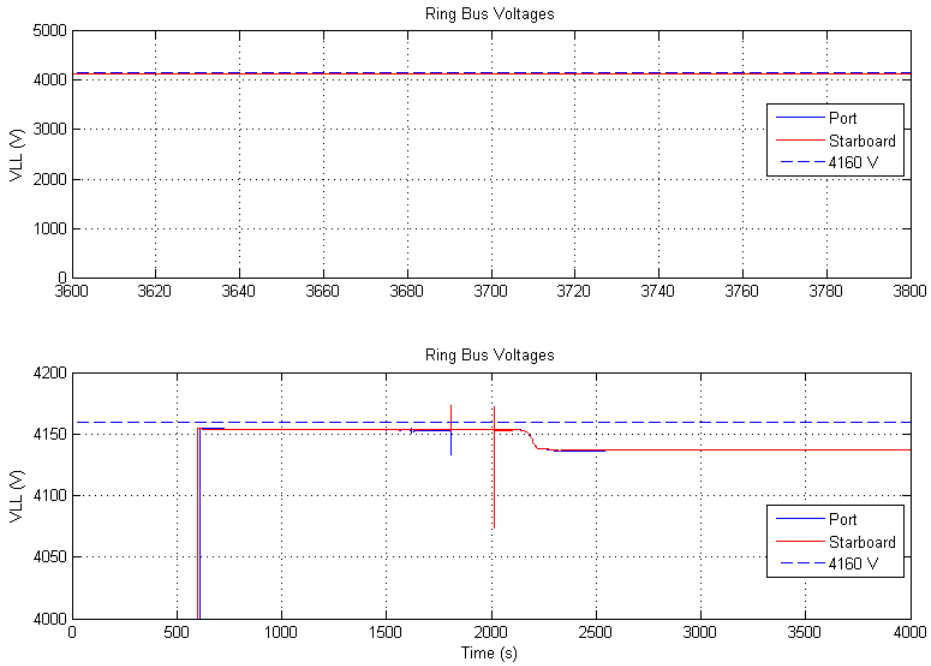

Fig. 5.2.4: Port and Starboard Bus Voltages.

Fig. 5.2.5 shows several plots related to the port propulsion drive, it includes motor speed, motor torque, motor power, DC link voltage, inverter current, and motor voltage. The DC link capacitor was initially charged to the nominal bus voltage at the start of the simulation, which explains the drop in the DC link voltage before the start of the acceleration. It is noticed, however, that the DC link voltage dropped from the nominal 5618 V to about 5000 V or by 11%

from nominal during the acceleration. This is within the 30% run condition set in the propulsion supervisory controller which monitors the DC link voltage to control the operational status of the propulsion drives.

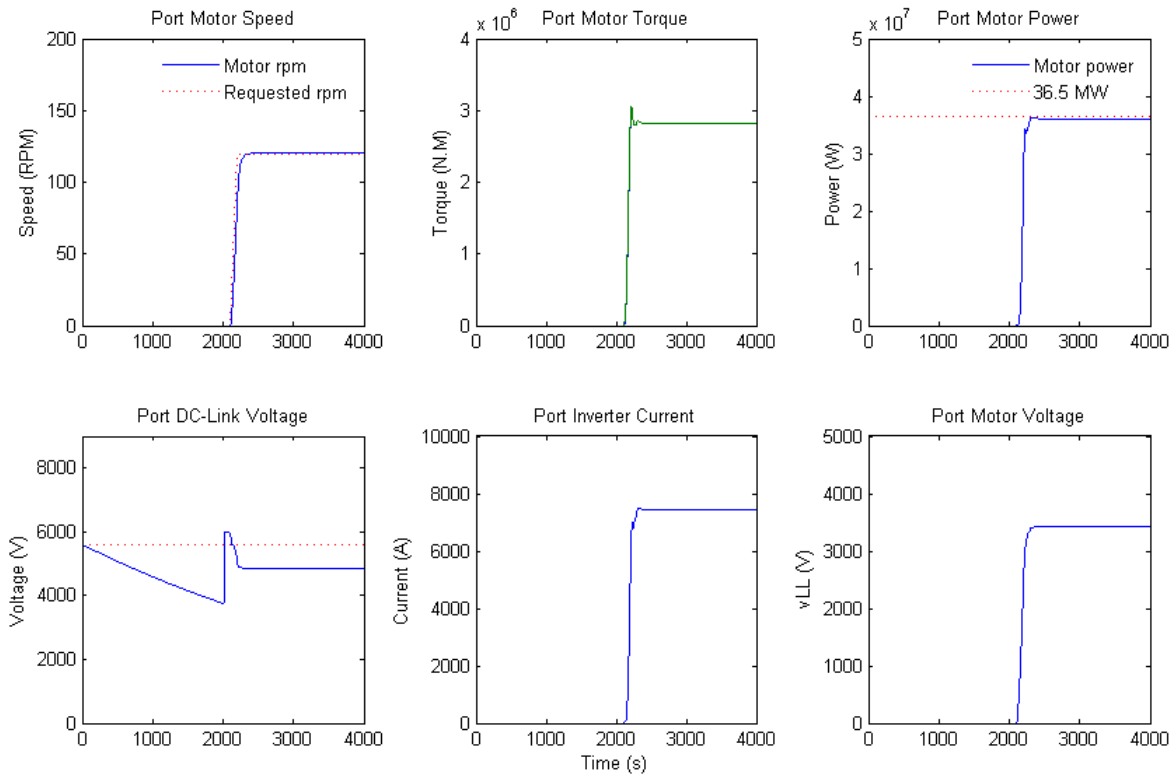

Fig. 5.2.5: Port Propulsion Data.

The Starboard propulsion data are shown in Fig. 5.2.6 and are similar to the port propulsion data. This was expected since the port and starboard busses were connected in parallel with the two propulsion drives sharing the voltage source.

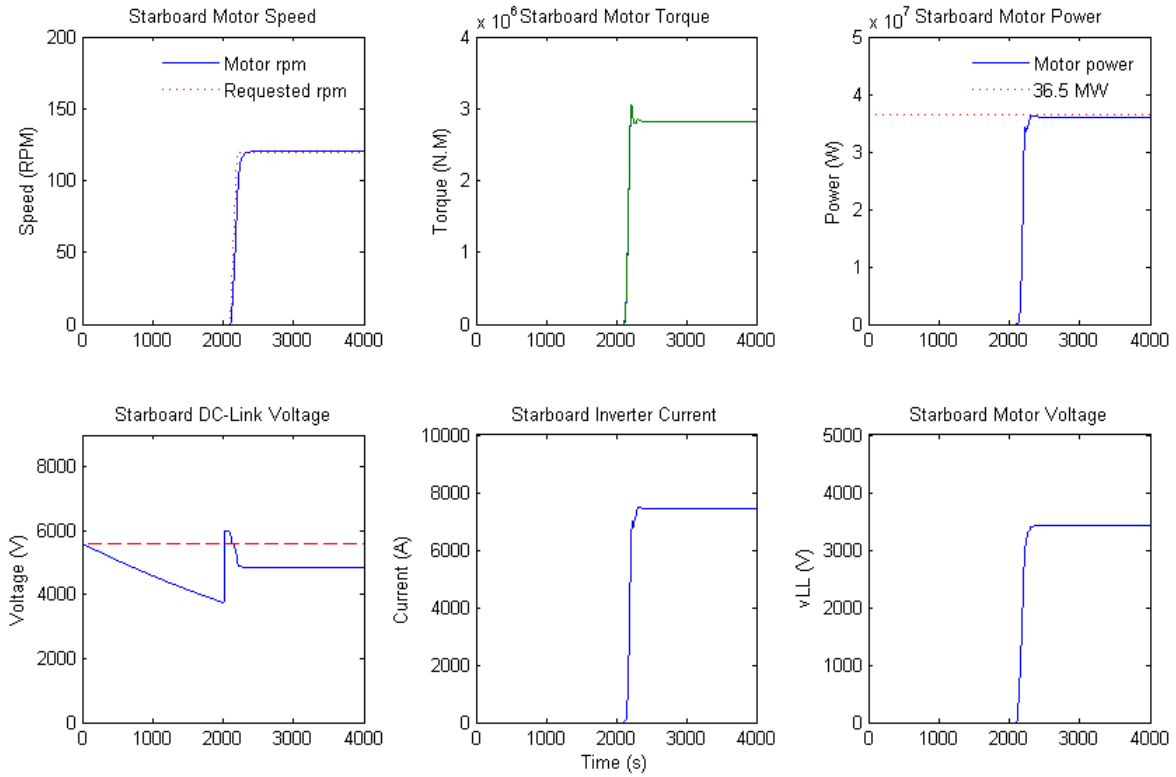

Fig. 5.2.6: Starboard Propulsion Data.

Fig. 5.2.7includes plots of power delivered to the six loads located in zone 1. The delivered power is calculated from the currents and voltages at the terminals of each load which indicates that all power system components involved in delivering the power to these loads are operating properly. This is the case, as can be clearly seen in the plots. Similar results are obtained for the other zonal loads. These are shown in Fig. 5.2.8 through Fig. 5.2.10. The plots that show very low power levels are for loads that are nominally zero and set to a small value to avoid numerical problems (these loads are selected from two possible load sets depending on the operational mode, battle or cruise mode; some loads operate in one mode but not in the other).

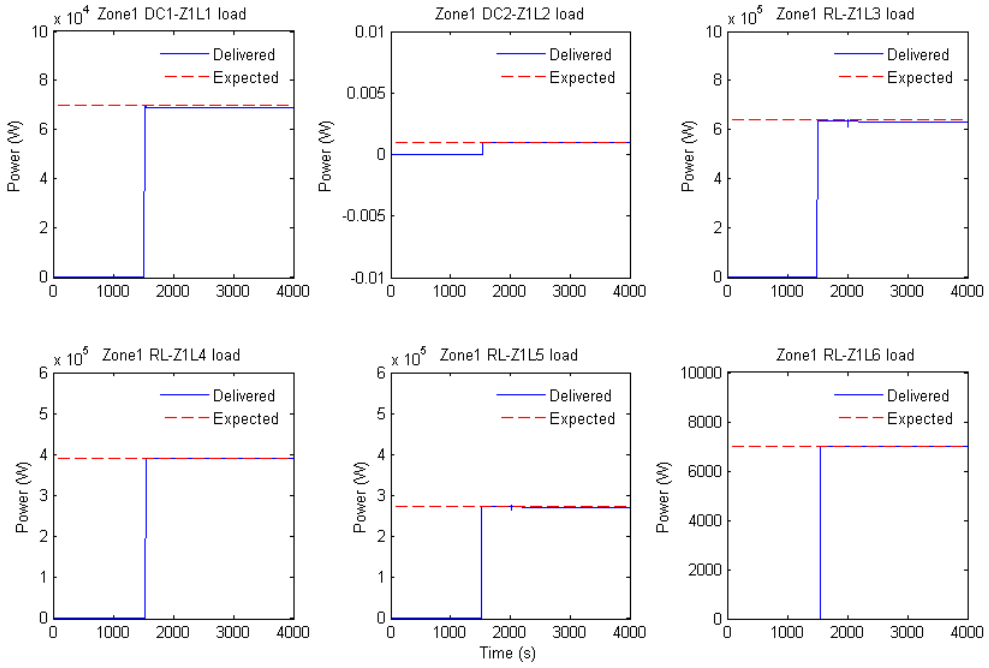

Fig. 5.2.7: Zone 1 Load Power.

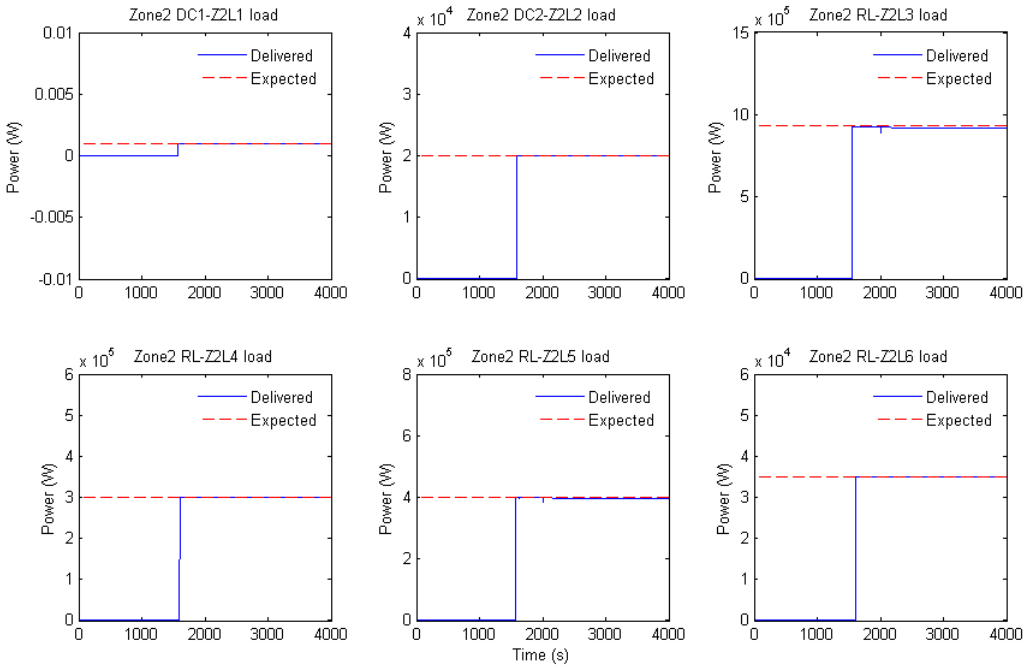

Fig. 5.2.8: Zone 2 Load Power.

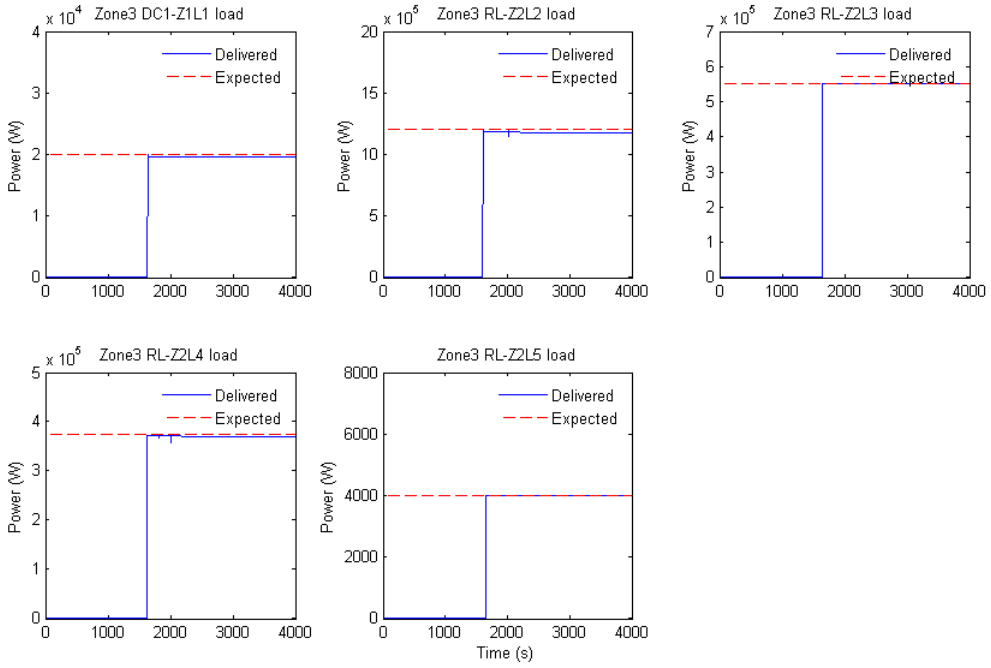

Fig. 5.2.9: Zone 3 Load Power.

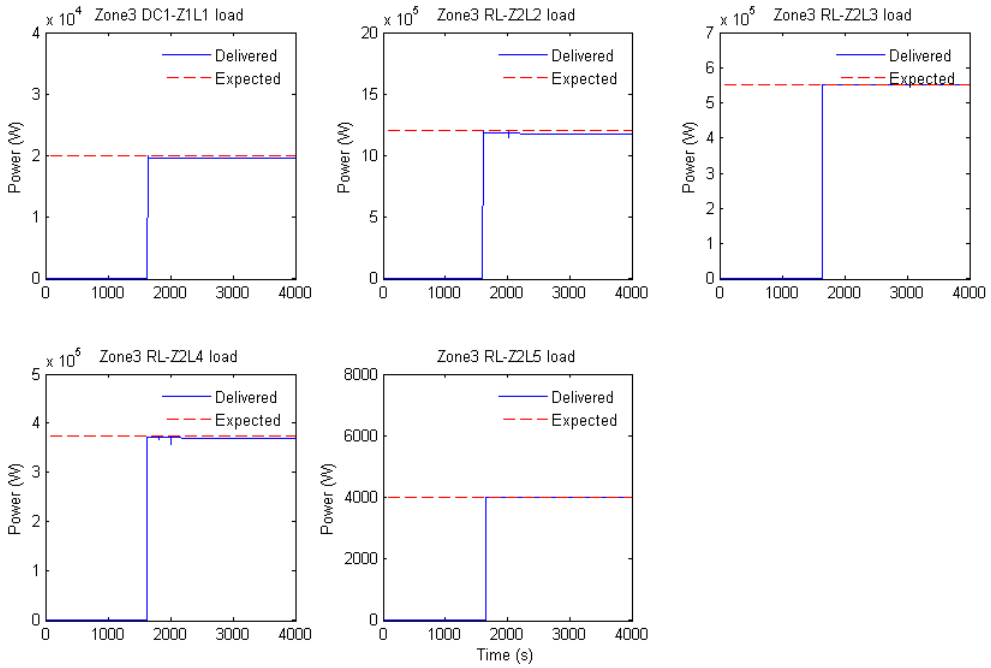

Fig. 5.2.10: Zone 4 Load Power.

Study 1 demonstrated that the HFAC average-value reduced-order power system model was indeed able to simulate a long scenario in a short period of time, as compared to waveform level system models, while the results are correct and useful. The short computer simulation time will allow design engineers and analysts to conduct multiple studies in short periods of time, thereby improving the design process considerably. In addition, Study 1 showed that the power system worked properly for the components that were active during the simulation, including the propulsion drives which were operating at their rated power. The generator synchronization controller worked well and the turbo-generators frequencies were kept very close to each other

and to the nominal system frequency. Initial observations indicate that exciters and governors parameters need to be selected more carefully in order to have better control of active and reactive power sharing.

5.2.2 Pulsed Load Response

In this study, the pulsed load operated in conjunction with all the loads onboard the ship which include all zonal loads, propulsion loads, and the special load. The aim of this second study is to analyze the response of the power system to high power pulses extracted directly from the ship electric grid. Two pulses are fired while the ship is operating in split-plant mode and another pulse is fired after the port and starboard busses main distribution busses are connected in parallel. The simulation sequence of events is listed in Table 5.2.4.

Table 5.2.4: Study 2 Simulation Sequence of Events.

Seq. #	Event start (end) time	Event Description
0	0	Ship at rest, power off, prop drive caps charged to 5600 V
1	0-(300)	START SIMULATION–Accelerate turbo-gens to rated speed
2	310	Turn excitation field on
3-6	600,610,620,630	Close all 4 generator breakers sequentially (10 sec apart)
7-18	700,710,720,730,740,750, 760,770,780,785,790,795	Close ring bus breakers for split-plant configuration sequentially (12 breakers)
19	800	Close zone distribution breakers simultaneously (8 breakers)
20	850	Close special load distribution breakers (HV breakers)
21	870	Close generic pulsed load breakers
22-25	1000,1100,1200,1300	Close zone 1 through 4 load breakers sequentially
26-28	1410,1415,1420	Enable operation of zone 1 ZAR and NIM
29-31	1425,1430,1435	Enable operation of zone 2 ZAR and NIM
32-34	1440,1445,1450	Enable operation of zone 3 ZAR and NIM
35-37	1455,1460,1465	Enable operation of zone 4 ZAR and NIM
38-43	1500,1510,1520,1530,1540,1550	Operate zone 1 loads sequentially (10 sec apart)
26-29	1560,1570,1580,1590,1600,1610	Operate zone 2 loads sequentially (10 sec apart)
30-34	1620,1630,1640,1650,1660	Operate zone 3 loads sequentially (10 sec apart)
35-39	1670,1680,1690,1700,1710	Operate zone 4 loads sequentially (10 sec apart)
40	1900	Close special load breakers
41	1950	Enable operation of special load ZAR
42	1980	Operate Special Load
43	2000	Close propulsion breakers
44	2010	Enable propulsion start-up (Spd* = 1)
45	2015	Operate propulsion (Opd* = 1)
46	2100	Start ship acceleration from rest to cruise speed (~20 Knots)
47	2700	Set pulsed load in standby mode
48,49	(3100-3140)-(3200-3240)	Operate pulsed load–fire 2 10MW shots (40s wide/60s apart)
50,51	3500,3510	Close port bus corner breakers (4 gens in parallel)
52	3700	Operate pulsed load –fire 1 10MW shot - gens paralleled
53	4000	END SIMULATION – record simulation time

The setup of load connections to the port and starboard busses is given in Table 5.2.5 and Table 5.2.6. When steady state is reached, the power system operates at 41% of capacity when pulsed power is not used and at 54% capacity during pulsed load operation.

Table 5.2.5: Study 2 Zonal Load Levels.

Loads	Port Bus (kW)	Starboard Bus (kW)
Z1L1	150	
Z1L2		615
Z1L3	715	
Z1L4	400	
Z1L5		910
Z1L6		0
Z2L1	1	
Z2L2		75
Z2L3		1400
Z2L4	750	
Z2L5	975	
Z2L6	40	
Z3L1		40
Z3L2	1200	
Z3L3		1900
Z3L4	750	
Z3L5		0
Z4L1		60
Z4L2		480
Z4L3	1750	
Z4L4		675
Z4L5	0	
Sub Total	6731	6155
Zone Total	12886	

Table 5.2.6: Study 2 Load Summary.

Load Type	Port Bus (kW)	Starboard Bus (kW)
Special Load	3750	
Pulsed Load Standby	1000	200
Pulsed Load Operation	1200	10000
Propulsion Load	7100	7100
Zone Total	6731	6155
Sub Total	19781	23455
Total	43236 (10000 pulsed)	

Simulation Results:

- The total events time for study 2 is 66 minutes (~ 4000 s)
- The computer execution time for the simulation is 5.5 minutes (330 s)
- Computer used: Dell Precision T7500 64-bit
- Processor: Intel Xeon® X5680 @ 3.3 GHz / 24 GB RAM

The turbo-generator speeds are shown in Fig. 5.2.11. As in study 1, the generator synchronization controller maintained the generators speeds (frequencies) under very good control and close to the nominal system frequency. Spikes in the speed traces during the pulses are less than 1% and occur during turn-on and turn-off of the pulsed load. Overall, pulsed power operation didn't affect system frequency considerably.

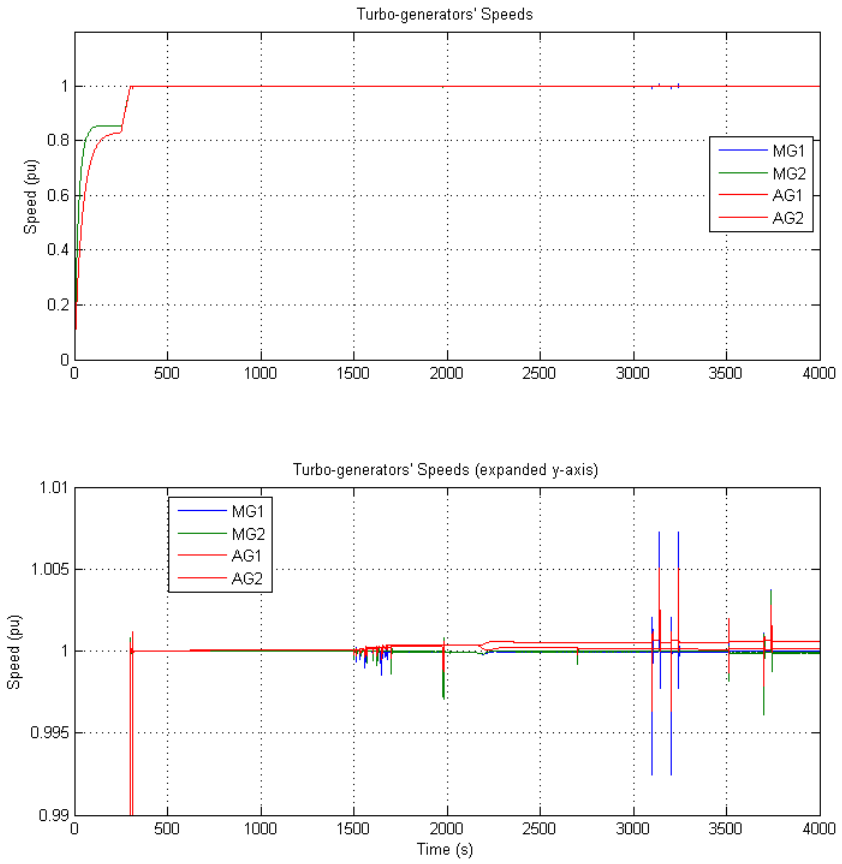

Fig. 5.2.11: Generator Response to Pulsed Load Operation.

The generator output powers are shown in Fig. 5.2.12 and Fig. 5.2.13. The results correlate well with the pulse events. The dual pulse power appears on the starboard generators only where the pulse load is connected for high power intake as expected since the system is still operating in the split-plant configuration. The single pulse power appears on all four generators power traces, as expected since the four generators are connected in parallel in that case. The results also show power sharing among the turbo-generators during pulsed load operation. It is important to mention here that some parameters such as the exciters parameters are found to be sensitive to the generators power sharing response. In our modeling efforts we haven't addressed control of reactive power in details and how to share it among the four generators which is

normally done through field control. The controls can be set to share reactive power among the four generators or assign it to a single generator for example. This issue needs to be addressed in future studies in order to establish the most effective strategy to handle reactive power given the electric ship power system constraints and operational modes.

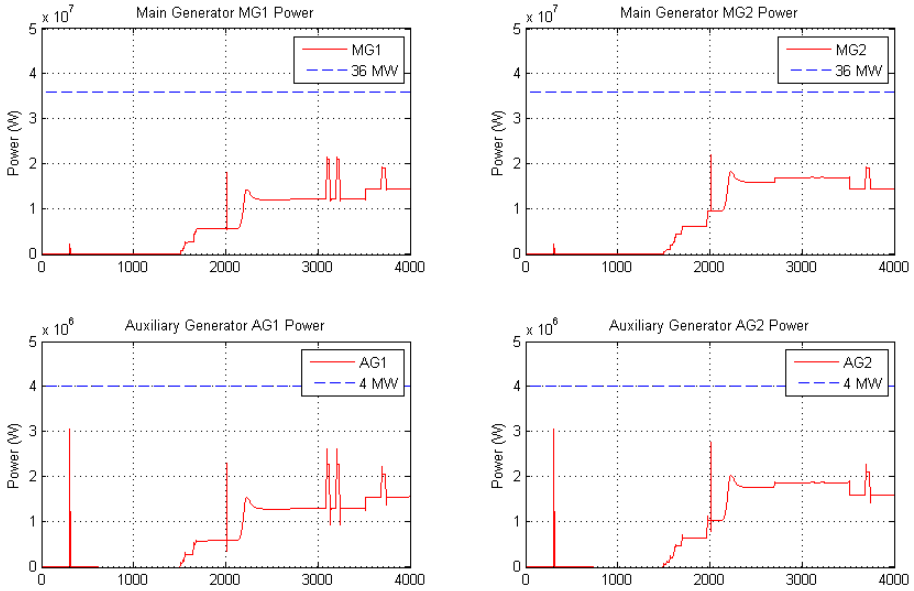

Fig. 5.2.12: Generator Power Sharing during Pulsed Load Operation.

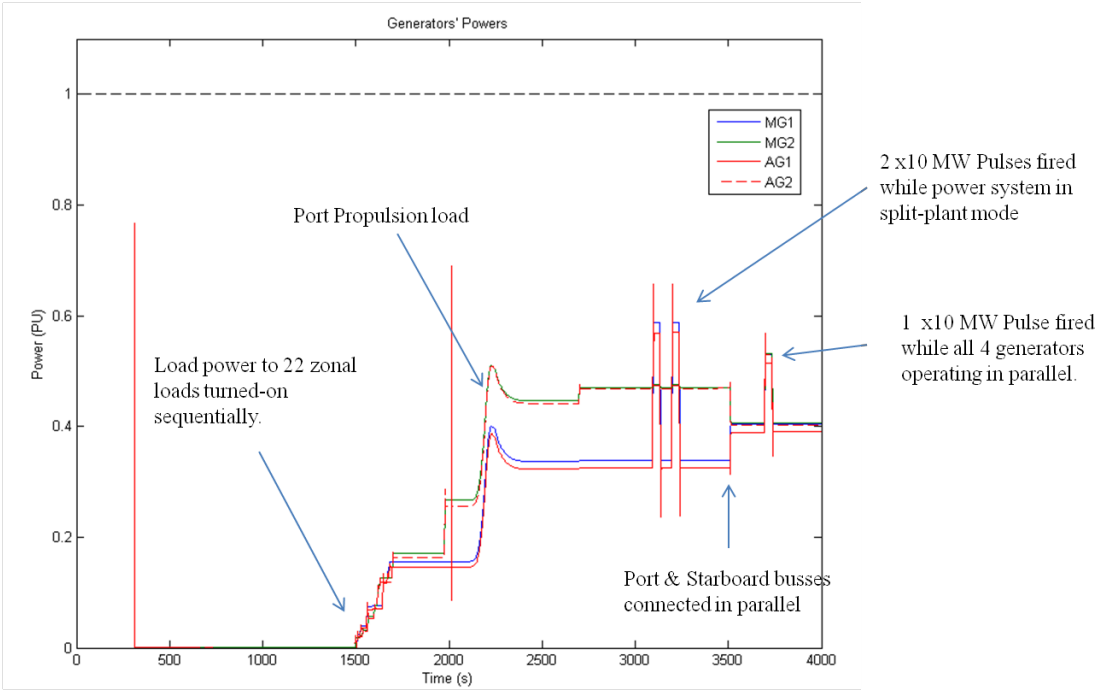

Fig. 5.2.13: Generator Power Sharing (single axis).

Ring bus voltages are shown in Fig. 5.2.14. The port and starboard busses remained stable during the pulse operation with voltage spikes during pulse turn-on and turn-off.

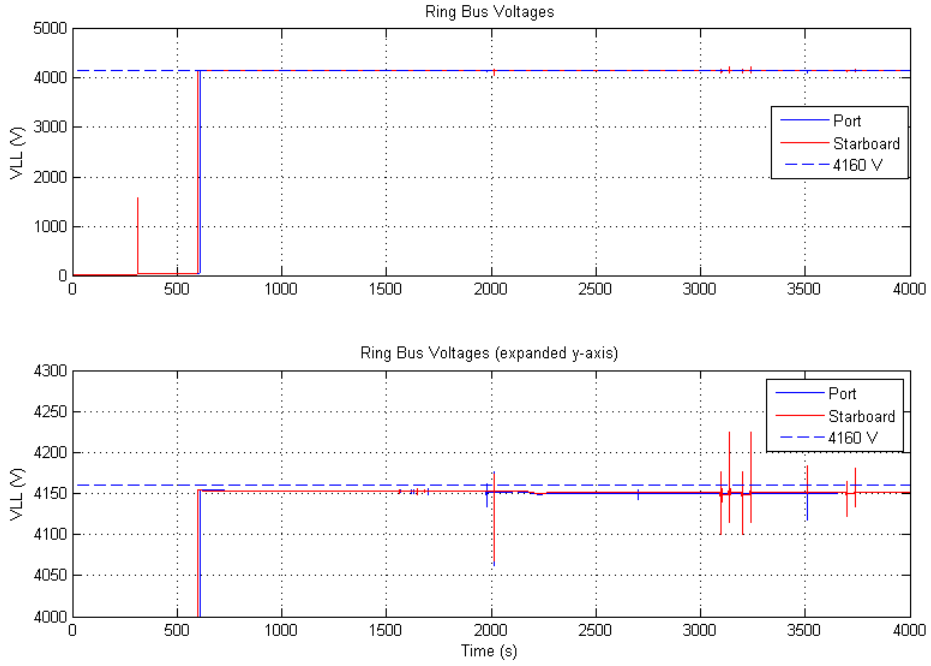

Fig. 5.2.14: Ring Bus Voltage During Pulsed Load Operation.

Port propulsion response to the pulsed load operation is shown in Fig. 5.2.15. The port propulsion drive remained unaffected. The starboard propulsion response is shown in Fig. 5.2.16. Some spikes appear in some traces such as the DC link voltage and inverter current.

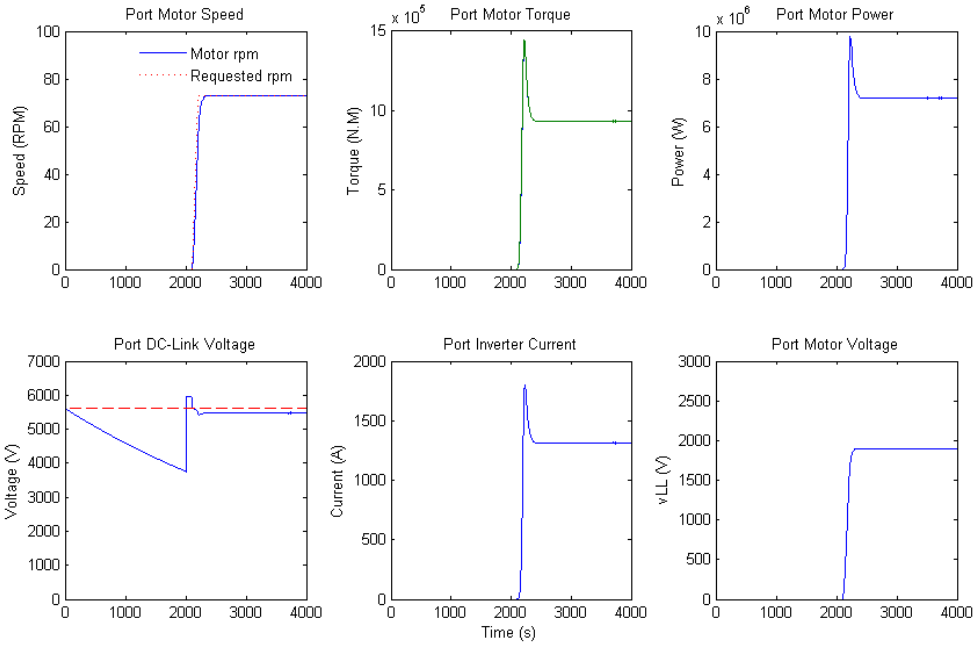

Fig. 5.2.15: Port Propulsion Response to Pulsed Load Operation.

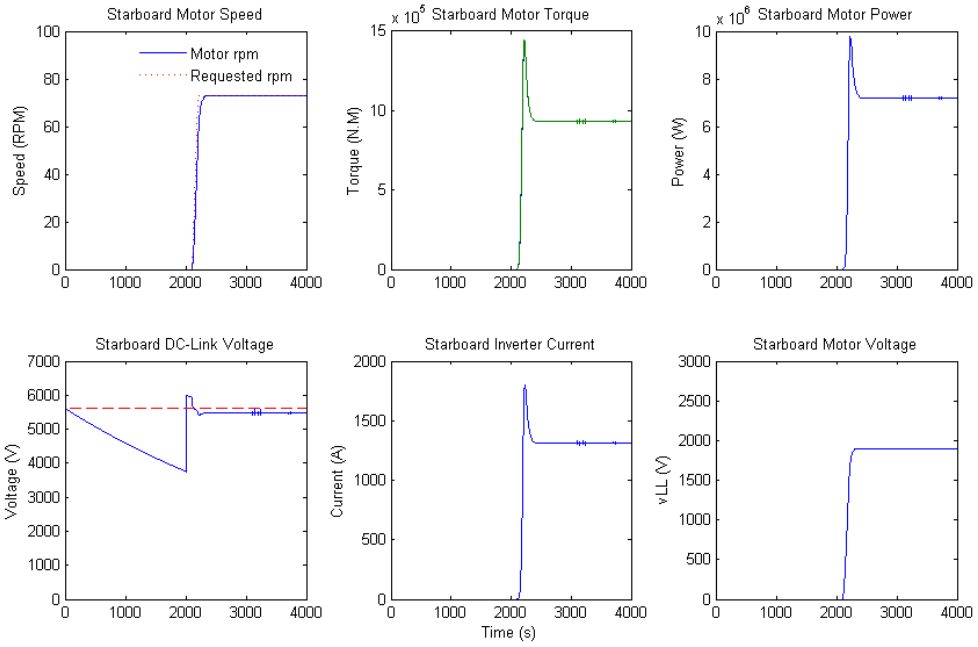

Fig. 5.2.16: Starboard Propulsion Response to Pulsed Load Operation.

Zonal load power traces are shown, for completeness, in Fig. 5.2.17, Fig. 5.2.18, Fig. 5.2.19, and Fig. 5.2.20 respectively for zones 1, 2, 3, and 4. Except for the loads that are connected to the starboard bus which exhibit some low amplitude spikes on their delivered power traces, the zonal loads are unaffected by the pulsed load operation.

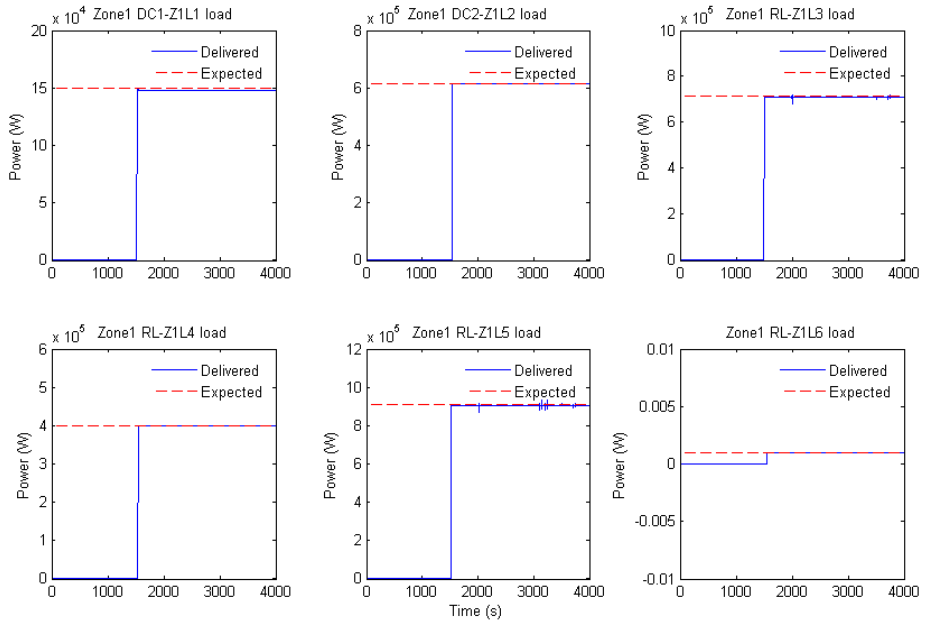

Fig. 5.2.17: Zone 1 Loads.

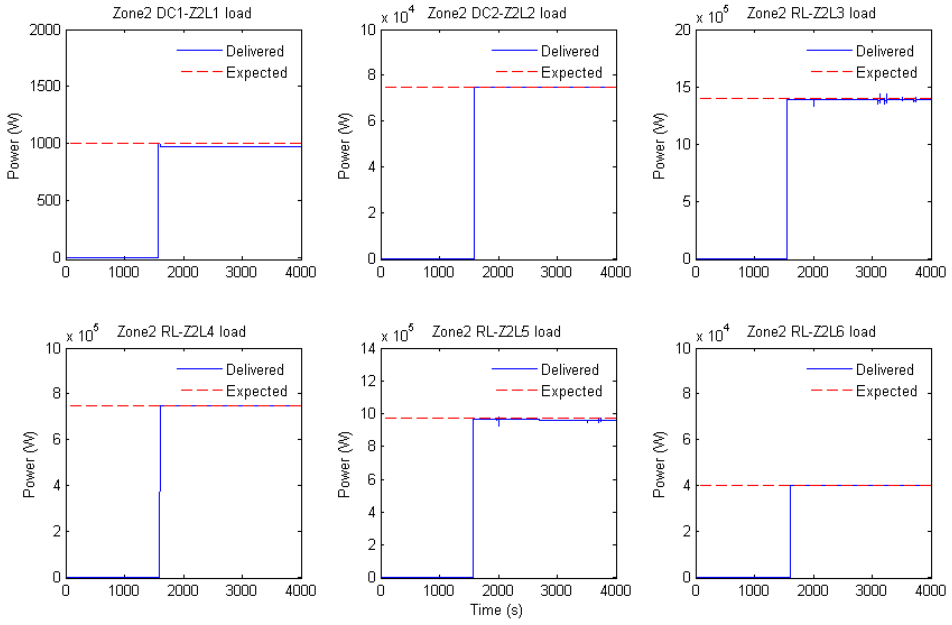

Fig. 5.2.18: Zone 2 Loads.

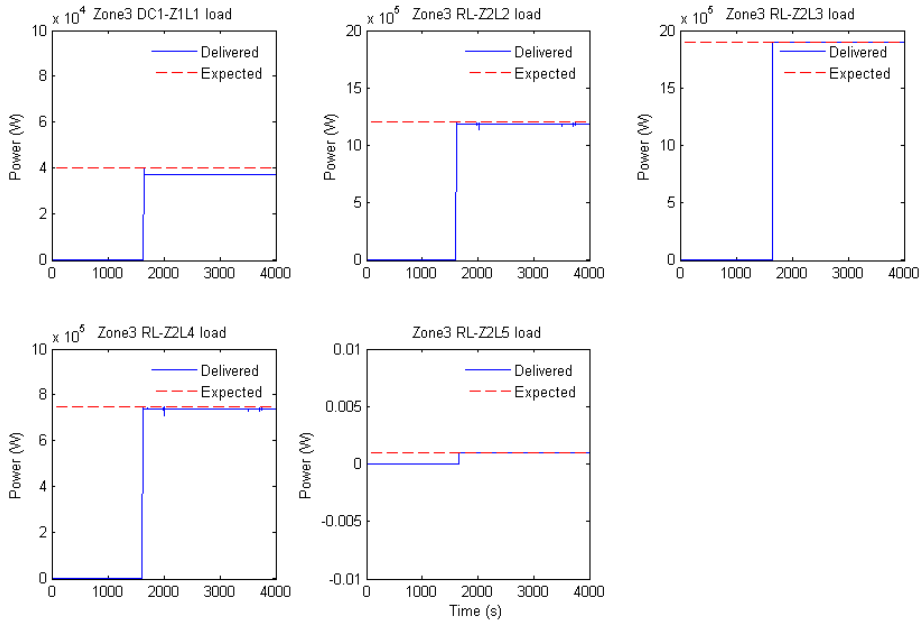

Fig. 5.2.19: Zone 3 Loads.

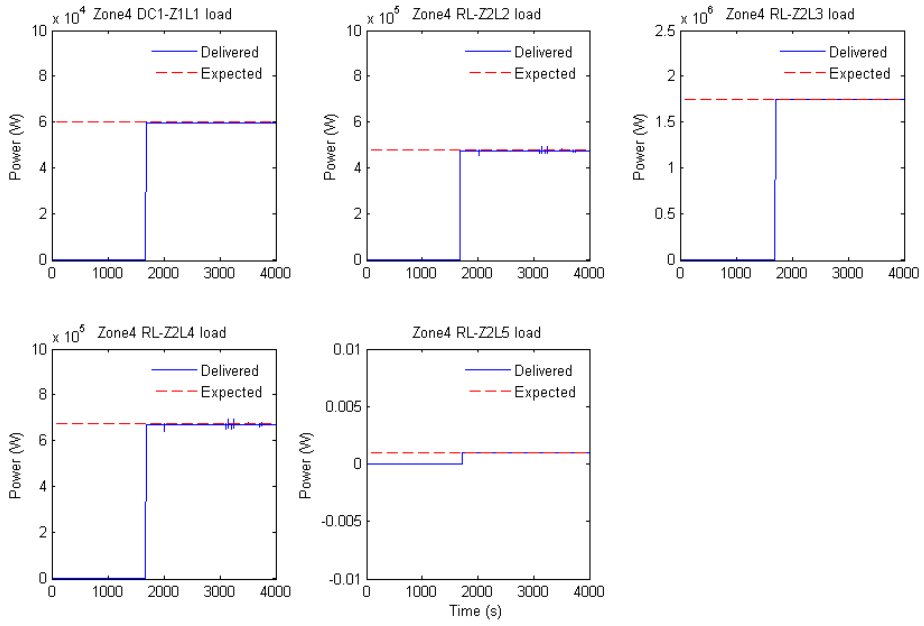

Fig. 5.2.20: Zone 4 Loads.

The special load, fed from the port bus, remains unaffected by the pulsed load operation. The transformer output voltage, the zonal rectifier DC output voltage that feeds the special load and the special load current are shown in Fig. 5.2.21.

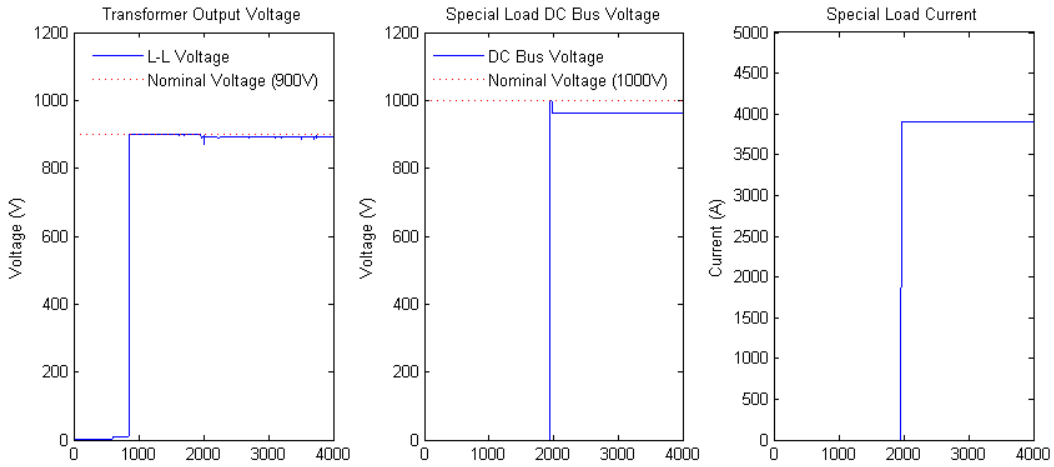

Fig. 5.2.21: Special Load.

Study 2 demonstrated that an analysis of the effect of pulsed load operations on the power system can be accomplished in very short period of time using an average-value reduced-order power system model such as the HFAC power system model just developed. It was found that for 10 MW pulses extracted directly from the ship electric grid, the effects on the power system were not significant. Further analyses can be conducted quickly for higher power levels for example and/or under different ship operational scenarios.

5.2.3 Loss of Generator

The simulation for study 3 was set-up correctly with all sub-systems, components, and loads operating with their supervisory control systems modeled as defined. In this study, the loss of a generator during operation was expected to trigger a response from the supervisory control systems which were expected to sense voltage drops or spikes across various loads and take appropriate actions, mainly disconnecting and re-connecting loads and modifying load demands as prescribed in the scenario. For the chosen scenario, which was setup a-priori through a sequence of events, the initial run was not successful.

During the simulation, when the main port generator breaker opened, as programmed to simulate the loss of the generator during operation, the simulation simply came to a virtual stop as various supervisory controllers were automatically activated in response to the fault event while others didn't. Due to a lack of time, only a short period was spent investigating the cause. First, the breaker of the auxiliary generator connected with the faulty generator, i.e. the second generator connected to the port bus, failed to open as expected since it would have sensed a very large current and opened. Few attempts were made to help this breaker open earlier by reducing its time constant as well as other approaches but without success. It was also found that the propulsion drive dc link voltage dropped very quickly after the fault started and it appeared that the propulsion supervisory controller detected the DC link voltage drop below the running limit and stopped operating the propulsion, as it was supposed to. However, it seems that at that point, the supervisory controller continued sensing the voltage it was controlling since the fault was

still there, and in the process continued its computations which with other factors perhaps, slowed the simulation to a point where it couldn't be completed. Perhaps, the supervisory controllers need to be instructed what to do in this situations such as stop all computations until a reset signal is sent or perform other less computing-intensive actions. These are just some possibilities, but a further look at this problem, which does not seem to be a major one, is needed.

6 MEDIUM VOLTAGE DC SYSTEM

6.1 System Description

The third instantiation of the notional power system is a Medium Voltage DC (MVDC) power system. The adaptation of the notional power system in Fig. 3.1.1 used in modeling the MVDC system is depicted in Fig. 6.1.1. The busses shown are medium voltage DC busses, and the sectionalizing switches on the DC busses are modeled by Simscape's electrical switches. The power generation modules are connected through electrical nodes on their respective buses. The propulsion system and pulse load inject current onto the buses through current injection blocks; meaning these two systems are not connected through electrical nodes, they utilize a signal flow modeling technique. For this system to proper manage the power on the bus, a proportional load sharing scheme discussed in Section 8.2.4 of Appendix A was implemented.

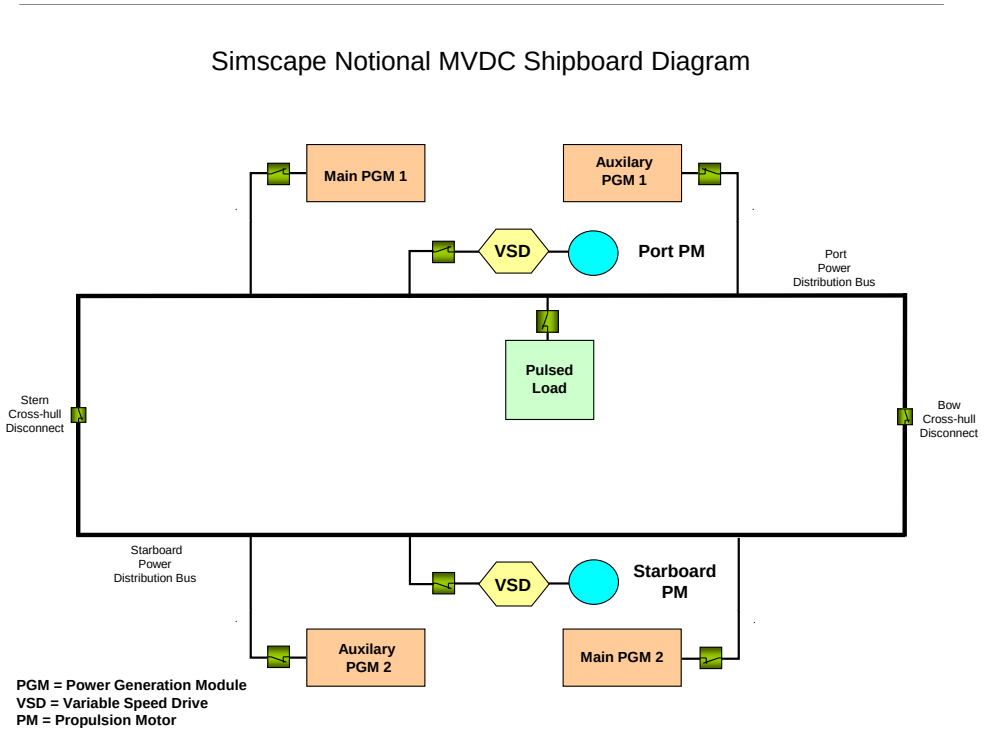

Fig. 6.1.1: Topology for Simscape Notional MVDC System.

The zonal load center for the MVDC system is depicted in Fig. 6.1.2. The starboard and port busses are dc busses that feed the dc loads through isolated dc/dc converters (IDCDC). Low-frequency (60 Hz) ac loads are fed through a non-isolated inverter module (NIM). However, because of the difficulties encountered using Simscape, it did not prove possible to implement the MVDC zones.

Fig. 6.1.2: Notional MVDC Zone.

DC Generator Set (GenSet)

For this notional system, the corresponding DC WRSM generator model described in Section 8.2.2 of Appendix A was not used. Rather, the AC WRSM generator model described in Section 8.2.2 of Appendix A was combined with a modified version of the diode rectifier described in Section 8.2.9 of Appendix A to create an electrical node based DC WRSM module to represent the main and auxiliary power generation units that power the DC bus. The IEEE Type AC8B – simplified exciter described in Section 8.2.3 of Appendix A, the gas turbine (Section 8.2.5 of Appendix A) and proportional power sharing control (Section 8.2.4, Appendix A) models where implemented using Simulink. Parameter tables for the ATG and MTG instantiation are shown in Sections 9.1, and 9.2 of Appendix B.

6.1.1 Auxiliary PGM and Turbine

Fig. 6.1.3 depicts the response of the Auxiliary PGM and its associated turbine (abbreviated ATG) voltage, electrical speed, and power to a 1 p.u. command from steady state conditions.

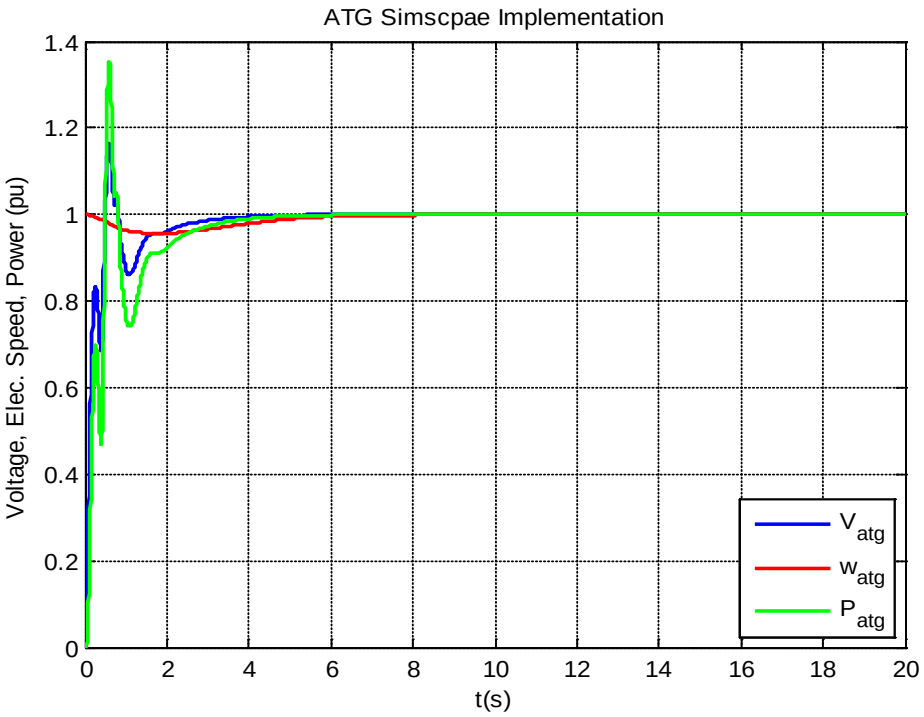

Fig. 6.1.3: ATG Response to 1pu Power Command.

Propulsion and Pulsed Loads

The notional fixed-pitch propeller model utilizes a salient permanent magnet synchronous machine, and a two-level bridge as described in Section 8.2.5 of Appendix A. The propulsion system takes a measured bus voltage as an input. The current output from the DC link is then injected on the respective buses. The propulsion system is modeled using signal flow. For simplicity and the need for shorter simulation times, the hydrodynamic characteristics in the propulsion module are represented by a speed-squared relationship between electrical speed and torque of the PM machine. The propulsion System parameters are listed in Section 9.5 of Appendix B. The pulsed load model as in Section 8.2.10 of Appendix A; parameters are listed in Section 9.7 of Appendix B. Fig. 6.1.4 depicts the Propulsion System response to a 1pu Speed Request.

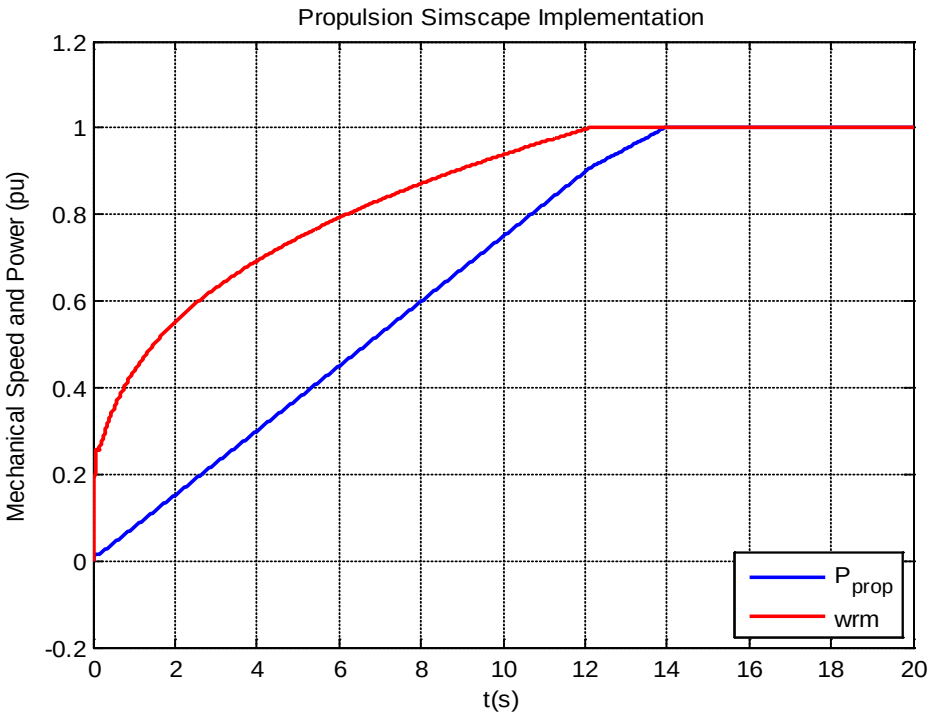

Fig. 6.1.4: Propulsion System Response to 1pu Speed Request.

6.2 Studies

6.2.1 Ship Startup

In this study, the port Main PGM and associated turbine (MTG) and Auxiliary PGM and associated turbine (ATG) are brought from zero RPM up to maximum, steady-state operating speed independently, i.e. not connected to the port DC bus, and with 0.01% base loading. Once the generators have stabilized, the port DC bus is energized at 10s. Fig. 6.2.1 shows plots of ATG and MTG per-unit power, their respective prime mover speeds, and the port DC bus voltage.

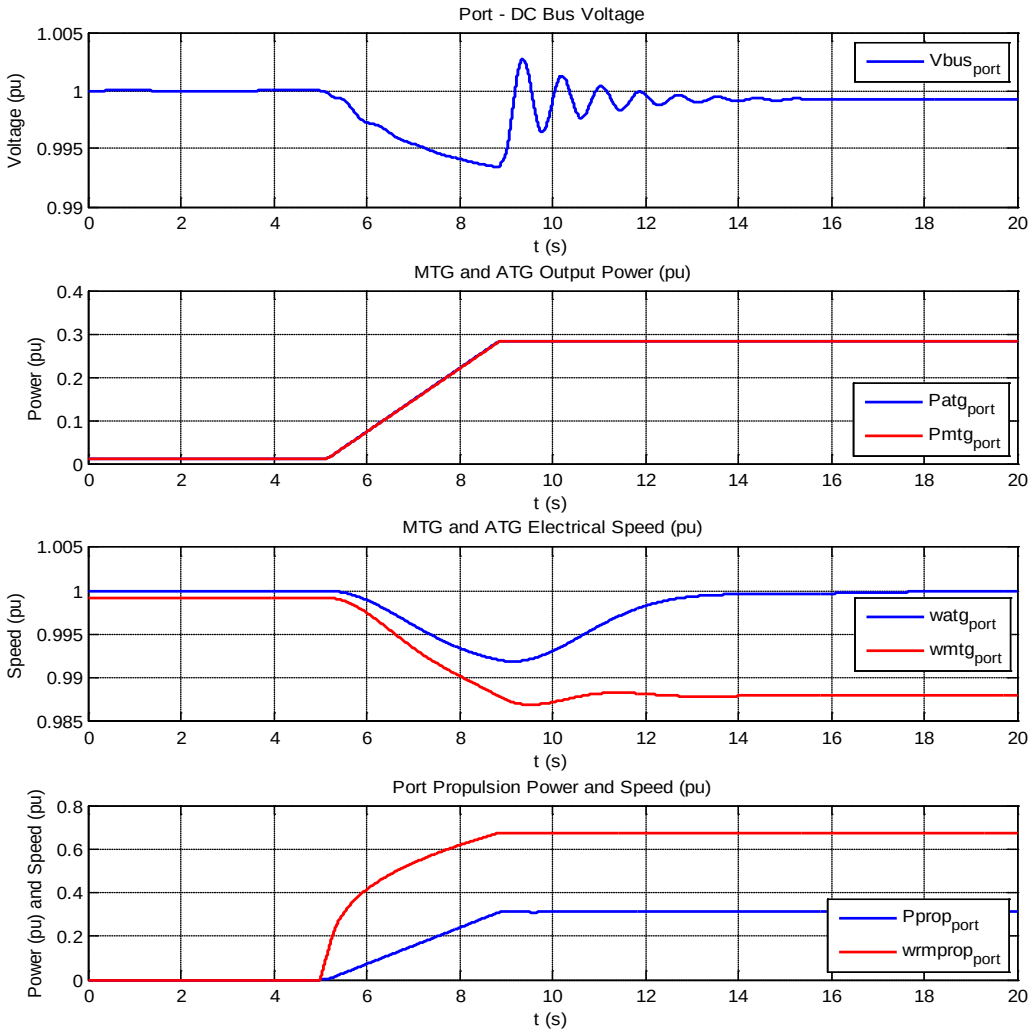

Fig. 6.2.1: Port Bus Response to 0.7pu Propulsion Speed Command.

Fig. 6.2.1 shows that with an increase in propulsion motor power and speed, the MTG and ATG's prime movers respond, the DC bus voltage sags and the GenSet load-sharing controls cause the generator to track the requested bus power. As expected, after the propulsion module reaches the requested motor speed, the controls for the prime mover bring the system back to steady-state operation, and the exciters regulate the DC bus voltage to its nominal value.

6.2.2 Pulsed Load Response

With the generators stable in steady-state operation and a supplying power to a 70% speed propulsion motor load, a notional pulse load is applied to the port DC bus at 5s. The notional pulse load ramps the level of current drawn by a constant-current load from zero amperes to a preset magnitude at a fixed ramp rate. At its peak, the load draws a constant current magnitude of 3 kA for a duration of 3.33s before quickly ramps down. The rate at which the pulse is removed is governed by a limit of 10kA/s. It is important to note that, if the pulse ramp were modeled as an ideal step pulse, Simscape would go unstable and crash due to its inability to

discretize through such an event. Fig. 6.2.2 shows the pulse load profile and Fig. 6.2.3 plots the per-unit power of the ATG and MTG, their representative prime mover speeds, the port DC bus voltage, and the port propulsion module per-unit power and mechanical speed.

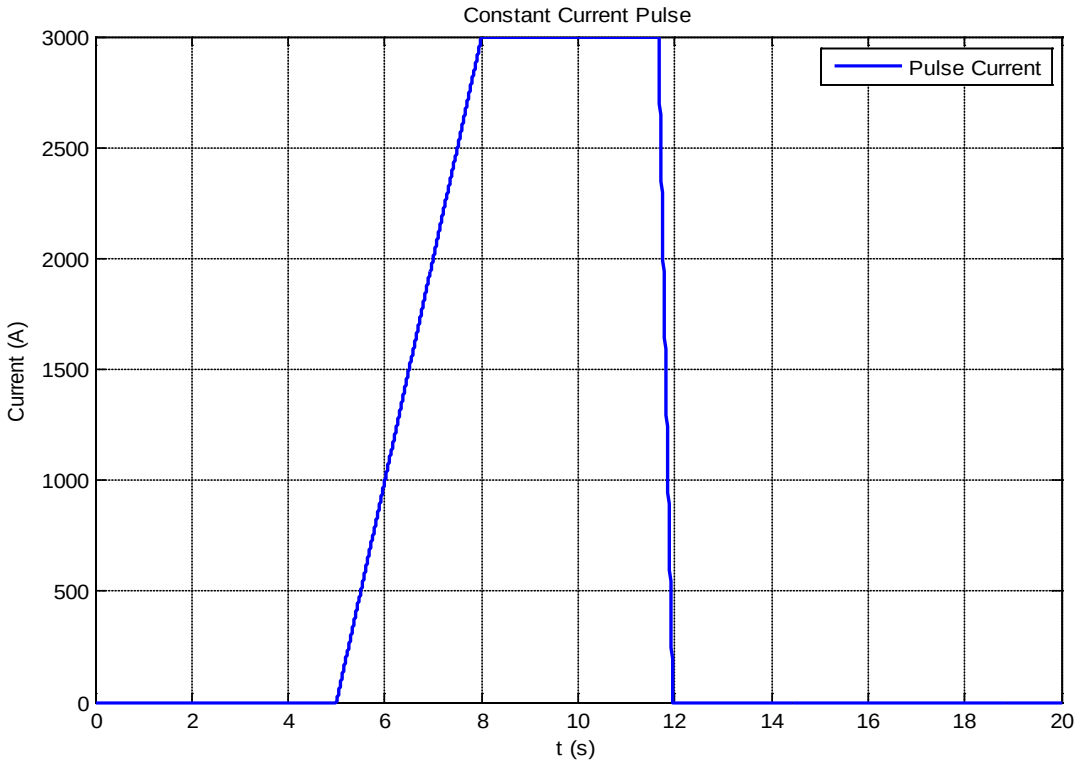

Fig. 6.2.2: Notional Pulsed Load Profile.

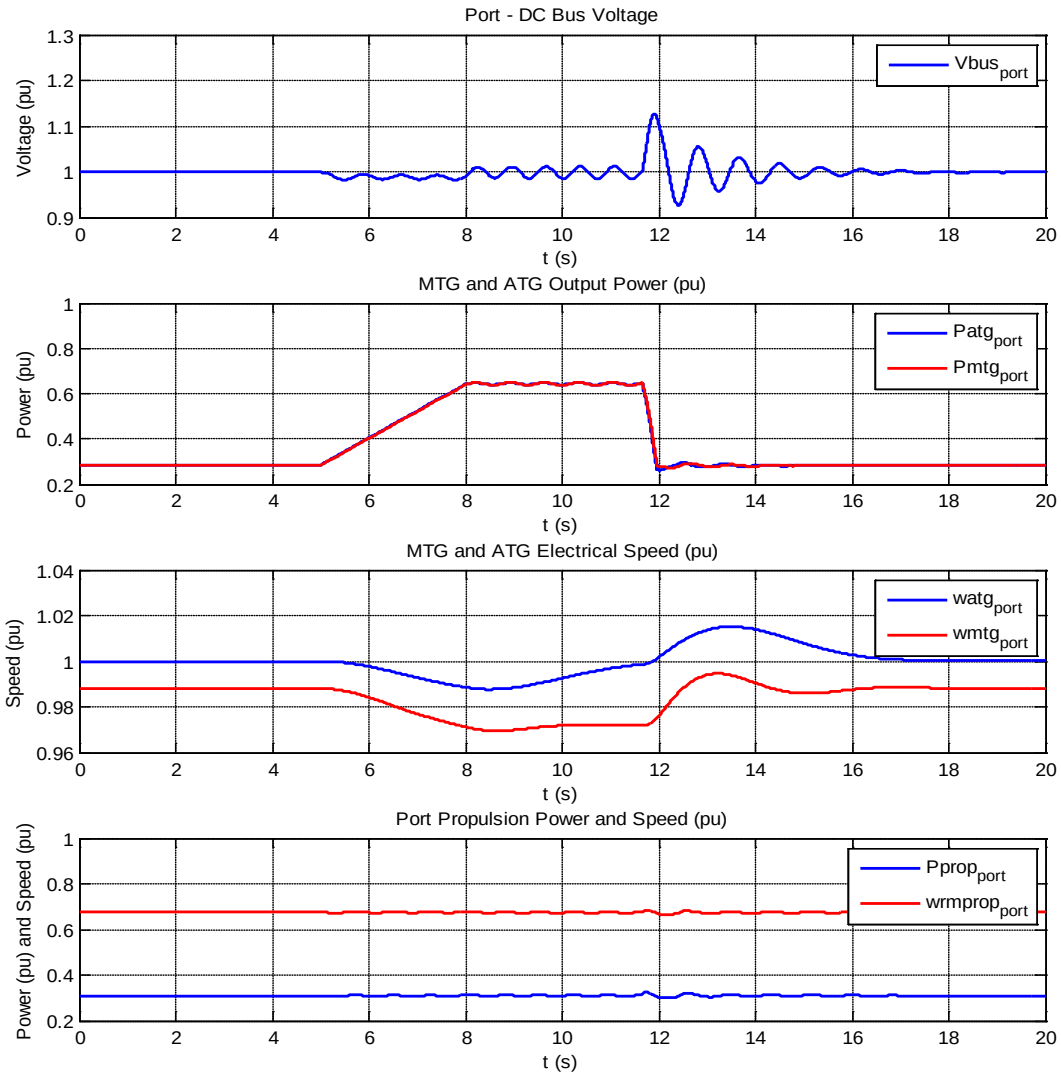

Fig. 6.2.3: Port Bus Response to Pulsed Load Application.

When the pulse is applied, the MTG and ATG's prime movers respond, the DC bus voltage starts oscillating and the exciters work to regulate the DC bus voltage to the its nominal value, while the load-sharing controls cause the delivered power from the two GenSets to track the total requested power of loads fed by the bus. A small disturbance is seen in the propulsion module's power and speed performance. This is due to the DC bus voltage working to maintain nominal voltage, since measured DC bus voltage is the only input to the propulsion module. When the pulse is removed, an overshoot occurs on the DC bus voltage and in the generators' prime mover speeds. This instability eventually dampens out, and the system performance stabilizes back to steady-state operation.

7 CONCLUSIONS

The simulation results for each study confirm that the averaged-value reduced-order models are appropriate early stage design tools. In particular, the simplified system models were shown to execute much faster than the detailed dynamic models evaluated in previous work, and were, in all cases, faster than real time.

However, the implementation of these simplified models was made difficult due to the infancy of the Simscape development environment. Currently, it is not well suited for the design and analysis of large, multi-component system simulations. In particular, the solver must be carefully tuned following the modification or addition of a component. The solver seems highly sensitive to initial conditions; and will occasionally ignore specified initial conditions. Its choice of configuration setting seems to alternate between its own and Simulink's in an unpredictable way. It is highly sensitive to tolerance levels and consistency tolerance. It includes only two implicit solvers, Simulink's ode15s and ode23s, which are the recommended type of solvers for the set of DAEs that are used in the models. Simulation errors are frequently observed in which the solver is unable to converge properly. Much time is wasted tracking down the error, as the solver generated error messages are often very vague in their descriptions.

In the course of developing the system models, some actions were found to be useful. For help in debugging code when compiling Simscape into a Simulink library, evoking

```
addpath([matlabroot '/toolbox/physmod/common/foundation/core/m']);
```

at the Matlab prompt is helpful. Because of the difficulty debugging models, set up the Simscape code to read out quantities of interest is also helpful.

As stated in the Executive Summary, however, perhaps the most important recommendation would simply be to avoid the use of Simscape altogether until further improvements from the software manufacturer are realized, and to go to a more mature product such as Simulink. In [1], it was shown that Simulink, using a user-defined solution to the interconnection equations, proved highly effective and should provide a much more robust approach.

8 APPENDIX A: COMPONENT MODELS

Model Reporting Structure

The model structure adopted in this work consists of describing the model in terms of its mathematical definition. To this end, the model reporting structure consists of a description of the model inputs, outputs, parameters, interface equations, and states before describing the mathematical model equations. The input and output definition refers to the model time domain structure and not the component functionality. The next aspect of the model reporting structure is to address the status of the validation of each model. The final area of the model reporting is the relevant references.

Inputs:
The inputs consist of the variables that are needed to either compute the time derivatives of the state variables of the model or to compute the output variables.

Outputs:
The model outputs are those variables associated with the model which are typically of direct interest to the system analyst or are typically needed by other system components. These variables are typically computed based on model state variables and/or model input variables.

Parameters:
The model parameters are those quantities in the model which are constant for a given component, such as control gains and circuit element values.
Interface Equations:
The interface equations are the algebraic equations that define the outputs of the component as a function of inputs and states that are solved by the system solver.

States:
The model states are those variables which are governed by ordinary differential equations and hence cannot change instantaneously. A major element of the every model is the computation of the time derivative of the state variables in terms of the inputs and states.

Model Equations:
The model equations are a listing of the mathematical equations within the model that are needed to obtain the time-derivatives of the state variables and output variables in terms of the input variables and state variables.

Validation:
The model validation section provides comments on the model maturity and the confidence level of the appropriate model.

References:
The reference section lists the applicable references for the presented component model.

8.1 Component Models

In this section, each of the component models needed to represent the MVAC, HFAC, and MVDC systems is represented.

8.1.1 Synchronous Reference Frame Estimator

The ac systems used herein feature multiple synchronous machines. Since the network equations must be solved in a single synchronous reference frame, the position of this reference frame must be defined. This model defines the position of the synchronous reference frame [5.1.1]. Note that this 'model' is different than most of the models in this report in that it does not represent a physical component. Rather, it defines the synchronous reference frame which is used for system analysis purposes. Nevertheless, it will be treated as if it were a component model for documentation purposes.

Inputs:

$\boldsymbol{\omega}_{rAG}$ Vector of angular electrical speeds of all active generators (rad/s)

Outputs:

ω_e The estimated angular speed of the synchronous reference frame (rad/s)

Parameters:

$\boldsymbol{P}_{bAG}$ Vector of base power rating of all active generators (W)

Interface Equations:
None

States:
None

Model Equations:

The angular speed of the synchronous reference frame is a weighted average of the rotor speeds of all of the active generators. The weighting factor used is the base power of each generator. The calculation of the synchronous reference frame speed is found using

$$\omega_e = \frac{\sum_{i \in AG} P_{bAG,i} \omega_{rAG,i}}{\sum_{i \in AG} P_{bAG,i}} \tag{8.2.1}$$

Validation:

This is not a component, but rather a definition. Hence validation is not relevant.

References:

[5.1.1] P. Krause, O. Wasynczuk, S. Sudhoff, and S. Pekarek, "Analysis of Electric Machinery and Drive Systems," 3rd Edition, New York: John Wiley and Sons/IEEE Press, 2013.

8.1.2 AC WRSM Generator Model

The ac wound rotor synchronous machine model in this work is that of a wound-field synchronous machine with two *q*-axis damper windings and one d-axis damper winding. The model is defined in [5.2.1] and outlined herein. The reduced order of the model refers to the neglecting of the fast stator dynamics in the model definition. The structure of the model is as follows.

Inputs:

$\mathbf{v}^e_{qds}$ A vector of *q*- and *d*-axis terminal voltages (v^e_{qs} and v^e_{ds}) in the synchronous ref. frame (V)

ω_{rm} The mechanical rotor speed (rad/s)

v_{fd} The referred field voltage (V)

ω_e The radian frequency of the synchronous reference frame (rad/s)

Outputs:

$\mathbf{i}^e_{qds}$ A vector of *q*- and *d*-axis currents (i^e_{qs} and i^e_{ds}) into the machine in the synchronous ref. frame (A)

T_e The electrical torque of the machine (positive for motor operation) (Nm)

i_{fd} The referred field current into the machine (A)

Parameters:

r_s The referred resistance of the stator windings (Ω)

r_{kq1} The referred resistance of the 1st *q*-axis damper winding (Ω)

r_{kq2} The referred resistance of the 2nd *q*-axis damper winding (Ω)

r_{fd} The referred resistance of the *d*-axis field winding (Ω)

r_{kd} The referred resistance of the *d*-axis damper winding (Ω)

L_{mq} The *q*-axis mutual inductance (H)

L_{md} The *d*-axis mutual inductance (H)

L_{lkq1} The referred leakage inductance of the 1st *q*-axis damper winding (H)

L_{lkq2} The referred leakage inductance of the 2nd *q*-axis damper winding (H)

L_{lfd} The referred leakage inductance of the *d*-axis field winding (H)

L_{lkd} The referred leakage inductance of the *d*-axis damper winding (H)

Interface Equations:

The interface equation for the generator may be expressed

$$\mathbf{v}^e_{qds} = \underbrace{\begin{bmatrix} Z^e_{qq} & Z^e_{qd} \\ Z^e_{dq} & Z^e_{dd} \end{bmatrix}}_{\mathbf{Z}^e_{qd}} \mathbf{i}^e_{qds} + \underbrace{\begin{bmatrix} e^{"e}_q \\ e^{"e}_d \end{bmatrix}}_{\mathbf{e}^{"e}_{qd}} \tag{8.2.2}$$

where

$$Z_{qq}^{e} = r_s + \frac{\omega_r}{2}\sin\left(2\delta\right)\left(L_d^{"} - L_q^{"}\right) \tag{8.2.3}$$

$$Z_{qd}^{e} = \omega_r\left(L_d^{"} - \left(L_d^{"} - L_q^{"}\right)\sin\left(\delta\right)^2\right) \tag{8.2.4}$$

$$Z_{dq}^{e} = \omega_r\left(-L_q^{"} - \left(L_d^{"} - L_q^{"}\right)\sin\left(\delta\right)^2\right) \tag{8.2.5}$$

$$Z_{dd}^{e} = r_s - \frac{\omega_r}{2}\sin\left(2\delta\right)\left(L_d^{"} - L_q^{"}\right) \tag{8.2.6}$$

and

$$e_q^{"e} = \omega_r\left(\sin\left(\delta\right)\lambda_q^{"} + \cos\left(\delta\right)\lambda_d^{"}\right) \tag{8.2.7}$$

$$e_d^{"e} = \omega_r\left(-\cos\left(\delta\right)\lambda_q^{"} + \sin\left(\delta\right)\lambda_d^{"}\right) \tag{8.2.8}$$

In (8.2.3) through (8.2.8), δ is the torque angle which is a state. The impedances in (8.2.3) through (8.2.6) have units of Ohms and the voltages in (8.2.7) through (8.2.8) have units of V. In (8.2.3) through (8.2.8),

$$L_q^{"} = L_{ls} + \left(\frac{1}{L_{mq}} + \frac{1}{L_{lkq1}} + \frac{1}{L_{lkq2}}\right)^{-1} \tag{8.2.9}$$

$$L_d^{"} = L_{ls} + \left(\frac{1}{L_{md}} + \frac{1}{L_{lkd}} + \frac{1}{L_{lfd}}\right)^{-1} \tag{8.2.10}$$

and

$$\lambda_q^{"} = \frac{L_{mq}\left(\frac{\lambda_{kq1}}{L_{lkq1}} + \frac{\lambda_{kq2}}{L_{lkq2}}\right)}{1 + \frac{L_{mq}}{L_{lkq1}} + \frac{L_{mq}}{L_{lkq2}}} \tag{8.2.11}$$

$$\lambda_d^{"} = \frac{L_{md}\left(\frac{\lambda_{kd}}{L_{lkd}} + \frac{\lambda_{fd}}{L_{lfd}}\right)}{1 + \frac{L_{md}}{L_{lkd}} + \frac{L_{md}}{L_{lfd}}} \tag{8.2.12}$$

Model States:

δ Torque angle (rad)

λ_{kq1} The referred Flux linkage of 1st q-axis damper winding (Vs)

λ_{kq2} The referred Flux linkage of 2nd q-axis damper winding (Vs)

λ_{fd} The referred Flux linkage of d-axis field winding (Vs)

λ_{kd} The referred Flux linkage of d-axis damper winding (Vs)

Model Equations:

The time derivative of the torque angle is calculated as

$$\frac{d\delta}{dt} = \omega_r - \omega_e \tag{8.2.13}$$

The time derivatives of the rotor states are found using the sequence

$$\mathbf{i}_{qds}^{e} = \mathbf{Z}_{qd}^{e\ -1}\left(\mathbf{v}_{qds}^{e} - \mathbf{e}_{qd}^{"e}\right) \tag{8.2.14}$$

$${}^{e}\mathbf{K}^{r} = \begin{bmatrix} \cos(\delta) & -\sin(\delta) \\ \sin(\delta) & \cos(\delta) \end{bmatrix} \tag{8.2.15}$$

$$\mathbf{i}_{qds}^{r} = {}^{e}\mathbf{K}^{r}\mathbf{i}_{qds}^{e} \tag{8.2.16}$$

$$i_{kq1} = \frac{\left(L_{lkq1}\lambda_{kq2} - L_{mq}\lambda_{kq1} + L_{mq}\lambda_{kq2} - L_{lkq1}L_{mq}i_{qs}^{r}\right)}{L_{lkq2}\left(L_{lkq1} + L_{mq}\right) + L_{lkq1}L_{mq}} \tag{8.2.17}$$

$$i_{kq2} = \frac{\left(L_{lkq2}\lambda_{kq1} - L_{mq}\lambda_{kq2} + L_{mq}\lambda_{kq1} - L_{lkq2}L_{mq}i_{qs}^{r}\right)}{L_{lkq1}\left(L_{lkq2} + L_{mq}\right) + L_{lkq2}L_{mq}} \tag{8.2.18}$$

$$i_{fd} = \frac{\left(L_{lfd}\lambda_{kd} - L_{md}\lambda_{fd} + L_{md}\lambda_{kd} - L_{lfd}L_{md}i_{ds}^{r}\right)}{L_{lkd}\left(L_{lfd} + L_{md}\right) + L_{lfd}L_{md}} \tag{8.2.19}$$

$$i_{kd} = \frac{\left(L_{lkd}\lambda_{fd} - L_{md}\lambda_{kd} + L_{md}\lambda_{fd} - L_{lkd}L_{md}i_{ds}^{r}\right)}{L_{lfd}\left(L_{lkd} + L_{md}\right) + L_{lkd}L_{md}} \tag{8.2.20}$$

whereupon the time derivatives of the rotor states are found using

$$\frac{d\lambda_{kq1}}{dt} = -r_{kq1}i_{kq1} \tag{8.2.21}$$

$$\frac{d\lambda_{kq2}}{dt} = -r_{kq2} i_{kq2} \tag{8.2.22}$$

$$\frac{d\lambda_{fd}}{dt} = v_{fd} - r_{fd} i_{fd} \tag{8.2.23}$$

$$\frac{d\lambda_{kd}}{dt} = -r_{kd} i_{kd} \tag{8.2.24}$$

The stator flux linkages are found

$$\lambda_{qs} = L_{ls} i_{qs}^r + L_{mq}\left(i_{qs}^r + i_{kq1} + i_{kq2}\right) \tag{8.2.25}$$

$$\lambda_{ds} = L_{ls} i_{ds}^r + L_{md}\left(i_{ds}^r + i_{fd} + i_{kd}\right) \tag{8.2.26}$$

and the torque is calculated using

$$T_e = \frac{3}{2}\frac{P}{2}\left(\lambda_{ds} i_{qs}^r - \lambda_{qs} i_{ds}^r\right) \tag{8.2.27}$$

Validation:

This model has been widely used in the power engineering community for decades. Note that this model does not include saturation. Further, it is a reduced order model, so initial fault response will not be correctly predicted.

References:

[5.2.1] P. Krause, O. Wasynczuk, S. Sudhoff, and S. Pekarek, "Analysis of Electric Machinery and Drive Systems," 3rd Edition, New York: John Wiley and Sons/IEEE Press, 2013.

8.1.3 AC WRSM Exciter Model

The WRSM exciter model represents a rotating, rectifier type exciter based upon IEEEAC8B [5.3.1], and is depicted in Fig. 8.2.1.

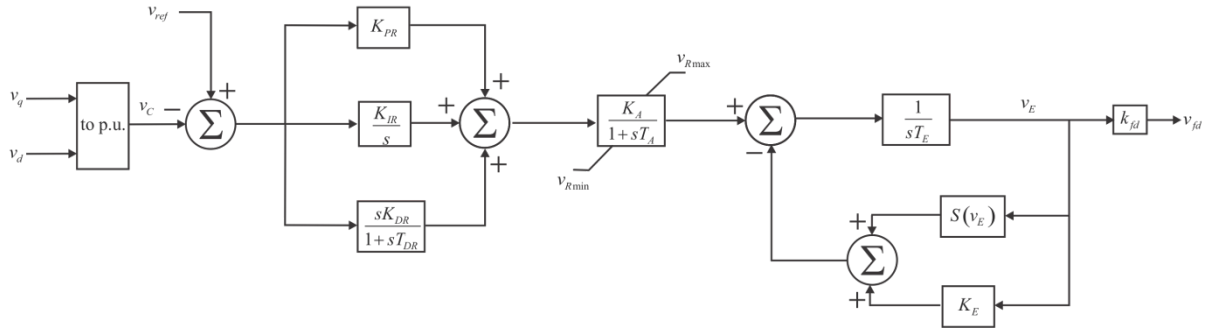

Fig. 8.2.1: Synchronous Generator Exciter Model.

The model structure is as follows.

Inputs:

v_q The *q*-axis terminal voltage (V)

v_d The *d*-axis terminal voltage (V)

Outputs:

v_{fd} The referred exciter voltage (V)

Parameters:

v_{ref} The per-unit line-line reference voltage (pu)

K_{PR} Automatic Voltage Regulator (AVR) proportional gain (pu)

K_{IR} AVR integral gain (pu)

K_{DR} AVR derivative gain (pu)

T_{DR} AVR derivative time constant (s)

K_A AVR power stage gain (pu)

T_A AVR power stage time constant (s)

$v_{R\max}$ AVR positive ceiling voltage (pu)

$v_{R\min}$ AVR negative ceiling voltage (pu)

T_E Exciter field time constant (s)

K_E Exciter field proportional gain (pu)

v_{rated} Rated line-line voltage of the synchronous machine (V)

Interface Equations:

None

Model Equations:

The model equations are not explicitly given here as they are readily formulated from Fig. 8.2.1. The per-unit line-line measured voltage is obtained from the *q*- and *d*-axis voltages using

$$v_c = \sqrt{\frac{3}{2}} \frac{\sqrt{v_q^2 + v_d^2}}{v_{rated}} \tag{8.2.28}$$

where v_{rated} is the rated rms line-neutral voltage of the synchronous machine.

The saturation block in Fig. 8.2.1 is defined as

$$S(v_E) = Ae^{Bv_E} \tag{8.2.29}$$

where A (1.0119) and B (0.875) are calculated using selected points on the voltage saturation curve, i.e. the open-circuit voltage vs. exciter field voltage curve.

The physical field voltage is obtained by scaling V_E, the per-unit value of the field voltage.

$$v_{fd} = k_{fd} V_E \tag{8.2.30}$$

where

$$k_{fd} = \frac{\sqrt{\frac{2}{3}} v_{rated} r_{fd}}{\omega_r L_{md}} \tag{8.2.31}$$

Validation:

This is a behavioral model commonly used in the power engineering community. However, it does not represent any physical excitation system.

References:

[5.3.1] L.M. Hajagos and M.J. Basler, "Changes to IEEE 421.5 recommended practice for excitation system models for power stability studies", IEEE/PES 2005 Meeting, San Francisco, CA.

8.1.4 AC Generator Real Time Synchronization Controller

The AC generator synchronization controller is used for MVAC and HFAC systems, where synchronization of paralleled generators is important. In MVAC and HFAC power distribution systems for an Electric Ship, multiple AC generators are present. Depending on the system operating mode, the overall system may break up into unconnected subsystems – for example unconnected starboard and port busses fed by separate AC generators. At some point, system reconfiguration may cause previously disconnected parts of the electrical distribution system to be interconnected. This may lead to large transients if the overall system is not properly synchronized. This section describes a supervisory controller called Real-Time Synchronization Controller (RTSC), which solves this problem by keeping all parts of the electrical distribution system synchronized at all times, even when they are not electrically connected. This requires both frequency and phase synchronization for all AC generators. The RTSC accomplishes this by augmenting the conventional frequency droop control for generators. At any given time, one interconnected subsystem is considered the reference subsystem and all other systems are target subsystems. The RTSC forces the target subsystems to be phase-synchronized with the reference subsystem. For more information on the RTSC see [5.4.1]. The discussion refers to a set of generators, each consisting of a gas turbine, as described in Section 8.2.5, connected to an AC WRSM generator, as described in Sections 8.2.1 through 8.2.3.

Inputs:

$\omega_{rm,ref}$	Reference turbine speed (pu)
P_i	Output power of *i*th generator (W)
$\mathbf{v}_{qd,\text{ref}}$	A vector of *q*- and *d*-axis terminal voltages for the reference subsystem (V)
$\mathbf{v}_{qd,\text{target}}$	A vector of *q*- and *d*-axis terminal voltages for the target subsystem (V)

Outputs:

$\Delta\omega_{speed_i}$	Offset added to the common speed reference $\omega_{rm,ref}$ for the *i*th generator by the RTSC controller (pu)

Parameters:

D_i	Droop setting of speed regulator for *i*th generator (pu)
P_{rated_i}	Rated power of *i*th generator (W)
ω_I	Cutoff frequency of Low-Pass Filter I (rad/s)
ω_{II}	Cutoff frequency of Low-Pass Filter II (rad/s)

Model Equations:

In order for interconnected generators to operate reliably in parallel and share generated power in proportion to their respective power rating, speed regulators of generators are set in droop mode, so that the generator frequency has a constant proportional relationship to the turbine's output mechanical power, as shown in Fig. 8.2.2. This is accomplished by using appropriate settings for the speed governor equation. For explanation purposes it is assumed that the relationship between output power and speed offset may be adequately approximated as

$$G(s) = \frac{W\left(Xs+1\right)}{Ys+Z} \tag{8.2.32}$$

A droop characteristic is obtained for $X=0$, $Z=1$ $W=K_D$ and the droop is given by

$$droop = \frac{1}{K_D} \tag{8.2.33}$$

Using conventional droop control, an error proportional to the power delivered by the generators will be present in the generator speed and consequently in the electrical frequency. The RTSC frequency control introduces an offset in the droop function, so that in steady state the per-unit frequency is exactly one, as shown in Fig. 8.2.3. The offset in the droop function is created by adding a variable offset dynamically to the speed regulator reference in each generator. For the *i*th generator, the speed reference $\omega_{rm,ref}$ used is the single-shaft and twin-shaft gas turbine model (Fig. 8.2.5 and Fig. 8.2.6) is modified according to

$$\omega_{rm,ref_i}(t) = \omega_{rm,ref} + \Delta\omega_{speed_i}(t) \tag{8.2.34}$$

where the frequency offset $\Delta\omega_{speed_i}(t)$ is the output of the RTSC controller for the *i*th generator. This quantity is given by

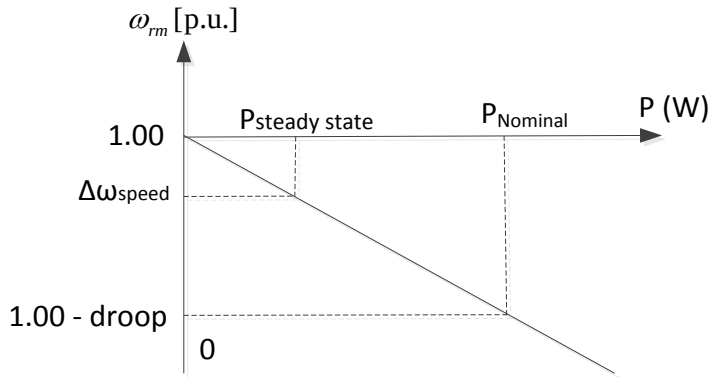

Fig. 8.2.2: Droop Function of Speed Regulator without RTSC.

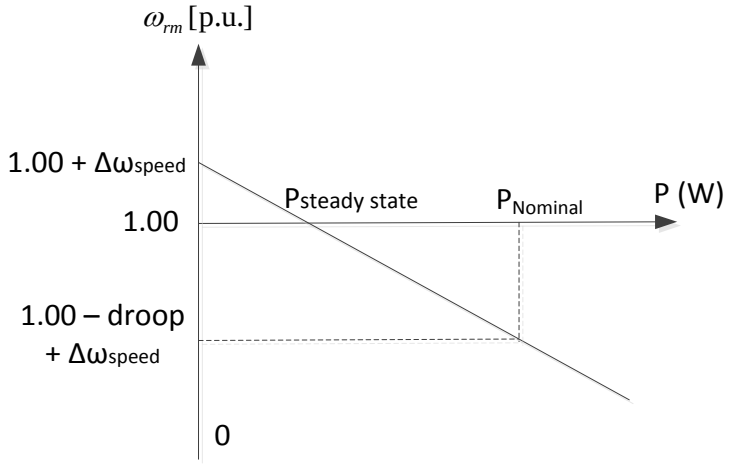

Fig. 8.2.3: Droop Function of Speed Regulator With RTSC.

$$\Delta\omega_{speed_i}(t) = D_i \cdot \frac{\sum_{j=1}^{n} K_{ij} P_j(t)}{\sum_{j=1}^{n} K_{ij} P_{rated\_j}} \tag{8.2.35}$$

where D_i is the droop setting of the speed regulator in the *i*th Generator, P_{rated_j} is the rated active power of the *j*th Generator, $P_j(t)$ is the instantaneous output power of the *j*th Turbine Engine, K_{ij} represents the relationship between the Generators *i* and *j*: $K_{ij} = 1$ if the two generators are located in the same subsystem; $K_{ij} = 0$ if the two generators are located in different subsystems; n is the total number of generators in the ESPS. The RTSC controller can determine the values of K_{ij} based on the status of the circuit breakers on the power distribution busses. The ratio on the right hand side of (8.2.35) represents the percentage loading of the generators in the subsystem containing Generator i with respect to their combined rated power. When implementing the RTSC in an ESPS, one subsystem is chosen as the reference subsystem and the other subsystems are set as the target subsystems. The criterion to choose reference subsystem is that it should have the largest power rating among all subsystems. As the control is

implemented in software, the reference subsystem can be chosen dynamically according to system operating state. The complete structure of the RTSC is shown in Fig. 8.2.4.

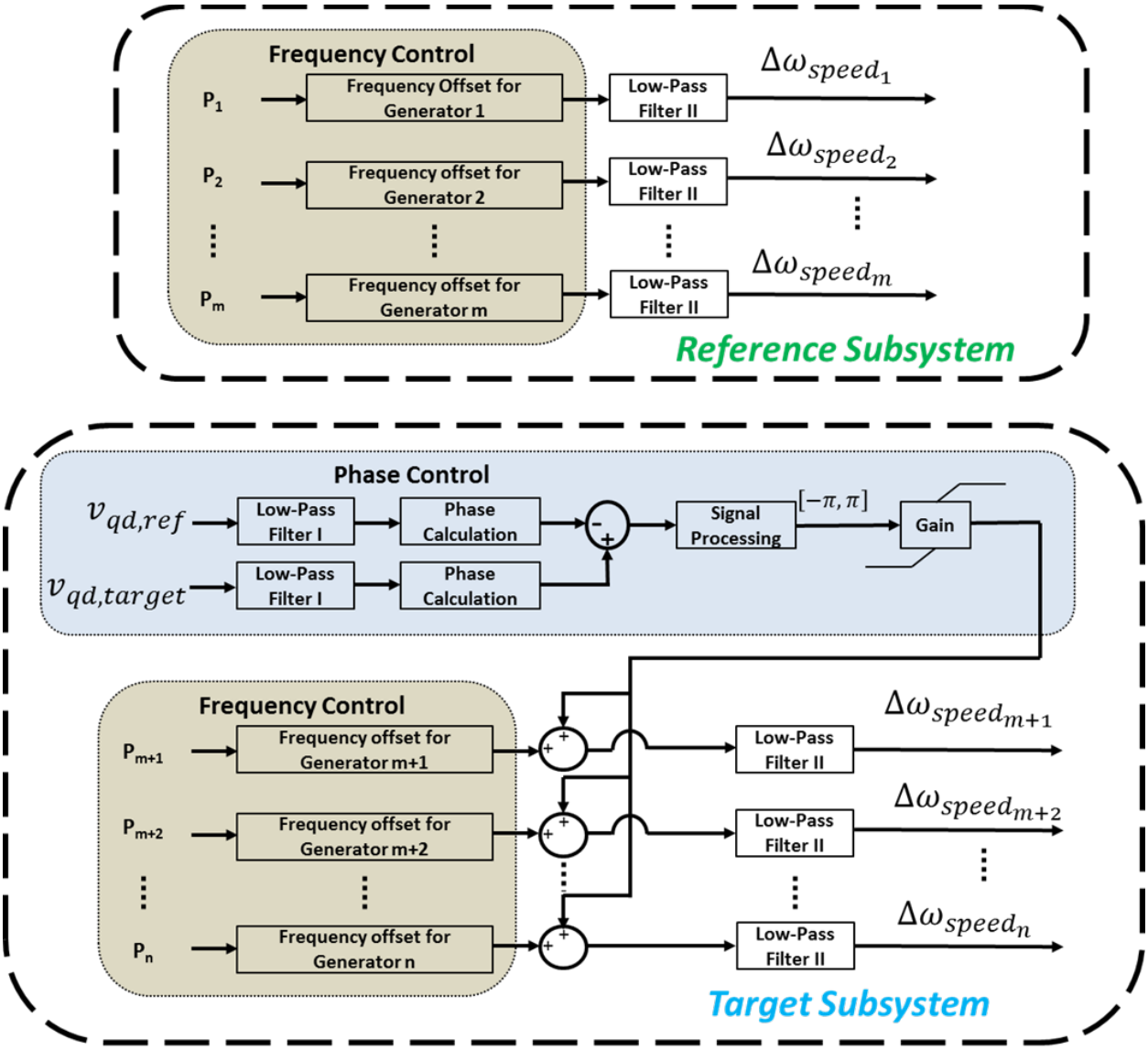

Fig. 8.2.4: Structure of the RTSC Consisting of Frequency Control and Phase Control.

In the figure only two subsystems are shown for simplicity: a reference subsystem, consisting of Generators 1 – *m*, and a target subsystem, consisting of Generators *m*+1 – *n*. Additional subsystems would be shown as separate target subsystems. Both the reference and the target subsystem have Frequency Control, but only the target subsystem has Phase Control. The goal of Phase Control is to keep voltages of the target subsystem and the reference subsystem in phase at all times.

Inside the Frequency Control part of the controller, the frequency offset block calculates for each generator the frequency offset as a function of real power generated using (8.2.35). The frequency offset goes through a first-order lowpass filter called Low-Pass Filter II, having the form

$$G_{LPF-II}(s) = \frac{1}{1+\frac{s}{\omega_{II}}} \tag{8.2.36}$$

For generators 1 – *m* belonging to the reference subsystem, this offset is added to the speed reference as in (8.2.34). For generators *m*+1 – *n* belonging to the target subsystem, the RTSC control includes also phase control.

In the Phase Control part of the controller, quantities $\mathbf{v}_{qd,\text{ref}}$ and $\mathbf{v}_{qd,\text{target}}$ are the vectors of *q*- and *d*-axis voltages for the reference and the target subsystem, respectively. Low-Pass Filter I (LPF-I) is a first-order lowpass filter used to eliminate the harmonics resulting from non-linear load current and it has the form

$$G_{LPF-I}(s) = \frac{1}{1+\frac{s}{\omega_{I}}} \tag{8.2.37}$$

For a generator having *q*-axis terminal voltage v_q and d-axis terminal voltage v_d, the Phase Calculation block calculates the absolute phase as

$$\theta_v = \text{atan}\,2\left(v_d, v_q\right) \tag{8.2.38}$$

The phase difference between the target subsystem and the reference subsystem voltages is calculated as

$$\Delta\theta_v = \theta_{v,\text{target}} - \theta_{v,\text{ref}} \tag{8.2.39}$$

and sent to the Signal Processing block, which constrains its value from [-2π, 2π] to [-π, π] using phase wrap. The phase control offset is produced by the Gain block in Fig. 8.2.4 and is added to the frequency control offset. For details on the design of Low-Pass Filter I and Low-Pass Filter II, please refer to [5.4.1].

As a result of the RTSC control of Fig. 8.2.4 in steady state all subsystems operate at the nominal frequency (p.u. frequency of one) and the voltages of all target subsystems are in phase with the reference subsystem.

Validation:

This component model is of a control, not of a physical component. Therefore, it has to be considered in terms of effectiveness, not fidelity. The reader is referred to [5.4.1] for a discussion of the effectiveness of this control.

References:

[5.4.1] E. Santi, and Y. Zhang, "Design of Real-Time Synchronization Controller in Electric Ship Power Systems," ESRDC Report, 2013.

[5.4.2] W.I. Rowen, "Simplified Mathematical Representations of Heavy-duty Gas Turbines", Journal of Engineering for Power, Vol. 105, 1983.

8.1.5 Generic Prime Mover Model

The gas turbine models used in this work consist of speed and acceleration control loops. The temperature control often associated with this type of gas turbine representation is omitted herein based upon the assumption that the critical turbine temperature will not be reached since temperature changes occur mostly during the startup of the turbine. The transfer function representing the speed governor allows for either droop or isochronous control. Setting the speed governor transfer function coefficient X=0 results in droop control where the output of the governor is directly proportional to the speed error, as can be seen in the turbine model diagrams in Fig. 8.2.5 and Fig. 8.2.6.

8.1.5.1 Single-shaft Gas Turbine

The single-shaft gas turbine model is depicted in Fig. 8.2.5.
The structure of the turbine model is as follows.

Inputs:

$\omega_{rm,ref}$ Reference speed (pu)

ω_{rm} Turbine speed (pu)

Outputs:

T_m Output torque (Nm)

Parameters:

W,X,Y,Z Speed governor parameters (pu)

$F_{l,\max}$ Maximum fuel limit (pu)

$F_{l,\min}$ Minimum fuel limit (pu)

K_{ia} Acceleration parameter (pu)

K_a Acceleration parameter (pu)

K_{fla} Fuel control parameter (pu)

K_{flb} Fuel control parameter (pu)

a,b,c Valve control parameters (pu)

τ_{fs} Fuel system time constant (s)

T_c Combustor time delay (s)

τ_{cp} Compressor time constant (s)

Interface Equations:

None

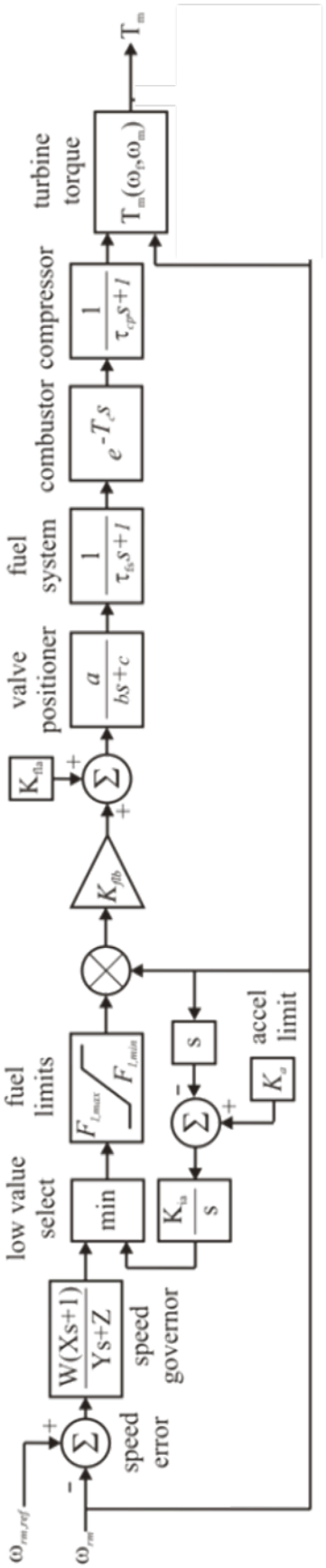

Fig. 8.2.5: Generic Single-Shaft Gas Turbine Model [5.5.1].

Model Equations:

The per unit turbine speed is found by dividing by the nominal speed of the turbine. The output torque, T_m in per-unit, is calculated using the turbine torque function [5.5.1]

$$T_{m,pu} = \frac{1}{K_{flb}}\left(\omega_f - K_{fla}\right) + \frac{1}{2}\left(1 - \omega_{rm}\right) \tag{8.2.40}$$

where ω_f is the output of the compressor block and the turbine shaft speed, ω_{rm}, is in per-unit. The actual torque in Nm is obtained using

$$T_{m,\mathrm{Nm}} = k_t T_{m,pu} \tag{8.2.41}$$

where

$$k_t = \frac{P_{\mathbf{nominal}}}{\omega_{\mathbf{nominal}}} \tag{8.2.42}$$

This gas turbine model and the overall parameters of the model can be different for gas turbines built by different manufacturers; however, the general model structure is an adequate representation for describing the dynamic behavior of a single-shaft gas turbine.

Validation:

The validity of this model is discussed in [5.5.1].

References:

[5.5.1] W.I. Rowen, "Simplified mathematical representations of heavy-duty gas turbines", Journal of Engineering for Power, Vol. 105, 1983.

8.1.5.2 Twin-shaft Gas Turbine

The model for the twin-shaft gas turbine is similar to the single-shaft gas turbine but with an additional control loop for the engine speed [5.5.2] and is depicted in Fig. 8.2.6.

Inputs:

$\omega_{rm,ref}$ Reference turbine speed (pu)

ω_{rm} Turbine speed (pu)

$\omega_{g,ref}$ Reference engine speed (pu)

ω_g Engine speed (pu)

Outputs:

T_m Output torque (Nm)

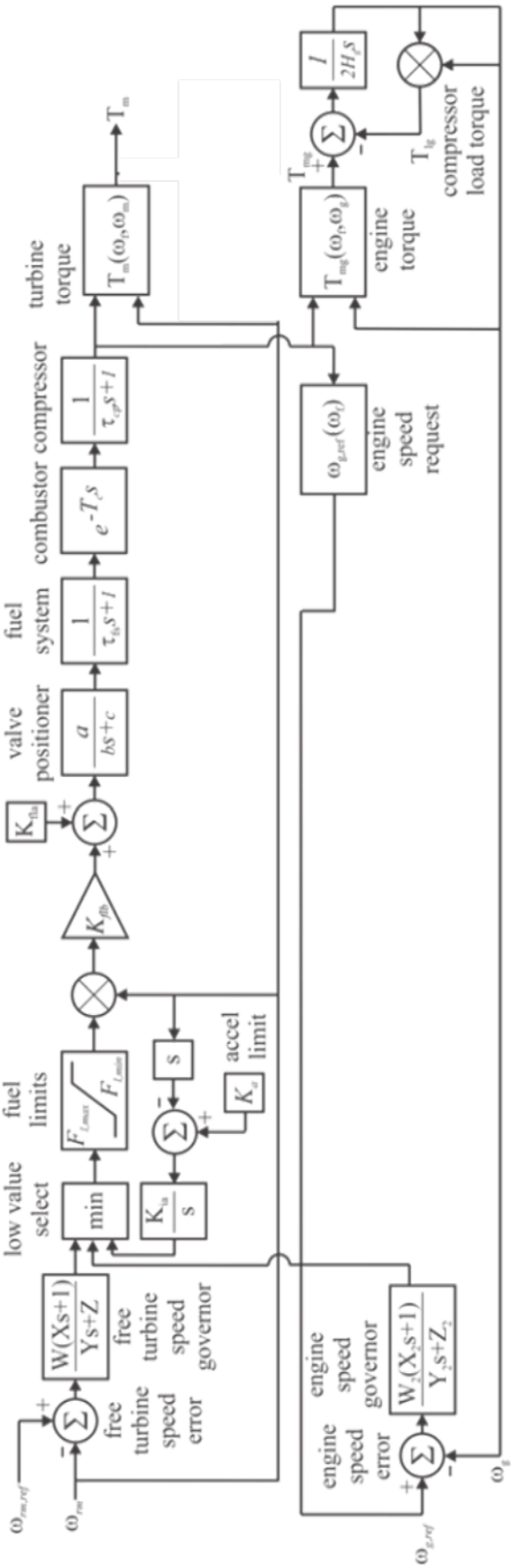

Fig. 8.2.6: Generic Twin-Shaft Gas Turbine Model.

Parameters:

W,X,Y,Z	Turbine speed governor parameters (pu)
W_2,X_2,Y_2,Z_2	Engine speed governor parameters (pu)
$F_{l,\max}$	Maximum fuel limit (pu)
$F_{l,\min}$	Minimum fuel limit (pu)
K_{ia} , K_a	Acceleration parameters (pu)
K_{fla} , K_{flb}	Fuel control parameters (pu)
a,b,c	Valve control parameters (pu)
τ_{fs}	Fuel system time constant (s)
T_c	Combustor time delay (s)
τ_{cp}	Compressor time constant (s)
H_g	Engine shaft inertial constant (pu)

Interface Equations:
None

Model Equations:

The per-unit turbine speeds are converted to per-unit by dividing by the nominal turbine speed. The per-unit torque is converted to Nm using (8.2.41) and (8.2.42).
The free turbine torque is calculated

$$T_m = \frac{1}{K_{flb}}\left(\omega_f - K_{fla}\right) + 0.6\left(1 - \omega_{rm}\right) \tag{8.2.43}$$

The engine torque is calculated

$$T_{mg} = \frac{1}{K_{flb}}\left(\omega_f - K_{fla}\right) + 3\left(1 - \omega_g\right) \tag{8.2.44}$$

The engine speed request is calculated

$$\omega_{g,ref} = p_1\omega_f + p_2 \tag{8.2.45}$$

Validation:

The validity of this model is discussed in [5.5.2].

References:

[5.5.2] L.N. Hannet, G. Jee, and B. Fardanesh, “A governor/turbine model for a twin-shaft combustion turbine,” IEEE Transactions on Power Systems, Vol. 10, no.1, pp. 133-140.

8.1.6 DC WRSM Generator Model

The dc WRSM model is depicted in Fig. 8.2.7 and consists of a WRSM connected to load commutated rectifier through an ac circuit breaker (CB). The component model is set forth in [5.6.1] and outlined herein.

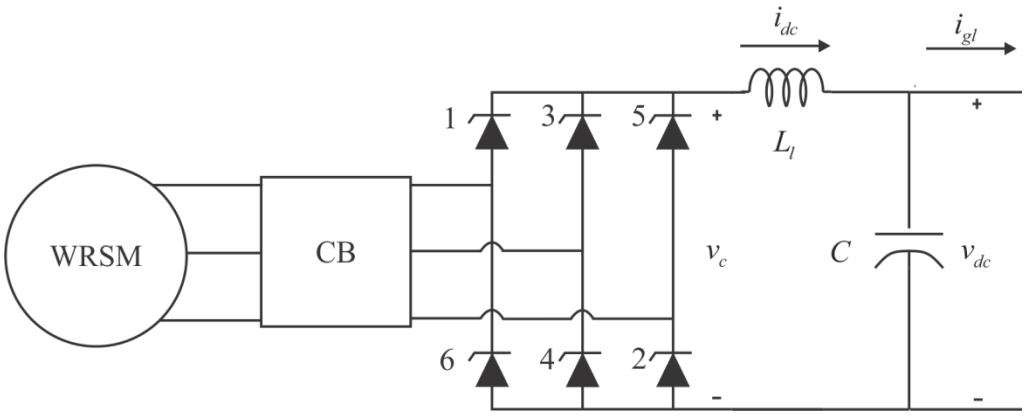

Fig. 8.2.7: Synchronous Machine Fed Load Commutated Converter.

The structure of the model is as follows:

Inputs:

i_{gl} The dc load current out of the generator (A)

ω_{rm} The mechanical rotor speed of the machine (rad/s)

v_{fd} The referred field voltage (V)

o^*_{gcb} The desired status of the generator circuit breaker

Outputs:

v_{dc} The dc output voltage of the generator (V)

T_e The electrical torque of the machine (positive for motor operation) (Nm)

i_{fd} The referred field current into the machine (A)

Parameters:

$v_{dc,\min}$ The dc bus voltage threshold (V)

i_{glf} The load current fault threshold (A)

L_l DC link inductance (H)

C DC link capacitance (F)

r_s The resistance of the stator windings (Ω)

r_{kq1} The referred resistance of the 1st *q*-axis damper winding (Ω)

r_{kq2} The referred resistance of the 2nd *q*-axis damper winding (Ω)

r_{fd} The referred resistance of the *d*-axis field winding (Ω)

r_{kd} The referred resistance of the *d*-axis damper winding (Ω)

L_{mq} The *q*-axis mutual inductance (H)

L_{md} The *d*-axis mutual inductance (H)

L_{lkq1} The referred leakage inductance of the 1st *q*-axis damper winding (H)

L_{lkq2} The referred leakage inductance of the 2nd *q*-axis damper winding (H)

L_{lfd} The referred leakage inductance of the *d*-axis field winding (H)

L_{lkd} The referred leakage inductance of the *d*-axis damper winding (H)

Interface Equations:
None

Model States:

v_{dc} The dc output voltage of the generator (V)

i_{dc} The dc current through the dc link inductor (V)

λ_{kq1} The referred Flux linkage of 1st *q*-axis damper winding (Vs)

λ_{kq2} The referred Flux linkage of 2nd *q*-axis damper winding (Vs)

λ_{fd} The referred Flux linkage of *d*-axis field winding (Vs)

λ_{kd} The referred Flux linkage of *d*-axis damper winding (Vs)

Model Equations:

The model equations for this component are broken in to six subsections. First, the subtransient model is defined, followed by the calculation of the firing and commutation angles. The third section considers the calculation of the stator currents and the fourth and fifth sections define the machine and dc link dynamics respectively. The final subsection relates to the exciter model.

8.1.6.1 Subtransient Model

It is useful to represent the reduced-order synchronous machine stator voltage equations in voltage-behind-reactance form utilizing subtransient quantities when coupled with a rectifier. For a synchronous machine with two *q*-axis damper windings and one *d*-axis damper winding, the subtransient inductances and flux linkages are expressed [5.6.1]

$$L_q'' = L_{ls} + \left(\frac{1}{L_{mq}} + \frac{1}{L_{lkq1}} + \frac{1}{L_{lkq2}} \right)^{-1} \tag{8.2.46}$$

$$L_d'' = L_{ls} + \left(\frac{1}{L_{md}} + \frac{1}{L_{lkd}} + \frac{1}{L_{lfd}} \right)^{-1} \tag{8.2.47}$$

$$\lambda_q^{"} = \frac{L_{mq}\left(\frac{\lambda_{kq1}}{L_{lkq1}} + \frac{\lambda_{kq2}}{L_{lkq2}}\right)}{1 + \frac{L_{mq}}{L_{lkq1}} + \frac{L_{mq}}{L_{lkq2}}} \tag{8.2.48}$$

$$\lambda_d^{"} = \frac{L_{md}\left(\frac{\lambda_{kd}}{L_{lkd}} + \frac{\lambda_{fd}}{L_{lfd}}\right)}{1 + \frac{L_{md}}{L_{lkd}} + \frac{L_{md}}{L_{lfd}}} \tag{8.2.49}$$

8.1.6.2 Firing Angle and Commutation Angle Calculations

The second step in modeling this system is the calculation of the firing angle and commutation angle. Assuming that that the circuit breaker is closed, the calculation of the firing angle (β) relative to rotor position is discussed in [5.6.1] and outlined herein. For uncontrolled operation the firing angle relative to rotor position is equal to $\beta_{\min}$ which is found by solving

$$\sqrt{3}\left(\lambda_q^{"}\cos\beta_{\min} + \lambda_d^{"}\sin\beta_{\min}\right) + 2\hat{i}_{dc}\left(L_q^{"} - L_d^{"}\right)\sin\left(2\beta_{\min} - \frac{\pi}{3}\right) = 0 \tag{8.2.50}$$

An intermediate variable *K* is the found by solving

$$K = \sqrt{3}\left(-\lambda_q^{"}\sin\beta + \lambda_d^{"}\cos\beta\right) + \left[\left(L_d^{"} - L_q^{"}\right)\cos\left(2\beta + \frac{2\pi}{3}\right) - \frac{1}{2}\left(L_q^{"} + L_d^{"}\right)\right]\hat{i}_{dc} \tag{8.2.51}$$

Whereupon the commutation angle, μ, is found by solving

$$\begin{aligned} &K - \sqrt{3}\left[-\lambda_q^{"}\sin\left(\beta+\mu\right) + \lambda_d^{"}\cos\left(\beta+\mu\right)\right] - \\ &\left[\left(L_q^{"} - L_d^{"}\right)\cos\left(2\beta + 2\mu - \frac{2\pi}{3}\right) + \frac{1}{2}\left(L_q^{"} + L_d^{"}\right)\right]\hat{i}_{dc} = 0 \end{aligned} \tag{8.2.52}$$

In the event that the circuit breaker is open, then $\beta_{\min}$, *K*, and μ can all be set to zero as they are unused.

8.1.6.3 Calculation of Stator Currents

The next step in the modeling of the system is the calculation of the average *q* and *d* axis currents. In the case that the circuit breaker is open, the *q*- and *d*-axis currents are set to zero. If the circuit breaker is closed, they are calculated using the following procedure.

The average values of the *q* and *d* axis currents are broken into commutation and conduction components. First, the conduction components are obtained using

$$\hat{i}_{qs,cond} = \frac{2\sqrt{3}}{\pi}\hat{i}_{dc}\left[\cos\left(\beta+\frac{2\pi}{3}\right)-\cos\left(\beta+\mu+\frac{\pi}{3}\right)\right] \tag{8.2.53}$$

$$\hat{i}_{ds,cond} = \frac{2\sqrt{3}}{\pi}\hat{i}_{dc}\left[\sin\left(\beta+\frac{2\pi}{3}\right)-\sin\left(\beta+\mu+\frac{\pi}{3}\right)\right] \tag{8.2.54}$$

During the interval following the firing of valve 3, the *a*-phase current is given by

$$\begin{aligned}\mathrm{i}_{\mathrm{as}}\left(\tilde{\theta}_r\right) = &\frac{K+\sqrt{3}\left(\lambda_q^{"}\sin\left(\tilde{\theta}_r+\beta\right)-\lambda_d^{"}\cos\left(\tilde{\theta}_r+\beta\right)\right)}{\left(L_q^{"}+L_d^{"}\right)-\left(L_q^{"}-L_d^{"}\right)\cos\left(2\tilde{\theta}_r+2\beta\right)} \\ &-\frac{\left[\left(L_q^{"}-L_d^{"}\right)\cos\left(2\tilde{\theta}_r+2\beta-\frac{2\pi}{3}\right)+\frac{1}{2}\left(L_q^{"}+L_d^{"}\right)\right]\hat{i}_{dc}}{\left(L_q^{"}+L_d^{"}\right)-\left(L_q^{"}-L_d^{"}\right)\cos\left(2\tilde{\theta}_r+2\beta\right)}\end{aligned} \tag{8.2.55}$$

where $\tilde{\theta}_r$ is the electrical rotor position offset such that valve 3 fires when $\tilde{\theta}_r$ = 0. The *q* and *d* axis currents can be expressed in terms of the *a*-phase current as

$$\mathrm{i}_{\mathrm{qs}}\left(\tilde{\theta}_r\right) = \frac{2\sqrt{3}}{3}\left[-\mathrm{i}_{\mathrm{as}}\left(\tilde{\theta}_r\right)\sin\left(\tilde{\theta}_r+\beta\right)-\hat{i}_{dc}\sin\left(\tilde{\theta}_r+\beta+\frac{\pi}{3}\right)\right] \tag{8.2.56}$$

$$\mathrm{i}_{\mathrm{ds}}\left(\tilde{\theta}_r\right) = \frac{2\sqrt{3}}{3}\left[\mathrm{i}_{\mathrm{as}}\left(\tilde{\theta}_r\right)\cos\left(\tilde{\theta}_r+\beta\right)+\hat{i}_{dc}\cos\left(\tilde{\theta}_r+\beta+\frac{\pi}{3}\right)\right] \tag{8.2.57}$$

Therefore, the commutation component of the average *q* and *d* axis currents is given by

$$\hat{i}_{qs,com} = \frac{\mu}{4\pi}\left[\mathrm{i}_{\mathrm{qs}}\left(0\right)+4\mathrm{i}_{\mathrm{qs}}\left(\frac{\mu}{4}\right)+2\mathrm{i}_{\mathrm{qs}}\left(\frac{\mu}{2}\right)+4\mathrm{i}_{\mathrm{qs}}\left(\frac{3\mu}{4}\right)+\mathrm{i}_{\mathrm{qs}}\left(\mu\right)\right] \tag{8.2.58}$$

$$\hat{i}_{ds,com} = \frac{\mu}{4\pi}\left[\mathrm{i}_{\mathrm{ds}}\left(0\right)+4\mathrm{i}_{\mathrm{ds}}\left(\frac{\mu}{4}\right)+2\mathrm{i}_{\mathrm{ds}}\left(\frac{\mu}{2}\right)+4\mathrm{i}_{\mathrm{ds}}\left(\frac{3\mu}{4}\right)+\mathrm{i}_{\mathrm{ds}}\left(\mu\right)\right] \tag{8.2.59}$$

and the average *q* and *d* axis currents are found using

$$\hat{i}_{qs} = \hat{i}_{qs,cond}+\hat{i}_{qs,com} \tag{8.2.60}$$

$$\hat{i}_{ds} = \hat{i}_{ds,cond}+\hat{i}_{ds,com} \tag{8.2.61}$$

8.1.6.4 Machine Dynamics

The next step is to calculate the flux linkages, the derivative of flux linkages, and the electrical torque of the machine which can be written as

$$\lambda_{qs} = L_q^{"} \hat{i}_{qs} + \lambda_q^{"} \tag{8.2.62}$$

$$\lambda_{ds} = L_d^{"} \hat{i}_{ds} + \lambda_d^{"} \tag{8.2.63}$$

$$\frac{d\lambda_{kq1}}{dt} = \frac{-r_{kq1}}{L_{lkq1}} \left(\lambda_{kq1} - L_q^{"} \hat{i}_{qs} - \lambda_q^{"} + L_{ls} \hat{i}_{qs} \right) \tag{8.2.64}$$

$$\frac{d\lambda_{kq2}}{dt} = \frac{-r_{kq2}}{L_{lkq2}} \left(\lambda_{kq2} - L_q^{"} \hat{i}_{qs} - \lambda_q^{"} + L_{ls} \hat{i}_{qs} \right) \tag{8.2.65}$$

$$\frac{d\lambda_{kd}}{dt} = \frac{-r_{kd}}{L_{lkd}} \left(\lambda_{kd} - L_d^{"} \hat{i}_{ds} - \lambda_d^{"} + L_{ls} \hat{i}_{ds} \right) \tag{8.2.66}$$

$$\frac{d\lambda_{fd}}{dt} = v_{fd} - \frac{r_{fd}}{L_{lfd}} \left(\lambda_{fd} - L_d^{"} \hat{i}_{ds} - \lambda_d^{"} + L_{ls} \hat{i}_{ds} \right) \tag{8.2.67}$$

The electrical torque of the synchronous machine (positive for generator operation) is found using

$$T_e = -\frac{3}{2}\frac{P}{2} \left(\lambda_{ds} \hat{i}_{qs} - \lambda_{qs} \hat{i}_{ds} \right) \tag{8.2.68}$$

The mechanical dynamics of the synchronous machine generator are expressed

$$J_g \frac{d\omega_{rm}}{dt} = T_{pm} - T_e \tag{8.2.69}$$

where T_{pm} is the prime mover torque.

8.1.6.5 DC Link Dynamics

The dc link dynamics are computed by first computing the commutating inductance L_c is given by

$$L_c(\beta) = \frac{1}{2}\left(L_q^{"} + L_d^{"} \right) + \left(L_d^{"} - L_q^{"} \right) \sin\left(2\beta + \frac{\pi}{6} \right) \tag{8.2.70}$$

and the transient commutating inductance expressed

$$L_t(\beta) = L_q^{"} + L_d^{"} + \left(L_d^{"} - L_q^{"} \right) \sin\left(2\beta - \frac{\pi}{6} \right) \tag{8.2.71}$$

The magnitude of the subtransient voltage is given by

$$E = |\omega_r| \sqrt{\left(\lambda_q^{"}\right)^2 + \left(\lambda_d^{"}\right)^2} \tag{8.2.72}$$

which is obtained from

$$e_q^{"} = \omega_r \lambda_d^{"} \tag{8.2.73}$$

$$e_d^{"} = -\omega_r \lambda_q^{"} \tag{8.2.74}$$

Next, the phase angle of the subtransient voltage is calculated as

$$\phi = \text{angle}\left(\lambda_d^{"} - j\lambda_q^{"}\right) \tag{8.2.75}$$

which is obtained from (8.2.73), (8.2.74), and

$$\phi = \text{angle}\left(e_q^{"} + je_d^{"}\right) \tag{8.2.76}$$

whereupon the firing angle relative to the voltage is given by

$$\alpha = \beta - \phi \tag{8.2.77}$$

The time derivative of the average dc current is expressed as

$$\frac{d\hat{i}_{dc}}{dt} = \begin{cases} \dfrac{\frac{3\sqrt{3}}{\pi} E\cos\alpha - \hat{v}_{dc} - \left(r_l + \frac{3}{\pi}\omega_r L_c(\beta)\right)\hat{i}_{dc}}{L_l + L_t(\beta)} & c_g \cdot \left((\hat{i}_{dc} > 0) + \left(\frac{3\sqrt{3}}{\pi} E\cos\alpha > \hat{v}_{dc}\right)\right) \\ -k\hat{i}_{dc} & \overline{c_g \cdot \left((\hat{i}_{dc} > 0) + \left(\frac{3\sqrt{3}}{\pi} E\cos\alpha > \hat{v}_{dc}\right)\right)} \\ \dfrac{-\hat{v}_{dc} - r_l\hat{i}_{dc}}{L_l} & \overline{c}_g \cdot (\hat{i}_{dc} > 0) \\ -k\hat{i}_{dc} & \overline{c}_g \cdot (\hat{i}_{dc} \le 0) \end{cases} \tag{8.2.78}$$

In (8.2.78), k is an artificial constant used to drive the dc link current to zero.

The time derivative of the capacitor voltage is found as

$$\frac{d\hat{v}_{dc}}{dt} = \begin{cases} \dfrac{\hat{i}_{dc} - i_{gl}}{C} & (\hat{v}_{dc} > 0) + (\hat{i}_{dc} > i_{gl}) \\ -k\hat{v}_{dc} & \overline{(\hat{v}_{dc} > 0) + (\hat{i}_{dc} > i_{gl})} \end{cases} \tag{8.2.79}$$

The terms to the right in (8.2.78) and (8.2.79) are Boolean, and that the over-bar denotes logical complement.

8.1.6.6 Generator Circuit Breaker Control

The circuit breaker control is depicted in Fig. 8.2.8. The inputs to the control are the desired status of the breaker, o^*_{gcb} , the dc voltage, v_{dc} , the minimum dc voltage, $v_{dc,\min}$, the load current, i_{gl} , and the fault current threshold, i_{glf} . The output of the control is the circuit breaker status, c_g .

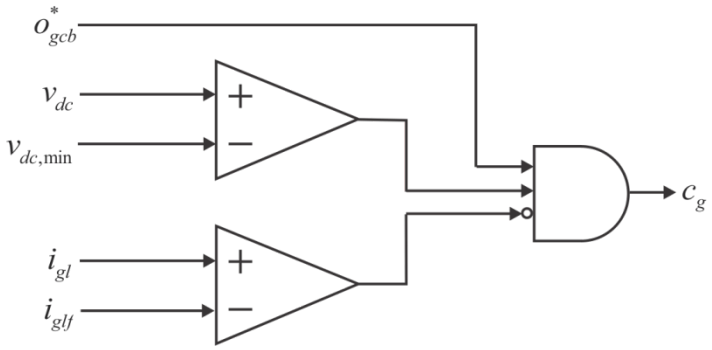

Fig. 8.2.8: DC Generator Circuit Breaker Control.

When a fault occurs the load current will rise above the fault current threshold causing the breaker status to go low and the breaker to open. In order to check if the fault is cleared, a low voltage supply is placed on the dc bus to trickle charge it. If there is no fault, then the dc voltage will rise above the minimum dc voltage value and, assuming the desired circuit breaker state is high, the circuit breaker will close. If the fault is still in place, the dc voltage will not rise and the circuit breaker will remain open.

Validation:

The generator rectifier model has been used extensively. It may be rigorously derived, and has been shown to accurately predict experimentally observed results. The main limitation is for very heavily loaded cases in which the thyristor conduction pattern changes.

References:

[5.6.1] Sudhoff, S.D.; Corzine, K. A.; Hegner, H.J.; Delisle, D.E., "Transient and dynamic average-value modeling of synchronous machine fed load-commutated converters," *Energy Conversion, IEEE Transactions on* , vol.11, no.3, pp.508,514, Sep 1996.

8.1.7 DC WRSM Exciter Model

The dc generator exciter is based upon IEEE AC8B [5.7.1] and is depicted in Fig. 8.2.9.

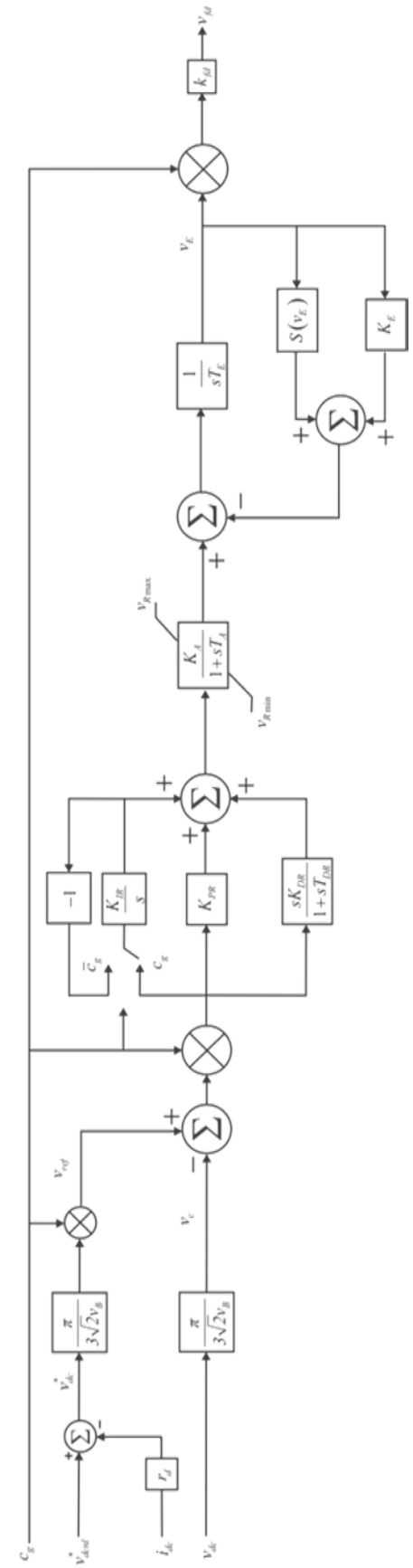

Fig. 8.2.9: DC Generator Exciter.

Inputs:

c_g Circuit breaker status (1 is closed, 0 is open)

i_{dc} The measured dc current (A)

v_{dc} The measured dc voltage (V)

Outputs:

v_{fd} The referred exciter voltage (V)

Parameters:

v_{dcnl}^* The no load dc voltage (V)

v_{rated} The rated dc link voltage (V)

v_B Base voltage (V)

r_d Droop resistance (Ω)

K_{PR} Automatic Voltage Regulator (AVR) proportional gain (pu)

K_{IR} AVR integral gain (pu)

K_{DR} AVR derivative gain (pu)

T_{DR} AVR derivative time constant (s)

K_A AVR power stage gain (pu)

T_A AVR power stage time constant (s)

$v_{R\max}$ AVR positive ceiling voltage (pu)

$v_{R\min}$ AVR negative ceiling voltage (pu)

T_E Exciter field time constant (s)

K_E Exciter field proportional gain (pu)

Interface Equations:

None

Model Equations:

The droop resistance is found

$$r_d = \frac{v_{dcnl}^* - v_{dcfl}^*}{i_{dcfl}} \tag{8.2.80}$$

in which v_{dcfl}^* is the desired full load voltage and i_{dcfl} is the full load dc current.

The reference voltage for the exciter, v_{ref}, is determined by converting the desired dc voltage, v_{dc}^*, to the rms line-line representation needed by the exciter. The desired dc voltage is obtained as the difference of the desired no load dc voltage and the dc current multiplied by r_d. The reference voltage is modulated by the circuit breaker status, c_g. The measured bus voltage for the exciter, v_C, is obtained as the rms line-line representation of the measured dc voltage.

The model equations for the exciter are not explicitly given here as they are readily formulated from Fig. 8.2.9.

The saturation block is defined as

$$S(v_E) = 1.0119e^{0.875v_E} \tag{8.2.81}$$

The integral term of the PI control is switched between either the error between the measured and reference voltages, or the negative of the integral term based upon the status of the circuit breaker. This winds down the integral term of the control if the circuit breaker opens due to a fault.

The referred field voltage is obtained from the per-unit field voltage v_E using

$$v_{fd} = c_g k_{fd} v_E \tag{8.2.82}$$

where k_{fd} is defined by (8.2.31).

Validation:

This is a behavioral model commonly used in the power engineering community to represent a rotating-rectifier type exciter and is discussed in [5.7.1].

References:

[5.7.1] L.M. Hajagos and M.J. Basler, "Changes to IEEE 421.5 recommended practice for excitation system models for power stability studies", IEEE/PES 2005 Meeting, San Francisco, CA.

8.1.8 Propulsion Drive Model

The propulsion drive consists of a dc link, an inverter, and a permanent magnet synchronous machine as depicted in Fig. 8.2.10. In ac applications, this drive modeled is used in conjunction with the rectifier model presented in the following section.

The dc link consists of a capacitor C_{dc} and a braking resistor r_{rb}. The inverter is an active current controlled inverter driving a slightly salient permanent magnet synchronous machine.

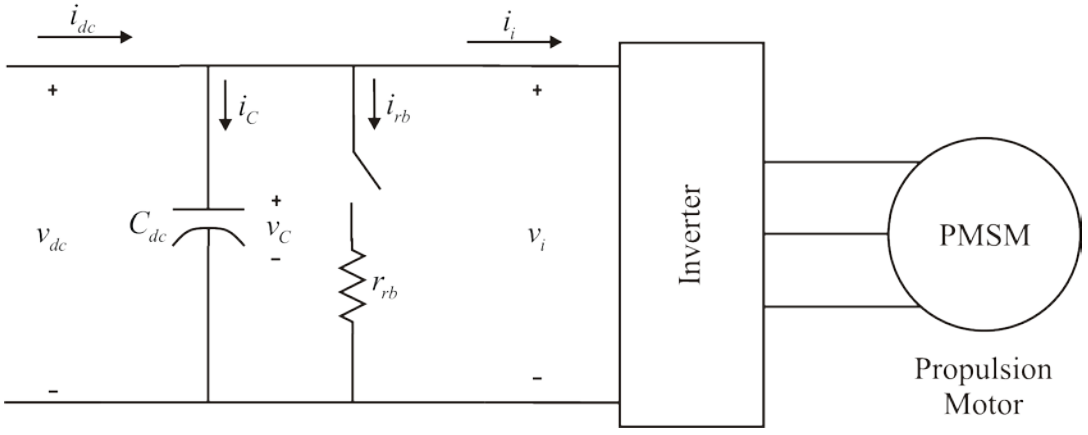

Fig. 8.2.10: DC Propulsion Drive

The model structure is as follows

Inputs:

v_{dc} The dc bus voltage (V)

ω_{rm} The mechanical speed of the propulsion drive (rad/s)

o_{pd}^{*} The desired operational status of the drive

ω_{rm}^{*} The desired mechanical speed of the propulsion drive (rad/s)

$T_{L,\text{est}}$ The estimated load torque of the propulsion drive (Nm)

Outputs:

v_{qs} The *q*-axis voltage of the propulsion motor (V)

v_{ds} The *d*-axis voltage of the propulsion motor (V)

P_i The power drawn from the inverter (W)

i_{qs} The *q*-axis current into the propulsion motor (A)

i_{ds} The *d*-axis current into the propulsion motor (A)

T_e The output electrical torque of the propulsion motor (Nm)

Parameters:

P The number of poles in the PMAC

λ_m The flux linkage due to the permanent magnet (Vs)

L_q The *q*-axis inductance of the machine (H)

L_d The *d*-axis inductance of the machine (H)

r_s The stator resistance of the machine (Ω)

C_{dc} The dc link capacitance value (F)

r_{rb} The resistor brake resistance value (Ω)

K_p The speed control proportional gain $\left(\frac{\text{Nm}}{\text{rad/s}}\right)$

K_i The speed control integral gain $\left(\frac{\text{Nm}}{\text{rad}}\right)$

ω_{rmr} The rated mechanical speed of the drive (rad/s)

T_{mx} The maximum allowable commanded torque (Nm)

T_{mn} The minimum allowable commanded torque (Nm)

$\dot{T}_{emxi}$ The maximum rate of change in commanded torque (Nm/s)

$\dot{T}_{emni}$ The minimum rate of change in commanded torque (Nm/s)

τ_{nsc} The non-linear stabilizing control time constant (s)

v_{fmx} The maximum non-linear stabilizing control voltage (V)

v_{fmn} The minimum non-linear stabilizing control voltage (V)

n_{nsc} The order of the non-linear stabilizing control

Δv_i An allowed margin for error in the inverter voltage (V)

Interface Equations:

States:

v_c The dc link capacitor voltage (V)

Model Equations:

8.1.8.1 PMAC Motor and Drive Model

The propulsion motor is a slightly salient PMSM. The model for this machine is defined in [5.8.1] and outlined herein. First, the electrical speed of the machine is

$$\omega_r = \frac{P}{2}\omega_{rm} \tag{8.2.83}$$

where ω_{rm} is the mechanical speed of the machine, and P is the number of poles. The machine model is defined using a *qd0* framework in the rotor reference frame. The reduced-order voltage equations in the rotor reference frame are presented in *qd* form as

$$v_{qs}^r = r_s i_{qs}^r + \omega_r L_d i_{ds}^r + \omega_r \lambda_m \tag{8.2.84}$$

$$v_{ds}^r = r_s i_{ds}^r - \omega_r L_q i_{qs}^r \tag{8.2.85}$$

where r_s is the stator winding resistance, L_q and L_d are the *q* and *d* axis inductances, λ_m is the flux linkage due to the permanent magnet, and ω_r is the angular velocity of the rotor. The inverter considered is an active current controlled inverter and so the currents obtained can be assumed to be the desired currents. Therefore the *q* and *d* axis currents are obtained using

$$i_{qs}^r = \begin{cases} \dfrac{4T_e^*}{3P\lambda_m} & o_{pd} \\ 0 & \overline{o}_{pd} \end{cases} \tag{8.2.86}$$

$$i_{ds}^r = \begin{cases} 0 & \overline{o}_{pd} \text{ or } \left(v_{aiv} \geq v_{riv}\right) \\ \dfrac{-b_{fw} + \sqrt{b_{fw}^2 - 4a_{fw}c_{fw}}}{2a_{fw}} & o_{pd} \text{ and } \left(v_{aiv} < v_{riv}\right) \end{cases} \tag{8.2.87}$$

where o_{pd} is the operational status of the drive, v_{aiv} is the available inverter voltage, v_{riv} is the required inverter voltage, and a_{fw}, b_{fw}, and c_{fw} are defined as

$$a_{fw} = r_s^2 + \omega_r^2 L_d^2 \tag{8.2.88}$$

$$b_{fw} = 2(r_s i_{qs}^r + \omega_r \lambda_m)\omega_r L_d - 2 r_s i_{qs}^r L_q \omega_r \tag{8.2.89}$$

$$c_{fw} = \frac{1}{3}(v_{ri}^2 - v_{aiv}^2) \tag{8.2.90}$$

The available inverter voltage is

$$v_{aiv} = v_i - \Delta v_i \tag{8.2.91}$$

where Δv_i represents an allowed margin. The required inverter voltage is

$$v_{riv} = \sqrt{3}\sqrt{(r_s i_{qs}^r + \omega_r \lambda_m)^2 + (\omega_r L_q i_{qs}^r)^2} \tag{8.2.92}$$

The inverter power is then found using

$$P_i = \frac{3}{2}\left(v_{qs}^r i_{qs}^r + v_{ds}^r i_{ds}^r\right) \tag{8.2.93}$$

and the inverter current is

$$i_i = \begin{cases} \dfrac{P_i}{v_i} & o_{pd} \\ 0 & \overline{o}_{pd} \end{cases} \tag{8.2.94}$$

8.1.8.2 DC Link and Resistor Brake

The dc link in the propulsion drive is depicted in Fig. 8.2.11. The dc link consists of a capacitor and the braking resistor.

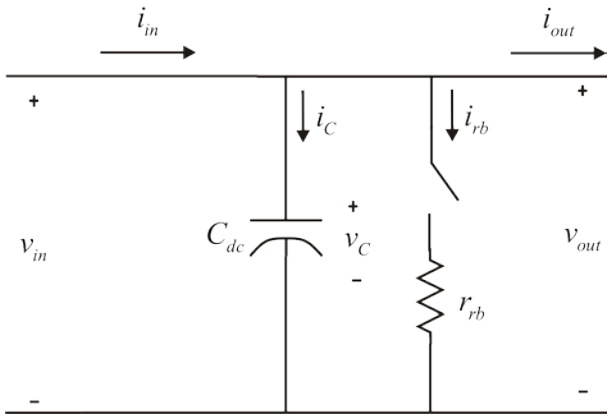

Fig. 8.2.11: DC Link.

The equations defining the dc link are

$$\frac{dv_c}{dt} = \frac{i_C}{C_{dc}} \tag{8.2.95}$$

$$i_{rb} = \begin{cases} 0 & o_{rb} = 0 \\ \dfrac{v_{out}}{r_{rb}} & o_{rb} = 1 \end{cases} \tag{8.2.96}$$

$$i_{in} = i_C + i_{rb} + i_{out} \tag{8.2.97}$$

where o_{rb} is the operational status of the resistor brake. The control for the resistor brake is depicted in Fig. 8.2.12. The output of the control, o_{rb}, is the operational status of the resistor brake and is determined by the level of the dc voltage at the input to the dc link. The threshold voltages for the resistor brake consist of an enable threshold, v_{rbe} and a disable threshold, v_{rbd}. The enable threshold, v_{rbe} is assumed to be greater than v_{rbd}. If the dc voltage is above v_{rbe}, the threshold for the brake to turn on, then o_{rb} is high, if the voltage goes below v_{rbd}, the voltage level to disable the resistive brake, o_{rb} goes low.

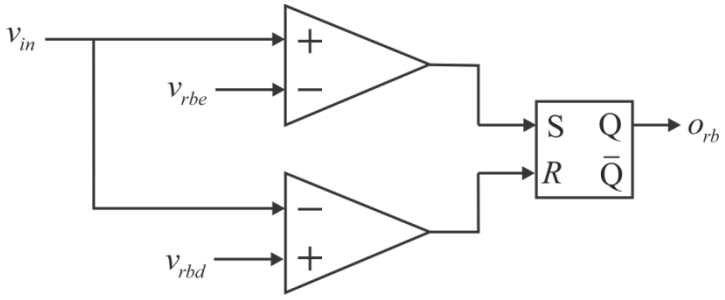

Fig. 8.2.12: Resistor Brake Control.

8.1.8.3 Propulsion Drive Control

The control for the propulsion drive is depicted in Fig. 8.2.13. The output of the control is T_e^*, the desired electrical torque for the propulsion motor. This torque value is obtained from a PI speed control followed by a slew rate limiter.

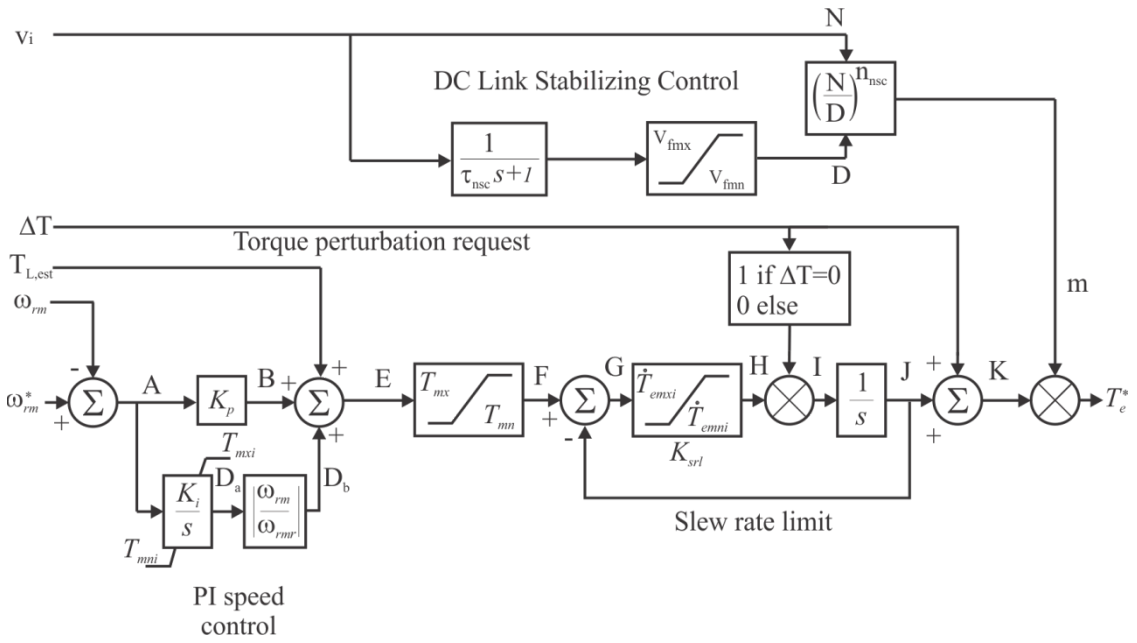

Fig. 8.2.13: Propulsion Control.

A torque perturbation request is facilitated and the dc link voltage stabilizing control is incorporated into the torque value that is subject to the operation state of the drive. The non-linear stabilizing control time constant is obtained using

$$\tau_{nsc} = 10\sqrt{\left(L_{dc} + 2L_c\right)\mathrm{C}_{dc}} \tag{8.2.98}$$

8.1.8.4 Propulsion Drive Supervisory Control

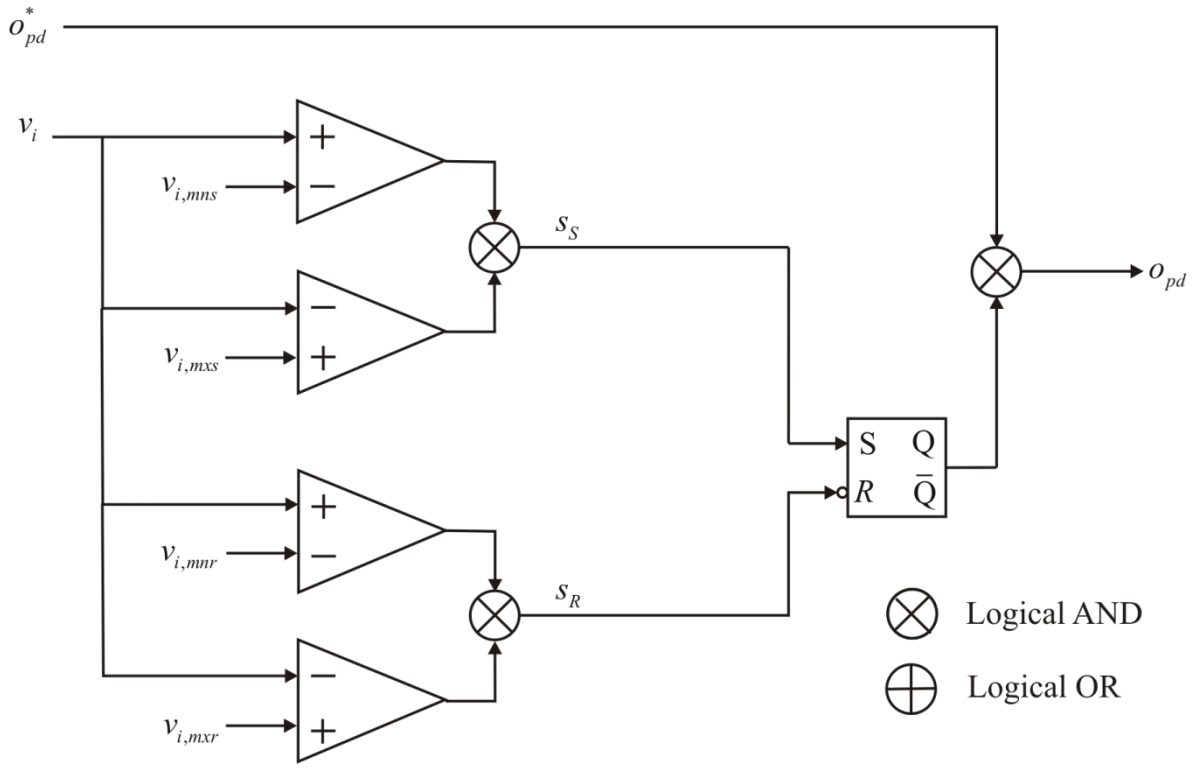

Fig. 8.2.14: DC Propulsion Supervisory Control.

The supervisory control for the propulsion drive is shown in Fig. 8.2.14. The output of the control is o_{pd}, the operational state of the drive. The inputs are o^*_{pd}, startup, and v_i, the desired operational state of the drive, whether the drive is in startup mode, and the dc voltage at the terminals of the inverter respectively. The operational state is determined by the inverter voltage being within startup limits during startup and within running limits during operation along with the desired operational status of the drive.

Validation:

With respect to the propulsion drive model, the propulsion motor and inverter module models are simple, well-established, and observed to be reasonably accurate. The control models again represent an intended control, and so must be judged in terms of effectiveness rather than in terms of accuracy.

References:

[5.8.1] P. Krause, O. Wasynczuk, S. Sudhoff, and S. Pekarek, "Analysis of Electric Machinery and Drive Systems," 3rd Edition, New York: John Wiley and Sons/IEEE Press, 2013.

8.1.9 Propulsion Drive Rectifier

For ac applications, in addition to the components listed in the previous section, the propulsion drive also includes a rectifier model. The propulsion drive rectifier model is depicted

in Fig. 8.2.15. Like the propulsion machine model, the transformer rectifier model utilizes the *qd* framework and is presented in detail in [5.9.1].

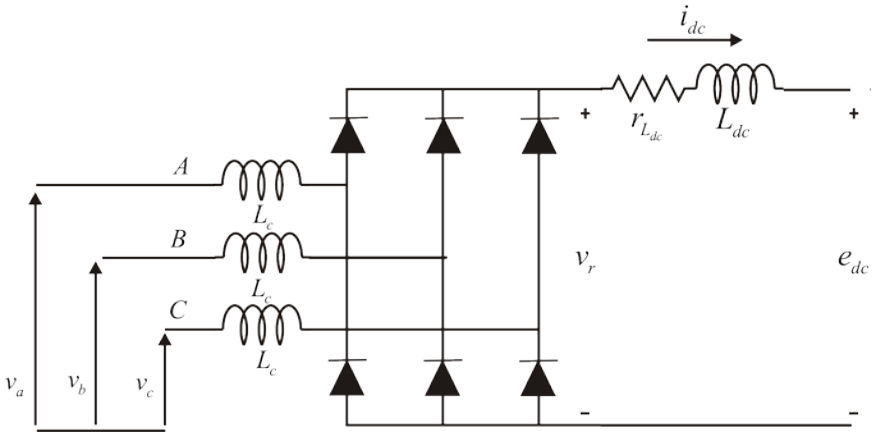

Fig. 8.2.15: Propulsion Drive Transformer Rectifier.

The structure of the ac propulsion load model is as follows.

Inputs:

v_q^a The *q*-axis voltage in the arbitrary reference frame (V)

v_d^a The *d*-axis voltage in the arbitrary reference frame (V)

Outputs:

i_q^a The *q*-axis current in the arbitrary reference frame (A)

i_q^a The *d*-axis current in the arbitrary reference frame (A)

Parameters:

L_c The commutating inductance of the rectifier (H)

L_{dc} The inductance of the dc link inductor (H)

r_{Ldc} The resistance of the dc link inductor (Ω)

Interface Equations:
None

States:

$\hat{i}_{dc}$ The average dc link inductor current (A)

Model Equations:

The model inputs are the *q* and *d* axis voltages of the ac input in the arbitrary reference frame and the outputs are the *q* and *d* axis currents in that same reference frame. To facilitate this, the frame-to-frame transformation

$$\mathbf{f}_{qd}^{g} = {}^{a}\mathbf{K}^{g}\mathbf{f}_{qd}^{a} \tag{8.2.99}$$

is used where

$$ {}^{a}\mathbf{K}^{g} = \begin{bmatrix} \cos\left(\theta_{ga}\right) & -\sin\left(\theta_{ga}\right) \\ \sin\left(\theta_{ga}\right) & \cos\left(\theta_{ga}\right) \end{bmatrix} $$

and where '*g*' denotes a generator reference frame wherein the *q*-axis voltage is positive and the *d*-axis voltage is zero. Applying (8.2.100) with

$$ \theta_{ga} = -\text{angle}\left(v_q^a - jv_d^a\right) \tag{8.2.100} $$

yields

$$ v_q^g = \sqrt{2}E \tag{8.2.101} $$

And

$$ v_d^g = 0 \tag{8.2.102} $$

where

$$ E = \frac{1}{\sqrt{2}}\sqrt{v_q^{a2} + v_d^{a2}} \tag{8.2.103} $$

In (8.2.101) and (8.2.104), v_q^a and v_d^a are the *q* and *d* axis voltages to the left of the ac side inductor L_c in Fig. 8.2.15. The average dc voltage to the right of the rectifier is defined as

$$ \hat{v}_r = \frac{3\sqrt{6}}{\pi}E\cos(\alpha) - \frac{3}{\pi}L_C\omega_g\hat{i}_{dc} - 2L_c\frac{d\hat{i}_{dc}}{dt} \tag{8.2.104} $$

where α is the firing delay angle. This average dc voltage can be related to e_{dc} by

$$ \hat{v}_r = r_{Ldc}\hat{i}_{dc} + L_{dc}\frac{d\hat{i}_{dc}}{dt} + e_{dc} \tag{8.2.105} $$

Therefore

$$ p\hat{i}_{dc} = \frac{\frac{3\sqrt{6}}{\pi}E\cos(\alpha) - \left(r_{Ldc} + \frac{3}{\pi}L_c\omega_g\right)\hat{i}_{dc} - e_{dc}}{L_{dc} + 2L_c} \tag{8.2.106} $$

The derivative of the average dc current is expressed

$$ \frac{d\hat{i}_{dc}}{dt} = \begin{cases} p\hat{i}_{dc} & \text{f} \\ -k\hat{i}_{dc} & \overline{\text{f}} \end{cases} \tag{8.2.107} $$

where *f* is

$$ f = \left(\hat{i}_{dc} \geq 0\right) \cup \left(p\hat{i}_{dc} > 0\right) \tag{8.2.108} $$

and k is a constant.

The commutation angle is determined using the following. First, assuming a firing delay angle of zero,

$$\alpha_s = 0 \tag{8.2.109}$$

The commutation angle is found using

$$\mu_s = -\alpha_s + \operatorname{acos}\left(\cos\left(\alpha_s\right) - \frac{2L_c\omega_g \hat{i}_{dc}}{\sqrt{6}E} \right) \tag{8.2.110}$$

This expression is only valid if several conditions are met. First,

$$\left| \cos\left(\alpha_s\right) - \frac{2L_c\omega_e \hat{i}_{dc}}{\sqrt{6}E} \right| \le 1 \tag{8.2.111}$$

The second and third conditions are that $\mu_s \le \frac{\pi}{3}$ and that $\mu_s + \alpha_s \le \pi$. If these conditions are met, then the firing delay angle and commutation angle are

$$\alpha = \alpha_s \tag{8.2.112}$$

and

$$\mu = \mu_s \tag{8.2.113}$$

Otherwise the firing delay angle and commutation angle are taken to be

$$\alpha = \frac{\pi}{3} - \operatorname{acos}\left(\operatorname{bound}\left(-1,1, \frac{2L_c\omega_g \hat{i}_{dc}}{\sqrt{6}E} \right) \right) \tag{8.2.114}$$

and

$$\mu = \frac{\pi}{3} \tag{8.2.115}$$

The expressions (8.2.115) and (8.2.116) assume 3-3 mode rectifier operation.

The first step in the calculation of the *q* and *d* axis currents is the calculation of the commutation interval currents defined as

$$\begin{aligned} \hat{i}^{g}_{qg,com} = {} & \frac{2\sqrt{3}}{\pi}\hat{i}_{dc}\left[\sin\left(\mu + \alpha - \frac{5\pi}{6} \right) - \sin\left(\alpha - \frac{5\pi}{6} \right) \right] \\ & + \frac{3}{\pi}\frac{\sqrt{2}E}{L_c\omega_g}\cos(\alpha)[\cos(\mu+\alpha) - \cos(\alpha)] \\ & + \frac{1}{4}\frac{3}{\pi}\frac{\sqrt{2}E}{L_c\omega_g}[\cos(2\alpha) - \cos(2\alpha + 2\mu)] \end{aligned} \tag{8.2.116}$$

$$\hat{i}^{g}_{dg,com} = \frac{2\sqrt{3}}{\pi}\hat{i}_{dc}\left[-\cos\left(\mu+\alpha-\frac{5\pi}{6}\right)+\cos\left(\alpha-\frac{5\pi}{6}\right)\right] + \frac{3}{\pi}\frac{\sqrt{2}E}{L_c\omega_g}\cos(\alpha)[\sin(\mu+\alpha)-\sin(\alpha)] + \frac{1}{4}\frac{3}{\pi}\frac{\sqrt{2}E}{L_c\omega_g}[\sin(2\alpha)-\sin(2\alpha+2\mu)]-\frac{3}{\pi}\frac{\sqrt{2}E}{L_c\omega_g}\frac{1}{2}\mu \quad (8.2.117)$$

The conduction interval ac currents are found using

$$\hat{i}^{g}_{qg,cond} = \frac{2\sqrt{3}}{\pi}\hat{i}_{dc}\left[\sin\left(\alpha+\frac{7\pi}{6}\right)-\sin\left(\alpha+\mu+\frac{5\pi}{6}\right)\right] \quad (8.2.118)$$

$$\hat{i}^{g}_{dg,cond} = \frac{2\sqrt{3}}{\pi}\hat{i}_{dc}\left[-\cos\left(\alpha+\frac{7\pi}{6}\right)+\cos\left(\alpha+\mu+\frac{5\pi}{6}\right)\right] \quad (8.2.119)$$

The ac currents are then the sum of the conduction and commutation interval ac currents.

$$\hat{i}_{qg} = \hat{i}_{q,com} + \hat{i}_{q,cond} \quad (8.2.120)$$

$$\hat{i}_{dg} = \hat{i}_{d,com} + \hat{i}_{d,cond} \quad (8.2.121)$$

These currents are then transformed back to the arbitrary reference frame using the inverse of the reference frame transformation (8.2.100). Namely, the currents into the rectifier are given by

$$\hat{i}^{a}_{q} = \hat{i}^{g}_{q}\cos\left(\theta_{ga}\right)+\hat{i}^{g}_{d}\sin\left(\theta_{ga}\right) \quad (8.2.122)$$

$$\hat{i}^{a}_{d} = -\hat{i}^{g}_{q}\sin\left(\theta_{ga}\right)+\hat{i}^{g}_{d}\cos\left(\theta_{ga}\right) \quad (8.2.123)$$

Validation:

This is also a well-established model. The chief limitations that will arise are that the accuracy of the model deteriorates if the ac bus voltages become highly disturbed. Further, the rectifier model is only valid in the 2-3 and 3-3 modes of operation. Finally, if the dc link or ac side inductances saturate, the accuracy of the model will decrease.

References:

[5.9.1] P. Krause, O. Wasynczuk, S. Sudhoff, and S. Pekarek, "Analysis of Electric Machinery and Drive Systems," 3rd Edition, New York: John Wiley and Sons/IEEE Press, 2013.

8.1.10 Generic Pulsed Load

The generic pulsed load exists in two contexts, dc and ac. The dc generic pulsed load is depicted in Fig. 8.2.16. The load is fed by two voltage level busses. A low voltage bus is used for the control and ancillaries and a high voltage bus is used for the bulk power. There are two

low voltage busses present for redundancy purposes. The low voltage busses are ac busses and the high voltage bus is dc. There are two modes considered in the pulsed load, standby and operational.

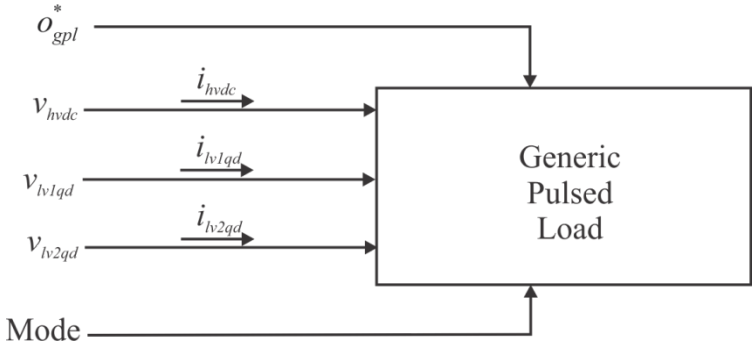

Fig. 8.2.16: DC Generic Pulsed Load.

The ac generic pulsed load is depicted in Fig. 8.2.17 . The load is once again fed by two voltage level busses, a high voltage bus and a low voltage bus. However, in this case the high voltage bus is an ac bus and is represented in *qd* form. The other inputs to the load are the same as those for the dc generic pulsed load.

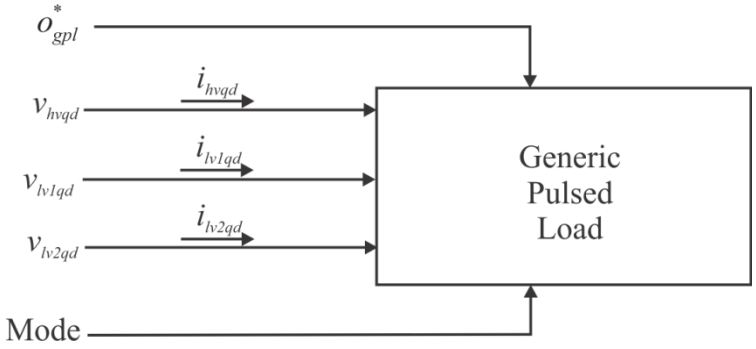

Fig. 8.2.17: AC Generic Pulsed Load.

The model structure for the generic pulsed load is as follows.

Inputs:

o^*_{gpl} The desired operational status of the load

$\boldsymbol{v}_{hvXX}$ The high voltage bus where XX is either *dc* or *qd* (V)

$\boldsymbol{v}_{lv1qd}$ The *qd* representation of the primary low voltage bus (V)

$\boldsymbol{v}_{lv2qd}$ The *qd* representation of the secondary low voltage bus (V)

Outputs:

$\boldsymbol{i}_{hvXX}$ The current on the high voltage bus where XX is either *dc* or *qd* (A)

$\boldsymbol{i}_{lv1qd}$ The ac current on the primary low voltage bus (A)

$\boldsymbol{i}_{lv2qd}$ The ac current on the secondary low voltage bus (A)

Parameters:

$v_{\mathrm{hv},mns}$ The minimum voltage to start for the high voltage bus (V)

$v_{\mathrm{hv},mxs}$ The maximum voltage to start for the high voltage bus (V)
$v_{\mathrm{hv},mnr}$ The minimum voltage to run for the high voltage bus (V)
$v_{\mathrm{hv},mxr}$ The maximum voltage to run for the high voltage bus (V)
$v_{lv1,mns}$ The minimum voltage to start for the primary bus (V)
$v_{lv1,mxs}$ The maximum voltage to start for the primary bus (V)
$v_{lv2,mns}$ The minimum voltage to start for the secondary bus (V)
$v_{lv2,mxs}$ The maximum voltage to start for the secondary bus (V)
$v_{lv1,mnr}$ The minimum voltage to run for the primary bus (V)
$v_{lv1,mxr}$ The maximum voltage to run for the primary bus (V)
$v_{lv2,mnr}$ The minimum voltage to run for the secondary bus (V)
$v_{lv2,mxr}$ The maximum voltage to run for the secondary bus (V)
P_{hvS} The high voltage standby mode real power level (W)
Q_{hvS} The high voltage standby mode reactive power level (W)
P_{lvS} The low voltage standby mode real power level (W)
Q_{lvS} The low voltage standby mode reactive power level (W)
P_{hvO} The high voltage operation mode real power level (W)
Q_{hvO} The high voltage operation mode reactive power level (W)
P_{lvO} The high voltage operation mode real power level (W)
Q_{lvO} The high voltage operation mode reactive power level (W)

Interface Equations:
None

States:
None

Model Equations:
None

8.1.10.1 DC Operation

For the dc application of the generic pulsed load, the high voltage bus is a dc bus where v_{hvdc} is the dc voltage on the bus and i_{hvdc} is the dc current being drawn from the bus. The low voltage bus is represented in *qd* form as

$$\boldsymbol{v}_{lvXqd} = \begin{bmatrix} v_{lvXq} \\ v_{lvXd} \end{bmatrix} \tag{8.2.124}$$

and

$$\boldsymbol{i}_{lvXqd} = \begin{bmatrix} i_{lvXq} \\ i_{lvXd} \end{bmatrix} \tag{8.2.125}$$

where *X* can be either *1* or *2* depending on which low voltage bus being referred to.

The dc power for each bus is defined in Table 8.2.1. The values for these power levels are listed in the Nominal System Parameters section of the document.

Table 8.2.1: DC Operation

	Mode	
Power	**Standby**	**Operational**
P_{hv}	P_{hvS}	P_{hvO}
P_{lv}	P_{lvS}	P_{lvO}
Q_{lv}	Q_{lvS}	Q_{lvO}

8.1.10.2 AC Operation

In the ac application of the generic pulsed load the high voltage bus is an ac bus as well as the low voltage busses. In this case the high voltage bus, like the low voltage bus, is represented in *qd* form as

$$v_{hvqd} = \begin{bmatrix} v_{hvq} \\ v_{hvd} \end{bmatrix} \tag{8.2.126}$$

and

$$i_{hvqd} = \begin{bmatrix} i_{hvq} \\ i_{hvd} \end{bmatrix} \tag{8.2.127}$$

The ac application of the generic pulsed load is similar to the dc operation, but also includes the apparent power levels for the two modes for each bus. These power levels are listed in Table 8.2.2. The values for these power levels are listed in the Nominal System Parameters section of the document.

Table 8.2.2: AC Operation

	Mode	
Power	**Standby**	**Operational**
P_{hv}	P_{hvS}	P_{hvO}
Q_{hv}	Q_{hvS}	Q_{hvO}
P_{lv}	P_{lvS}	P_{lvO}
Q_{lv}	Q_{lvS}	Q_{lvO}

8.1.10.3 Supervisory Control

The supervisory control for the generic pulsed load is shown in Fig. 8.2.18. The inputs to the control are the desired operational status of the pulsed load, o_{pd}^{*}, the measured high voltage

bus level, v_{hvm}, the measured first low voltage bus level, v_{lv1m}, and the measured second low voltage bus level, v_{lv2m}. The measured low voltage bus levels are obtained by

$$v_{lvXm} = \frac{1}{\sqrt{6}}\sqrt{v_{lvXq}^2 + v_{lvXd}^2} \tag{8.2.128}$$

where *X* can be either *1* or *2* depending on which low voltage bus being referred to. The dc application high voltage measurement is equal to v_{hvdc}, and the ac application high voltage bus measurement is obtained as

$$v_{hvm} = \frac{1}{\sqrt{6}}\sqrt{v_{hvq}^2 + v_{hvd}^2} \tag{8.2.129}$$

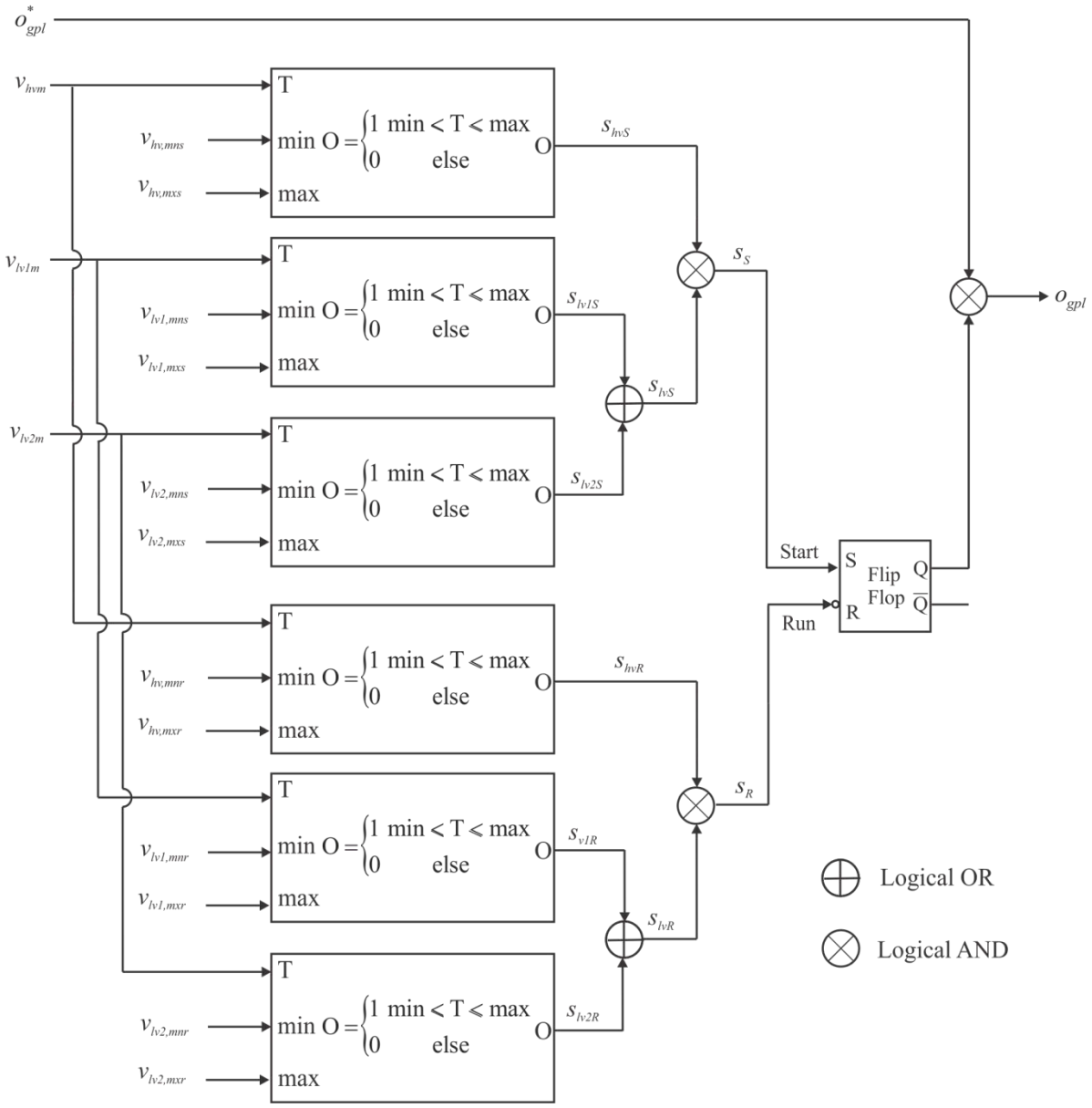

Fig. 8.2.18: GPL Supervisory Control.

There are two situations governed by the control. The first is during the startup condition and the second is during a running condition. These two conditions have different minimum and maximum voltage level requirements with the startup condition being the more stringent of the two. The output of the control is the operational state of the generic pulsed load and is dependent on the voltage levels for the three busses being within the limits for either the startup or running condition. The startup intermediate control variables s_{hvS}, s_{lv1S}, and s_{lv2S} are true if the corresponding bus voltages are within their ranges governed by the appropriate min and max voltage levels. One of the low voltage busses must be within the required range and the high voltage bus must be within the required range in order for the operational state of the drive to be enabled. This same control scheme is used for the running condition which if not satisfied resets the operational state of the pulsed load.

8.1.10.4 Model Outputs

The outputs of the generic pulsed load are the currents for the three busses. For the dc application where the high voltage bus is dc, the high voltage bus current, i_{hv}, is

$$i_{hv} = \begin{cases} 0 & o_{gpl} = 0 \\ \dfrac{P_{hvS}}{v_{hv}} & o_{gpl} = 1, \text{mode} = \text{standby} \\ \dfrac{P_{hvO}}{v_{hv}} & o_{gpl} = 1, \text{mode} = \text{operational} \end{cases} \tag{8.2.130}$$

In the ac application of the pulsed load, the high voltage bus is an ac bus and therefore, the *q*-axis current of the high voltage bus is

$$i_{hvq} = \begin{cases} 0 & o_{gpl} = 0 \\ \dfrac{v_{hvq}P_{hvS} - v_{hvd}Q_{hvS}}{\frac{3}{2}\left(v_{hvq}^2 + v_{hvd}^2\right)} & o_{gpl} = 1, \text{mode} = \text{standby} \\ \dfrac{v_{hvq}P_{hvO} - v_{hvd}Q_{hvO}}{\frac{3}{2}\left(v_{hvq}^2 + v_{hvd}^2\right)} & o_{gpl} = 1, \text{mode} = \text{operation} \end{cases} \tag{8.2.131}$$

and the *d*-axis current on the high voltage bus is

$$i_{hvd} = \begin{cases} 0 & o_{gpl} = 0 \\ \dfrac{v_{hvd} P_{hvS} + v_{hvq} Q_{hvS}}{\dfrac{3}{2}\left(v_{lv1q}^2 + v_{lv1d}^2\right)} & o_{gpl} = 1, \text{mode} = \text{standby} \\ \dfrac{v_{hvd} P_{hvO} + v_{hvq} Q_{hvO}}{\dfrac{3}{2}\left(v_{hvq}^2 + v_{hvd}^2\right)} & o_{gpl} = 1, \text{mode} = \text{operation} \end{cases} \tag{8.2.132}$$

Regardless of dc or ac application of the generic pulsed load, the low voltage bus is ac and the q-axis current on the first low voltage bus is

$$i_{lv1q} = \begin{cases} 0 & o_{gpl} = 0 \text{ or } s_{lv1R} = 0 \\ \dfrac{v_{lv1q} P_{lvS} - v_{lv1d} Q_{lvS}}{\dfrac{3}{2}\left(v_{lv1q}^2 + v_{lv1d}^2\right)} & o_{gpl} = 1 \text{ and mode} = \text{standby and } s_{lv1R} = 1 \\ \dfrac{v_{lv1q} P_{lvO} - v_{lv1d} Q_{lvO}}{\dfrac{3}{2}\left(v_{lv1q}^2 + v_{lv1d}^2\right)} & o_{gpl} = 1 \text{ and mode} = \text{operation and } s_{lv1R} = 1 \end{cases} \tag{8.2.133}$$

The *q*-axis current on the second low voltage bus is

$$i_{lv2q} = \begin{cases} 0 & o_{gpl} = 0 \text{ or } s_{lv1R} = 1 \text{ or } s_{lv2R} = 0 \\ \dfrac{v_{lv2q} P_{lvS} - v_{lv2d} Q_{lvS}}{\dfrac{3}{2}\left(v_{lv2q}^2 + v_{lv2d}^2\right)} & o_{gpl} = 1 \text{ and mode} = \text{standby and } s_{lv1R} = 0 \text{ and } s_{lv2R} = 1 \\ \dfrac{v_{lv2q} P_{lvO} - v_{lv2d} Q_{lvO}}{\dfrac{3}{2}\left(v_{lv2q}^2 + v_{lv2d}^2\right)} & o_{gpl} = 1 \text{ and mode} = \text{operation and } s_{lv1R} = 0 \text{ and } s_{lv2R} = 1 \end{cases} \tag{8.2.134}$$

The *d*-axis current on the first low voltage bus is

$$i_{lv1d} = \begin{cases} 0 & o_{gpl} = 0 \text{ or } s_{lv1R} = 0 \\ \dfrac{v_{lv1d} P_{lvS} + v_{lv1q} Q_{lvS}}{\frac{3}{2}\left(v_{lv1q}^2 + v_{lv1d}^2\right)} & o_{gpl} = 1 \text{ and mode} = \text{standby and } s_{lv1R} = 1 \\ \dfrac{v_{lv1d} P_{lvO} + v_{lv1q} Q_{lvO}}{\frac{3}{2}\left(v_{lv1q}^2 + v_{lv1d}^2\right)} & o_{gpl} = 1 \text{ and mode} = \text{operation and } s_{lv1R} = 1 \end{cases} \quad (8.2.135)$$

The d-axis current on the second low voltage bus is

$$i_{lv2d} = \begin{cases} 0 & o_{gpl} = 0 \text{ and } s_{lv1R} = 1 \text{ and } s_{lv2R} = 0 \\ \dfrac{v_{lv2d} P_{lvS} + v_{lv2q} Q_{lvS}}{\frac{3}{2}\left(v_{lv2q}^2 + v_{lv2d}^2\right)} & o_{gpl} = 1 \text{ and mode} = \text{standby and } s_{lv1R} = 0 \text{ and } s_{lv2R} = 1 \\ \dfrac{v_{lv2d} P_{lvO} + v_{lv2q} Q_{lvO}}{\frac{3}{2}\left(v_{lv2q}^2 + v_{lv2d}^2\right)} & o_{gpl} = 1 \text{ and mode} = \text{operation and } s_{lv1R} = 0 \text{ and } s_{lv2R} = 1 \end{cases} \quad (8.2.136)$$

If both of the low voltage busses are present and both i_{hv} and i_{hv} are high, then the first bus is selected as the bus used to power the control and ancillaries of the GPL.

Validation:

The model is an abstraction of the requirement of a generic pulsed load (or constant power load) which consumes the desired power, but no internal dynamics are represented.

References:

None

8.1.11 Generic Hydrodynamic Load

The generic hydrodynamic load model is defined in [5.12.1-5.12.3] and outlined herein. The model structure is as follows.

Inputs:

ω_{prop} Propeller angular frequency (rad/s)

Outputs:

T_{prop} Counter torque exerted on shaft (Nm)

V_{ship} Ship velocity (m/s)

Parameters:

ρ	Density of salt water (kg/m^3)
D	Propeller diameter (m)
η_r	Relative rotational efficiency (pu)
V_a	Propeller speed of advance (m/s)
υ	Modified advanced coefficient (pu)
$\mathrm{C_Q}(\upsilon)$	Open water propeller torque coefficient function
$\mathrm{C}\tau(\upsilon)$	Open water propeller thrust coefficient function
$\mathrm{w_T}(V_{ship})$	Taylor wake fraction
T_d	Thrust deduction factor
m_{ship}	Mass of ship (kg)
$F_{drag}(V_{ship})$	Hydrodynamic resistance (N vs knots)

Interface equation:
None

States:

V_{ship}	Ship velocity (m/s)

Model Equations:

The model definition for the generic hydrodynamic load is given in [5.12.1] and outlined herein. First, the propeller speed of advance is found utilizing the Taylor Wake fraction as

$$V_a = V_{ship}\left(1-\mathrm{w_T}\left(V_{ship}\right)\right) \tag{8.2.137}$$

Next, the thrust exerted on the ship is found using

$$F_{ship} = \mathrm{C_\tau}(\upsilon)\rho D^2(V_a{}^2 + (nD)^2)(1-T_d) \tag{8.2.138}$$

where

$$n = \frac{\omega_{prop}}{2\pi} \tag{8.2.139}$$

and

$$\upsilon = \frac{nD}{\sqrt{V_a{}^2 + (nD)^2}} \tag{8.2.140}$$

Next, the derivative of ship speed is found using

$$\frac{dV_{ship}}{dt} = \frac{1}{m_{ship}}\left[F_{ship1} + F_{ship2} - \mathrm{F_{drag}}\left(V_{ship}\right)\right] \tag{8.2.141}$$

where F_{ship1} and F_{ship2} are the thrust exerted on the ship by propellers one and two. Finally, the counter torque on the propeller shaft is found using

$$T_{prop} = \mathrm{C_Q}(\upsilon)\rho\left(\frac{D^3}{\eta_r}\right)(V_a{}^2 + (nD)^2) \tag{8.2.142}$$

Validation:

The hydrodynamic represented here is general and valid for a given set of torque and thrust coefficients, and ship resistance, which all depend on various factors including propeller type, ship hull form, and operating conditions such as sea state conditions, and the presence of cavitation, for example. Further discussion and analysis of ship propulsion can be found in [5.12.4] and [5.12.5].

References:

[5.12.1] E. J. Lecourt, Jr., "Using Simulation To Determine the Maneuvering Performance of the WAGB-20," Naval Engineer's Journal, January 1998, pp. 171-188.

[5.12.2] Syntek, "DD(X) Notional Baseline Modeling and Simulation Development Report," Internal Report, August 2003.

[5.12.3] Robert F. Roddy, David E. Hess, and Will Faler, "Neural Network Predictions of the 4-Quadrant Wageningen Propeller Series, NSWCCD-50-TR-2006/004, Naval Surface Warfare Center, Carderock Division, West Bethesda, MD, April 2006.

[5.12.4] K.J. Rawson, E.C. Tupper, "Basic Ship Theory," Longman Scientific and Technical, Volume 2 , 1994.

[5.12.5] V. Bertram, "Practical Ship Hydrodynamics," Elsevier Ltd, 2nd Edition, 2012.

8.1.12 Line Models

8.1.12.1 DC Line

This section sets forth descriptions of the ac and dc line models. The dc line is a resistive line and the model structure is as follows.

Inputs:

$v_{dc,x}$ The dc voltage at bus *x* (V)

$v_{dc,y}$ The dc voltage at bus *y* (V)

Outputs:

$i_{dc,xy}$ The dc current through the line from bus *x* to bus *y* (A)

Interface equation:

$$v_{dc,y} = v_{dc,x} - r_{dc} i_{dc,xy} \tag{8.2.143}$$

States:

None

Model Equation:

$$i_{dc,xy} = \frac{v_{dc,x} - v_{dc,y}}{r_{dc}} \tag{8.2.144}$$

Validation:

The chief sources of inaccuracy in this model are that temperature dependence and line inductance are neglected. This will cause the line model to tend to overestimate fault currents.

References:
None

8.1.12.2 AC Line

The ac line is an RL line and the model structure is as follows.

Inputs:

$\mathbf{v}^e_{qd,x}$ The vector of *q*- and *d*-axis voltages ($v^e_{q,x}$ and $v^e_{d,x}$) at bus *x* of the line in the synchronous ref. frame (V)

$\mathbf{v}^e_{qd,y}$ The vector of *q*- and *d*-axis voltages ($v^e_{q,y}$ and $v^e_{d,y}$) at bus *y* of the line in the synchronous ref. frame (V)

ω_e The radian frequency of the synchronous reference frame (rad/s)

Outputs:

$\mathbf{i}^e_{qd,xy}$ The *q*- and *d*-axis currents ($i^e_{q,xy}$ and $i^e_{d,xy}$) through the line from bus *x* to bus *y* in the synchronous ref. frame (A)

Interface equation:

$$\mathbf{v}^e_{qd,y} = \mathbf{v}^e_{qd,x} - \mathbf{Z}^e_{qd}\mathbf{i}^e_{qd,xy} \tag{8.2.145}$$

where

$$\mathbf{Z}^e_{qd} = \begin{bmatrix} r & \omega_e L \\ -\omega_e L & r \end{bmatrix} \tag{8.2.146}$$

States:
None

Model Equations:

$$\mathbf{i}^e_{qd,xy} = \left(\mathbf{Z}^e_{qd}\right)^{-1}\left(\mathbf{v}^e_{qd,x} - \mathbf{v}^e_{qd,y}\right) \tag{8.2.147}$$

Validation:

This line model neglects temperature dependence. The line inductance is included, but only in a steady-state sense. Thus, fault current will tend to be overestimated. . In addition, it is assumed that the line is balanced and symmetrical.

References:
None

8.1.13 AC Circuit Breaker Model

The ac circuit breaker model represents the opening and closing of the breaker as a change in resistance. This is done in such a way as to avoid discontinuities. The breaker either opens due to the measured current being greater than a threshold indicating a fault, or if the desired circuit breaker status (o_{acb}^{*}) is open. If the breaker trips due to an over-current, the desired circuit breaker status must be set low for a certain period of time in order to reset the circuit breaker. The model structure for the ac circuit breaker is as follows.

Inputs:

o_{acb}^{*} The desired circuit breaker status

I_s The measured current used to indicate a fault (A)

Outputs:

R_{cb} The resistance of the circuit breaker (Ω)

Parameters:

I_t The threshold current that defines a fault condition (A)

R_{closed} The closed resistance of the circuit breaker (Ω)

R_{open} The open resistance of the circuit breaker (Ω)

τ_o The time constant associated with a manual change of operational status (s)

τ_f The time constant associated with a fault detection (s)

Interface equation:
None

States:

o_{acb} The operational status of the circuit breaker

F The fault status of the circuit breaker

Model Equations:

There are two values in the control that define whether the breaker is in operation and if there is a fault condition. The operational status of the breaker is represented by o and the fault status of the breaker is represented by F . The governing equations for these two control values are

$$\dot{o}_{acb} = \begin{cases} 1 & o^*_{acb} = 1 \text{ and } o_{acb} \le 1 \\ -1 & o^*_{acb} = 0 \text{ and } o_{acb} \ge 0 \\ 0 & \left(o^*_{acb} = 0 \text{ and } o_{acb} < 0\right) or \left(o^*_{acb} = 1 \text{ and } o_{acb} > 1\right) \end{cases} \tag{8.2.148}$$

and

$$\dot{F} = \begin{cases} 1 & \left(I_s > I_t \text{ and } F < 1\right) \text{ or} \\ & \left(o_{acb} > 0 \text{ and } I_s < I_t \text{ and } \left(F > 0 \text{ and } F < 1\right)\right) \\ -1 & \left(o_{acb} \le 0 \text{ and } I_s < I_t \text{ and } F > 0\right) \\ 0 & \left(I_s > I_t \text{ and } F \ge 1\right) \text{ or} \\ & \left(I_s < I_t \text{ and } F \le 1\right) \text{ or} \\ & \left(o_{acb} > 0 \text{ and } I_s < I_t \text{ and } F \ge 1\right) \end{cases} \tag{8.2.149}$$

The derivatives of the control signals are then calculated as

$$\frac{do_{acb}}{dt} = \frac{1}{\tau_o}\dot{o}_{acb} \tag{8.2.150}$$

$$\frac{dF}{dt} = \frac{1}{\tau_F}\dot{F} \tag{8.2.151}$$

The status of the circuit breaker (open/closed) is then governed by

$$c = \min(o_{acb}, 1 - F) \tag{8.2.152}$$

and the resistance of the circuit breaker is

$$R = 10^{\log(R_{\max}) - c\left(\log(R_{\max}) - \log(R_{\min})\right)} \tag{8.2.153}$$

Validation:

It must be recognized that this model is completely behavioral in nature. Functionally, it will operate as a circuit breaker and interrupt a fault current and be re-closable. However, the dynamics of the circuit breaker are not based on physics and so the model does not correctly portray the short-time scale behavior of circuit breaker operation.

References:
None

8.1.14 Transformer

The *q* and *d*-axis equivalent circuits for the transformer model are depicted in Fig. 8.2.19 and Fig. 8.2.20.

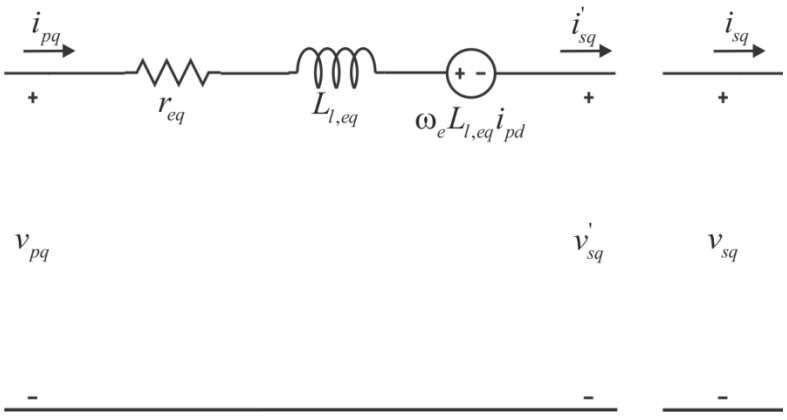

Fig. 8.2.19: Transformer *Q*-axis Equivalent Circuit.

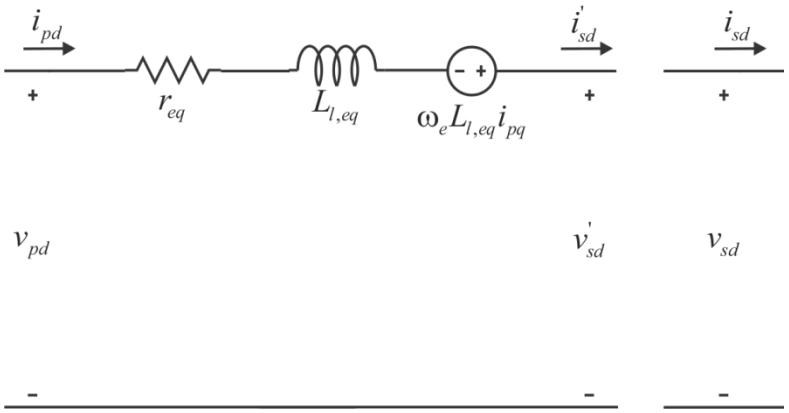

Fig. 8.2.20: Transformer *D*-axis Equivalent Circuit.

The equivalent resistance (r_{eq}) and inductance (L_{eq}) are found using

$$r_{eq} = r_p + r_s' \tag{8.2.154}$$

$$L_{l,eq} = L_{lp} + L_{ls}' \tag{8.2.155}$$

The model structure is as follows.

Inputs:

$v_{p,qd}$ The primary side voltage in the *qd* reference frame (V)

$i_{s,qd}$ The secondary side current in the *qd* reference frame (A)

ω_e The electrical speed of the synchronous reference frame (rad/s)

Outputs:

$v_{s,qd}$ The secondary side voltage in the *qd* reference frame (V)

$i_{p,qd}$ The primary side current in the *qd* reference frame (A)

Parameters:

r_p The primary side winding resistance (Ω)

$r_s^{'}$ The secondary side winding resistance referred to the primary side (Ω)

L_{lp} The primary side winding leakage inductance (H)

$L_{ls}^{'}$ The secondary side winding leakage inductance referred to the primary side (H)

N_p The number of turns on the primary winding

N_s The number of turns on the secondary winding

Interface Equations:

$$v_{pq} = r_{eq} i_{pq} + \omega_e L_{l,eq} i_{pd} + v_{sq}^{'} \tag{8.2.156}$$

$$v_{pd} = r_{eq} i_{pd} - \omega_e L_{l,eq} i_{pq} + v_{sd}^{'} \tag{8.2.157}$$

States:
None

Model Equations:

The relationship between the referred and non-referred quantities is

$$v_{sX}^{'} = \frac{N_p}{N_s} v_{sX} \tag{8.2.158}$$

and

$$i_{sX}^{'} = \frac{N_s}{N_p} i_{sX} \tag{8.2.159}$$

where X can either be *q* or *d*.

$$i_{sX}^{'} = i_{pX} \tag{8.2.160}$$

Lastly, the resistance and inductance are referred using

$$r_s^{'} = \left(\frac{N_p}{N_s} \right)^2 r_s \tag{8.2.161}$$

and

$$L_{ls}^{'} = \left(\frac{N_p}{N_s} \right)^2 L_{ls} \tag{8.2.162}$$

Validation:

The model described assumes a balanced three phase transformer. The magnetizing inductance is assumed to be infinite, and the leakage saturation and temperature effects are ignored. Since this is a reduced-order model, initial fault currents will tend to be over-predicted.

References:
None

8.1.15 Zonal Active Rectifier

The Zonal Active Rectifier is depicted in Fig. 8.2.21.

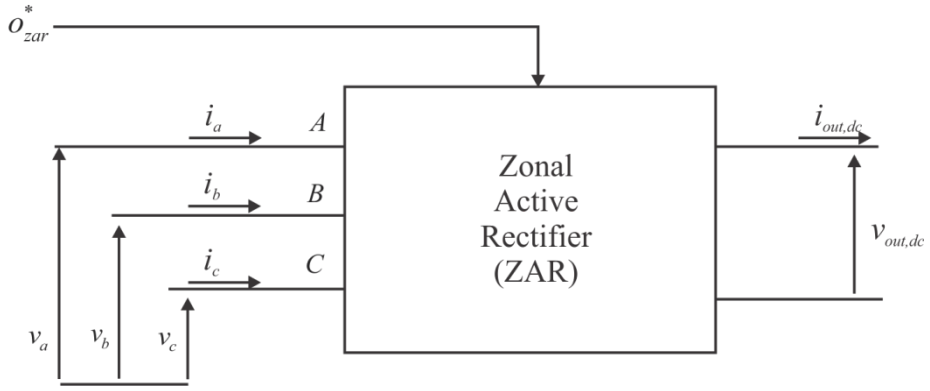

Fig. 8.2.21: Zonal Active Rectifier.

The model structure for the Zonal Active Rectifier is as follows.

Inputs:

$v_{in,qd}$ The ac side voltage in the *qd* reference frame (V)

$i_{out,dc}$ The dc output current (A)

o^*_{zar} The desired status of the component

Outputs:

$i_{in,qd}$ The ac side current in the *qd* reference frame (A)

$v_{out,dc}$ The dc output voltage (V)

Parameters:

r_d The droop resistance (Ω)

v^*_{out} The desired no load output voltage (V)

i_t The fault current threshold (A)

i_f The peak fault current (A)

Interface Equations:
None

States:
None

Model Equations:

The supervisory control for the Zonal Active Rectifier is shown in Fig. 8.2.22. The inputs to the control are the measured voltage level of the bus and the desired operational status of the load, o^*_{zar}. The output of the supervisory control is the operational state of the load, o_{zar}.

The supervisory control categorizes the bus voltage into two categories. The first category relates to being appropriate to start and the second relates to whether the bus voltage is appropriate to continue running. These two conditions have different minimum and maximum voltages level requirements with the startup condition being the more stringent of the two. The output of the control is the operational state of the load, o_{zar}, and is dependent upon the voltage levels of the buss being within the limits for either the startup or running condition. The intermediate control variables S_S and S_R are true if the bus voltage is within the ranges governed by the appropriate min and max voltage levels for component start or run. If the bus is within its required voltage range then the flip-flop is not reset. If it is out of range then the flip-flop is reset.

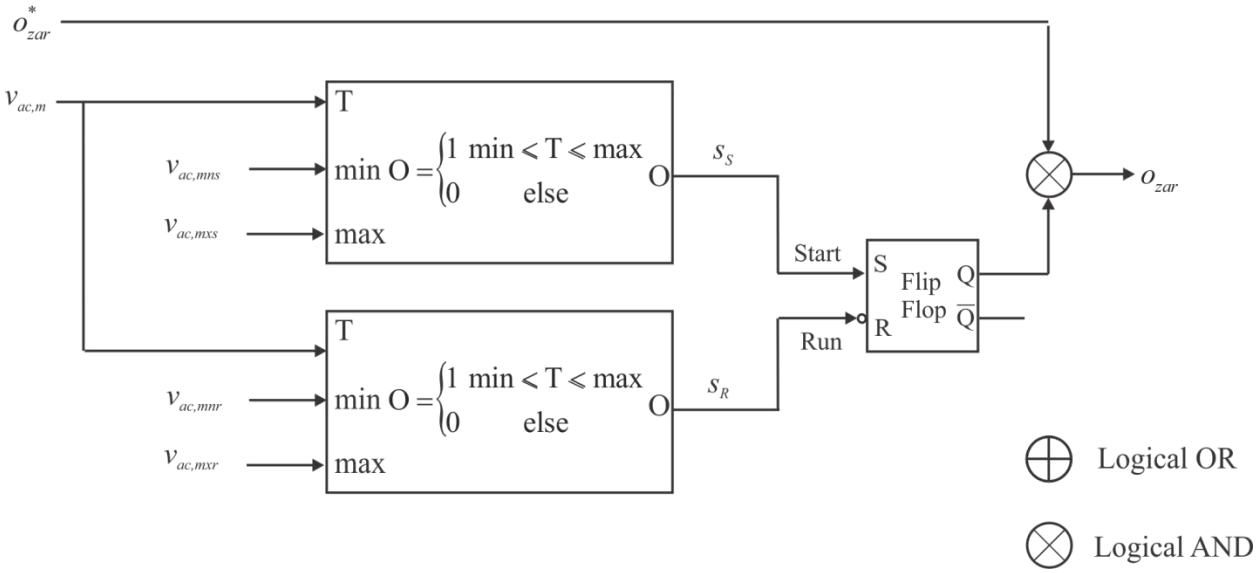

Fig. 8.2.22: Zonal Active Rectifier Supervisory Control.

The dc output voltage of the rectifier as a function of output current is depicted in Fig. 8.2.23.

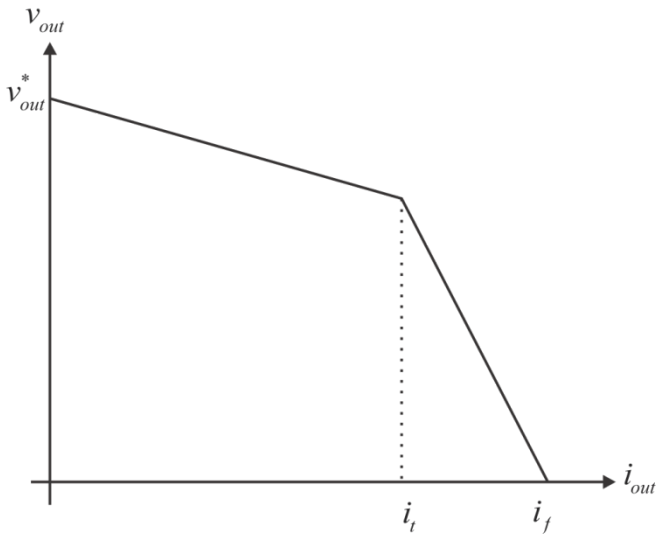

Fig. 8.2.23: Zonal Active Rectifier Output Voltage.

The output voltage is therefore expressed

$$v_{out} = \begin{cases} 0 & o_{zar} = 0 \text{ or } i_{out} > i_f \\ v_{out}^* - r_d i_{out} & o_{zar} = 1 \text{ and } i_{out} < i_t \\ m i_{out} + c & o_{zar} = 1 \text{ and } i_{out} \geq i_t \end{cases} \tag{8.2.163}$$

where

$$m = \frac{r_d i_t - v_{out}^*}{i_f - i_t} \tag{8.2.164}$$

and

$$c = \frac{\left(v_{out}^* - r_d i_t\right) i_f}{i_f - i_t} \tag{8.2.165}$$

The output power is found using

$$P_{out} = v_{out} i_{out} \tag{8.2.166}$$

and the input power is found using

$$P_{in} = \frac{P_{out}}{\eta_{inc}} + P_{nl} \tag{8.2.167}$$

where

$$\eta_{inc} = \frac{\Delta P_{out}}{\Delta P_{in}} \tag{8.2.168}$$

is the incremental efficiency. The *q* and *d*-axis currents can then be calculated using

$$i_q = \frac{\frac{2}{3} P_{in} v_q}{v_q^2 + v_d^2} \tag{8.2.169}$$

and

$$i_d = \frac{\frac{2}{3} P_{in} v_d}{v_q^2 + v_d^2} \tag{8.2.170}$$

Validation:

The behavior of this component is based on what is possible in terms of power balance. It is an abstraction of a desired component performance.

References:

None

8.1.16 Type 1 DC Load

The Type 1 dc load is depicted in Fig. 8.2.24 and is a resistive load fed by one of two busses. The first input bus is the primary power source and the second bus supplies backup power.

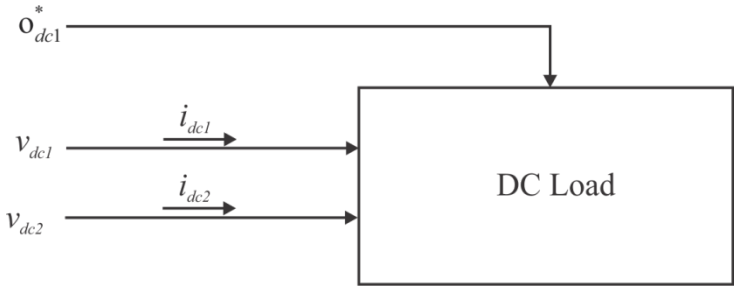

Fig. 8.2.24: Zonal DC Load.

The model structure is defined as follows.

Inputs:

o^*_{dc1} The desired operational status of the load

v_{dc1} The dc voltage on the primary bus (V)

v_{dc2} The dc voltage on the secondary bus (V)

Outputs:

i_{dc1} The dc current on the primary bus (A)

i_{dc2} The dc current on the secondary bus (A)

Parameters:

$v_{lv1,mns}$ The minimum voltage to start for the primary bus (V)

$v_{lv1,mxs}$ The maximum voltage to start for the primary bus (V)

$v_{lv2,mns}$ The minimum voltage to start for the secondary bus (V)

$v_{lv2,mxs}$ The maximum voltage to start for the secondary bus (V)

$v_{lv1,mnr}$ The minimum voltage to run for the primary bus (V)

$v_{lv1,mxr}$ The maximum voltage to run for the primary bus (V)

$v_{lv2,mnr}$ The minimum voltage to run for the secondary bus (V)

$v_{lv2,mxr}$ The maximum voltage to run for the secondary bus (V)

r_{dc} The resistance of the dc load (Ω)

Interface Equations:
None

States:
None

Model Equations:

The supervisory control for the load is depicted in Fig. 8.2.25. The inputs to the supervisory control are the measured dc voltages on each of the two busses, v_{dc1m} and v_{dc2m}, and the desired operational status of the load, o^*_{dc1}.

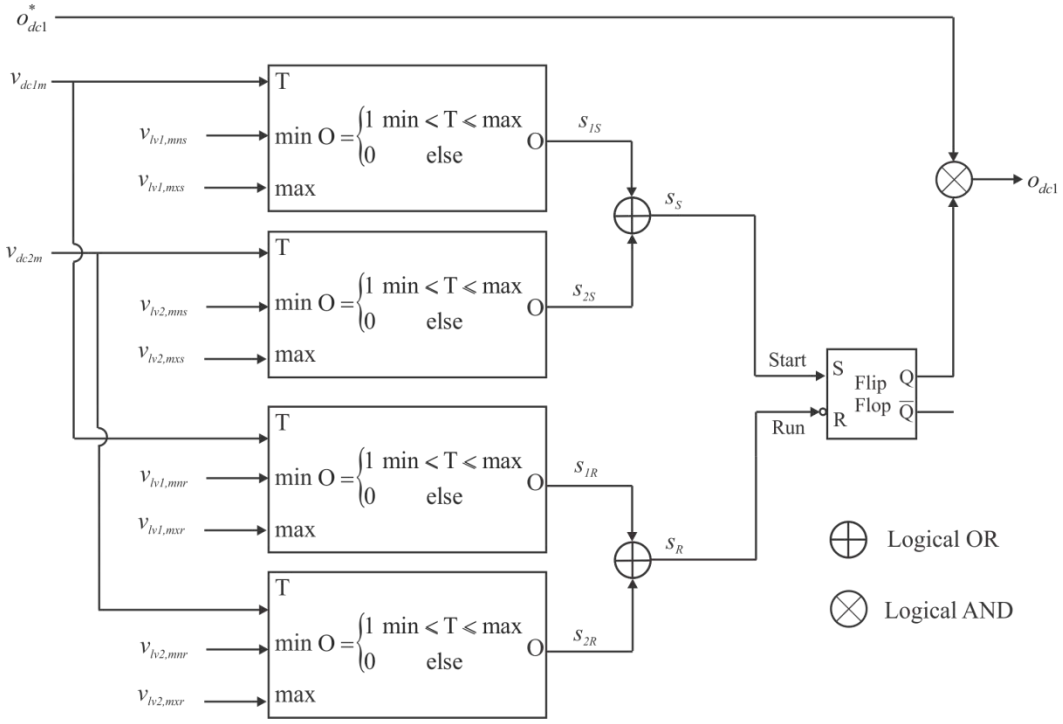

Fig. 8.2.25: Zonal DC Load Supervisory Control.

The supervisory control categorizes each bus voltage into two categories. The first category relates to being appropriate to start and the second relates to whether the bus voltages are appropriate to continue running. These two conditions have different minimum and maximum voltages level requirements with the startup condition being the more stringent of the two. The output of the control is the operational state of the load, o_{dc1}, and is dependent upon the voltage levels for each of the busses being within the limits for either the startup or running condition. The intermediate control variables s_{1S} and s_{2S} are true if the corresponding bus voltages are within their ranges governed by the appropriate min and max voltage levels for component start. One bus being within the required range makes the set input of the flip-flop to true. The intermediate control variables s_{1R} and s_{1R} are true if the corresponding bus voltages are within the range governed by the appropriate min and max voltage levels to run. If either of the two busses is within its required voltage range then the flip-flop is not reset. If they both are out of range then the flip-flop is reset.

The output of the dc load model are the two load currents, i_{dc1} and i_{dc2}, which are given by

$$i_{dc1} = \begin{cases} 0 & o_{dc1} = 0 \text{ or } s_{1R} = 0 \\ \dfrac{v_{dc1}}{r_{dc}} & o_{dc1} = 1 \text{ and } s_{1R} = 1 \end{cases} \tag{8.2.171}$$

$$i_{dc2} = \begin{cases} 0 & o_{dc1} = 0 \text{ or } s_{2R} = 0 \\ \dfrac{v_{dc2}}{r_{dc}} & o_{dc1} = 1 \text{ and } s_{1R} = 0 \end{cases} \tag{8.2.172}$$

Validation:

The behavior of this component is based on what is possible in terms of power balance. It is an abstraction of a desired component performance.

References:
None

8.1.17 Type 2 DC Load

The type 2 dc load is the same configuration as the Type 1 dc load depicted in Fig. 8.2.24, but represents a constant power load. The model structure for this load is identical to that of the Type 1 dc load. The supervisory control for the load is identical to that of the Type 1 dc load depicted in Fig. 8.2.25 with the output being o_{dc2} instead of o_{dc1}.

The outputs of the Type 2 dc load model are the two load currents, i_{dc1} and i_{dc2}, which are given by

$$i_{dc1} = \begin{cases} 0 & o_{dc2} = 0 \text{ or } s_{1R} = 0 \\ \dfrac{P_{dc}}{v_{dc1}} & o_{dc2} = 1 \text{ and } s_{1R} = 1 \end{cases} \tag{8.2.173}$$

$$i_{dc2} = \begin{cases} 0 & o_{dc2} = 0 \text{ or } s_{2R} = 0 \\ \dfrac{P_{dc}}{v_{dc2}} & o_{dc2} = 1 \text{ and } s_{1R} = 0 \end{cases} \tag{8.2.174}$$

8.1.18 AC Load

The ac load is an RL load fed by two ac busses and is depicted in Fig. 8.2.26. The first input bus is the primary power source and the second bus supplies backup power.

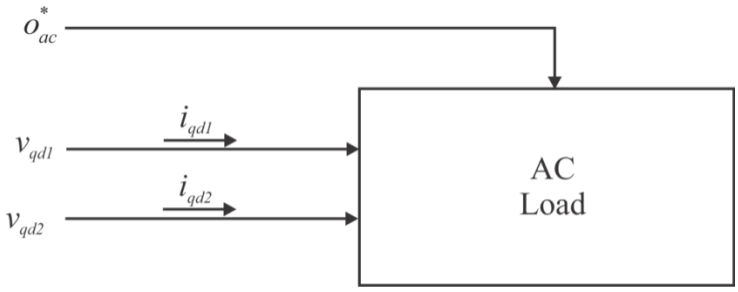

Fig. 8.2.26: Zonal AC Load.

The model structure is defined as follows.

Inputs:

o_{ac}^{*} The desired operational status of the load

v_{qd1} The ac voltage on the primary bus (V)

v_{qd2} The ac voltage on the secondary bus (V)

ω_e The electrical speed of the synchronous reference frame (rad/s)

Outputs:

i_{qd1} The ac current on the primary bus (A)

i_{qd2} The ac current on the secondary bus (A)

Parameters:

$v_{ac1,mns}$ The minimum voltage to start for the primary bus (V)

$v_{ac1,mxs}$ The maximum voltage to start for the primary bus (V)

$v_{ac2,mns}$ The minimum voltage to start for the secondary bus (V)

$v_{ac2,mxs}$ The maximum voltage to start for the secondary bus (V)

$v_{ac1,mnr}$ The minimum voltage to run for the primary bus (V)

$v_{ac1,mxr}$ The maximum voltage to run for the primary bus (V)

$v_{ac2,mnr}$ The minimum voltage to run for the secondary bus (V)

$v_{ac2,mxr}$ The maximum voltage to run for the secondary bus (V)

r_{ac} The resistance of the ac load (Ω)

L_{ac} The inductance of the ac load (Ω)

Interface Equations:

None

States:

None

Model Equations:

The supervisory control for the ac load is depicted in Fig. 8.2.27. The inputs to the control are the measured voltage levels for each of the busses and the desired operational status of the load, o_{ac}^{*}. The output of the supervisory control is the operational state of the load, o_{ac}.

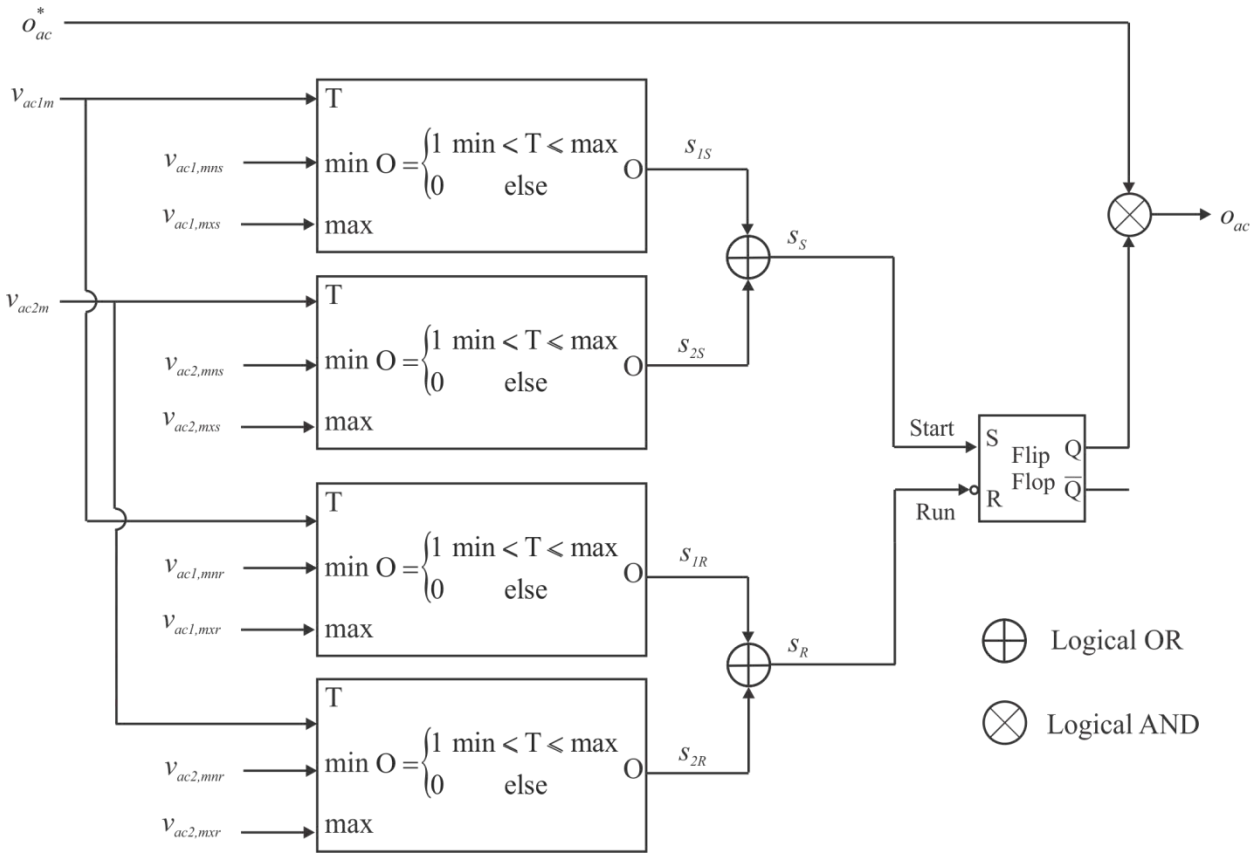

Fig. 8.2.27: Zonal AC Load Supervisory Control.

The measured voltage levels for the two busses are found using

$$v_{acXm} = \frac{1}{\sqrt{6}}\sqrt{v_{qX}^2 + v_{dX}^2} \tag{8.2.175}$$

where *X* can either be 1 or 2.

The supervisory control categorizes each bus voltage into two categories. The first category relates to being appropriate to start and the second relates to whether the bus voltages are appropriate to continue running. These two conditions have different minimum and maximum voltages level requirements with the startup condition being the more stringent of the two. The output of the control is the operational state of the load, o_{ac}, and is dependent upon the voltage levels for each of the busses being within the limits for either the startup or running condition. The intermediate control variables s_{1S} and s_{2S} are true if the corresponding bus voltages are within their ranges governed by the appropriate min and max voltage levels for component start. One bus being within the required range makes the set input of the flip-flop to true. The intermediate control variables s_{1R} and s_{1R} are true if the corresponding bus voltages are within the range governed by the appropriate min and max voltage levels to run. If either of the two busses is within its required voltage range then the flip-flop is not reset. If they both are out of range then the flip-flop is reset.

The model outputs for the ac load are the *q* and *d* axis currents for each of the busses, i_{q1}, i_{d1}, i_{q2} and i_{d2}, which are computed as

$$i_{q1} = \begin{cases} 0 & o_{ac} = 0 \text{ or } s_{ac1R} = 0 \\ \dfrac{r_{ac} v_{q1} - \omega L_{ac} v_{d1}}{r_{ac}^2 + \omega^2 L_{ac}^2} & o_{ac} = 1 \text{ and } s_{ac1R} = 1 \end{cases} \tag{8.2.176}$$

$$i_{d1} = \begin{cases} 0 & o_{ac} = 0 \text{ or } s_{ac1R} = 0 \\ \dfrac{r_{ac} v_{d1} + \omega L_{ac} v_{q1}}{r_{ac}^2 + \omega^2 L_{ac}^2} & o_{ac} = 1 \text{ and } s_{ac1R} = 1 \end{cases} \tag{8.2.177}$$

$$i_{q2} = \begin{cases} 0 & o_{ac} = 0 \text{ or } s_{ac2R} = 0 \\ \dfrac{r_{ac} v_{q2} - \omega L_{ac} v_{d2}}{r_{ac}^2 + \omega^2 L_{ac}^2} & o_{ac} = 1 \text{ and } s_{ac1R} = 0 \end{cases} \tag{8.2.178}$$

$$i_{d2} = \begin{cases} 0 & o_{ac} = 0 \text{ or } s_{ac2R} = 0 \\ \dfrac{r_{ac} v_{d2} + \omega L_{ac} v_{q2}}{r_{ac}^2 + \omega^2 L_{ac}^2} & o_{ac} = 1 \text{ and } s_{ac1R} = 0 \end{cases} \tag{8.2.179}$$

Validation:

This component model is an exact steady-state model of a balanced RL load, neglecting temperature variations. It does not include dynamics.

References:

None

8.1.19 Isolated DC-DC Converter

The IDCDC converter considered herein is an isolated, peak-current controlled, uni-directional DC-DC converter [5.21.1]. The topology is shown in Fig. 8.2.28. The control of the DC-DC converter is shown in Fig. 8.2.29. A simplified equivalent circuit used to derive the average value model (AVM) is seen in Fig. 8.2.30.

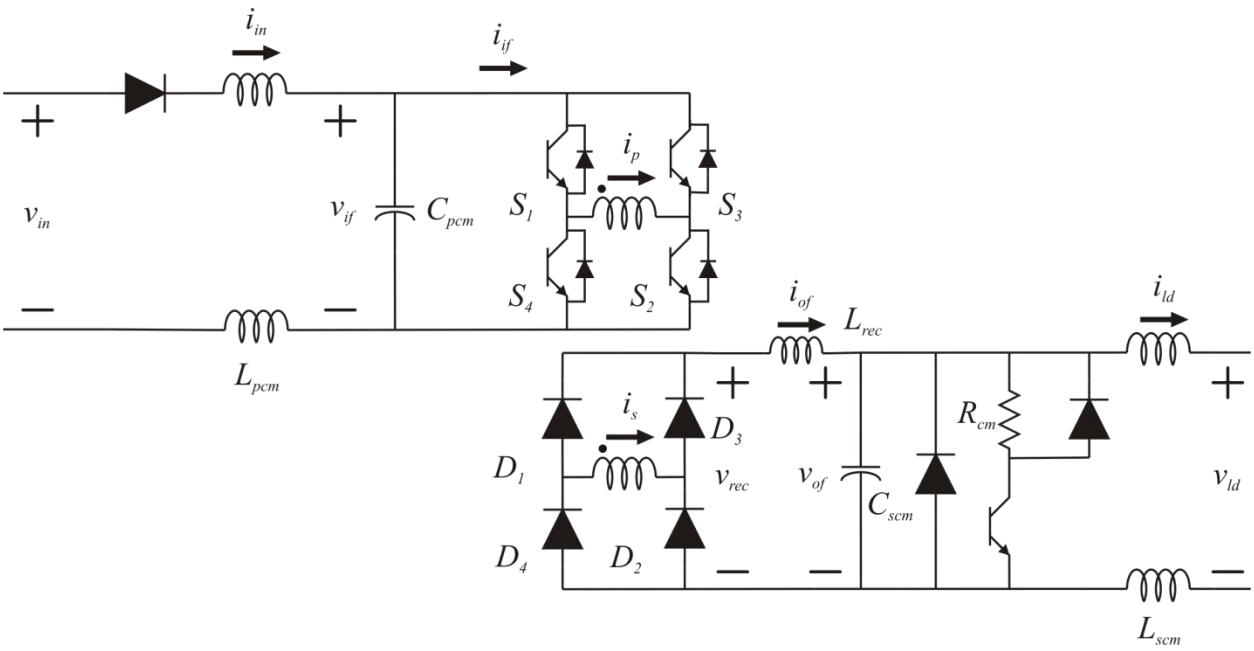

Fig. 8.2.28: DC-DC Converter Topology.

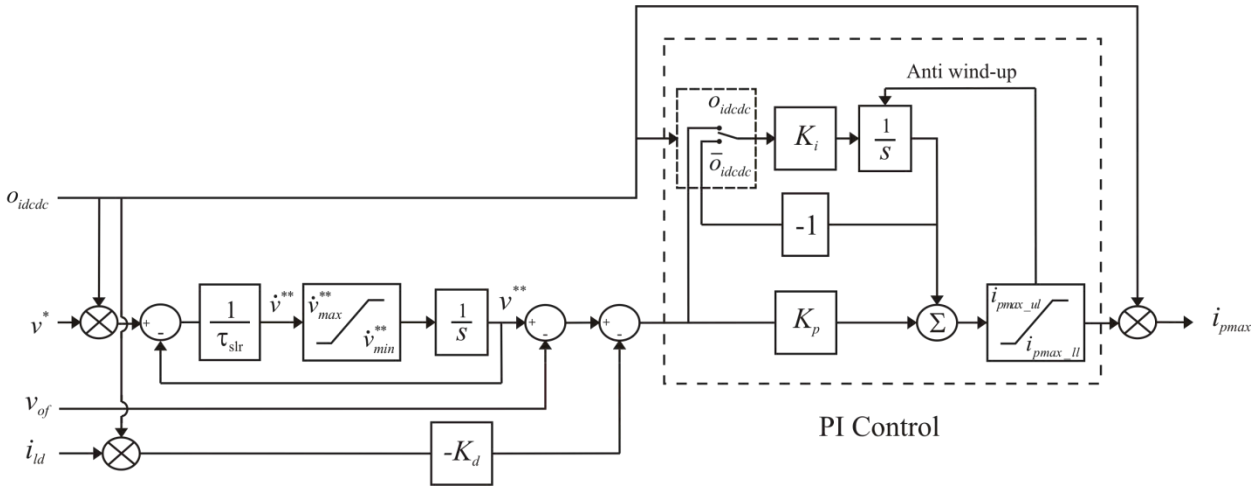

Fig. 8.2.29: DC-DC Converter Control.

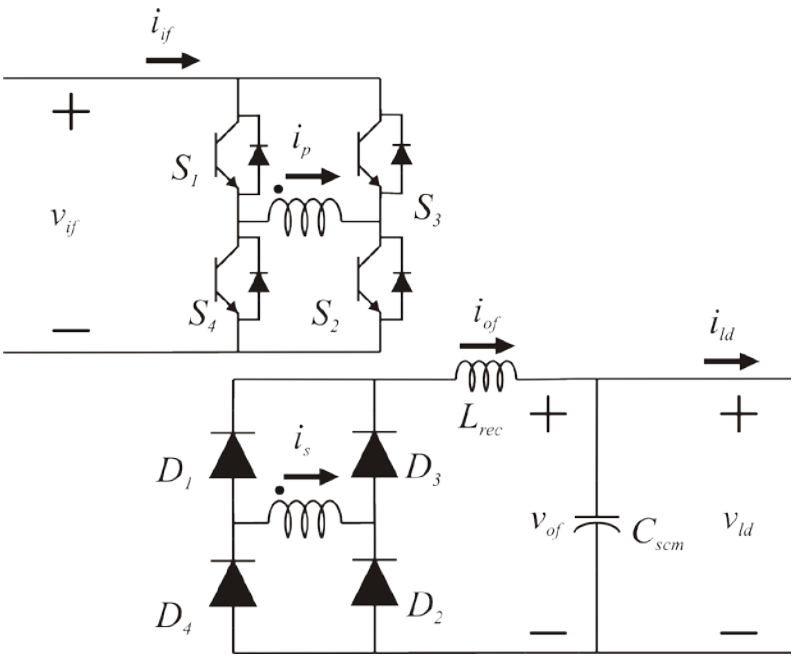

Fig. 8.2.30: AVM Simplified Topology.

The average value model of the IDCDC converter is as follows:

Inputs:

v^* The commanded output filter capacitor voltage (V)

v_{if} The input voltage of the DC-DC converter (V)

i_{ld} The load current drawn from the DC-DC converter (A)

Outputs:

i_{if} The current drawn by the DC-DC converter (A)

v_{of} Output filter capacitor voltage (V)

Parameters:

L_{pcm} Input filter inductance (H)

r_{pcm} Input filter inductor's resistance (Ω)

C_{pcm} Input filter capacitance (F)

L_m Transformer magnetizing inductance (H)

L_{lp} Transformer primary leakage inductance (H)

r_{lp} Transformer primary leakage resistance (Ω)

L_{ls} Transformer secondary leakage inductance (H)

r_{ls} Transformer secondary leakage resistance (Ω)

$\frac{N_1}{N_2}$ Transformer turns ratio (no units)

L_{rec} DC link inductance (H)

r_{rec} Resistance of DC link inductor (Ω)

L_{scm} Output filter inductance (H)

r_{scm} Output filter inductor's resistance (Ω)

C_{scm} Output filter capacitance (F)

K_p Proportional constant (Ω^{-1})

K_i Integral constant ($(\Omega s)^{-1}$)

K_d Droop constant (Ω)

i_{pmax_ul} Upper limit of maximum transformer primary current (A)

i_{pmax_ll} Lower limit of maximum transformer primary current (A)

f_{sw} Switching frequency of transformer (Hz)

T_{sw} Time period of switching of transformer (s)

τ_{slr} Slew rate limit constant (s)

τ_{awu} Anti-windup constant (s)

$\dot{v}^{**}_{min}$ Minimum rate of change of voltage command (Vs^{-1})

$\dot{v}^{**}_{max}$ Minimum rate of change of voltage command (Vs^{-1})

$v_{in,mns}$ Minimum voltage required at input to enable operation (V)

$v_{in,mxs}$ Maximum voltage allowed at input to enable operation (V)

$v_{in,mnr}$ Minimum voltage required to remain operational (V)

$v_{in,mxr}$ Maximum voltage allowed to remain operational (V)

Interface Equations:
None

States:

v^{**} The slew-rate limited voltage command (control) (V)

I_{PI} Integral term in the PI control (A)

v_{of} Output filter capacitor voltage (V)

Model Equations:

A supervisory control which turns the DC-DC converter on only if the input voltage is within as certain range of voltage and turns the DC-DC converter off if the input voltage is out outside of another range of voltage has also been implemented apart from the main peak-current control. This can be seen in Fig. 8.2.31.

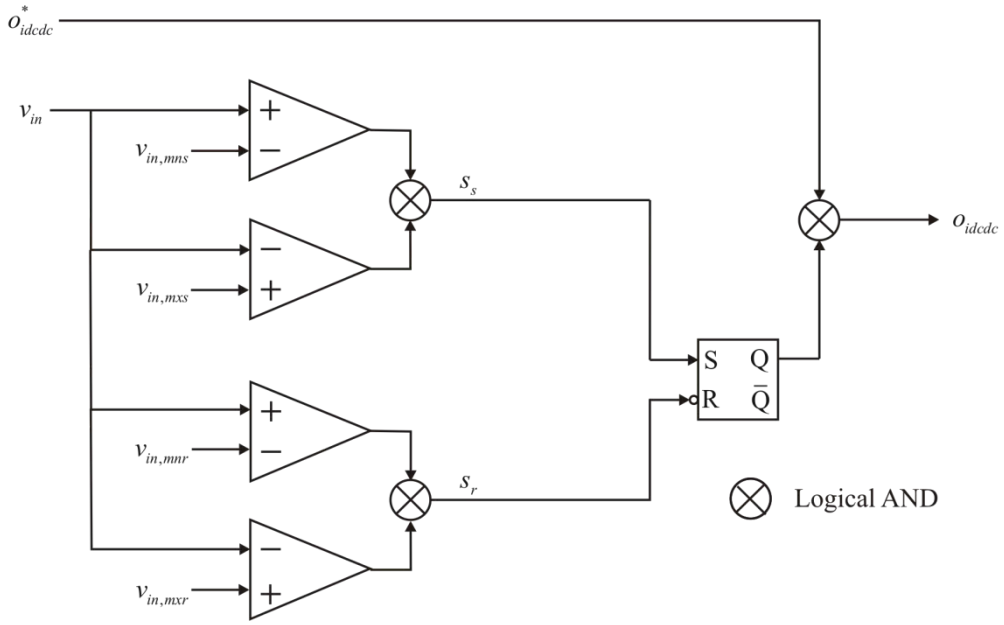

Fig. 8.2.31: Supervisory Control of the DC-DC Converter.

This supervisory control gives as output, o_{idcdc}, which is 1 if the DC-DC converter is operational and 0 if the DC-DC converter is non-operational.

First, the equations that determine the derivative of the states are presented. A variable, $\dot{v}^{**}$ is defined as follows.

$$\dot{v}^{**} = \frac{v^{*} - v^{**}}{\tau_{slr}} \tag{8.2.180}$$

where τ_{slr} is the slew-rate limit time constant. The time derivative of the slew-rate limited voltage command is obtained as

$$\frac{d}{dt}v^{**} = \begin{cases} \dot{v}^{**} & \text{if} \quad \dot{v}^{**}_{min} < \dot{v}^{**} < \dot{v}^{**}_{max} \\ \dot{v}^{**}_{max} & \text{if} \quad \dot{v}^{**} > \dot{v}^{**}_{max} \\ \dot{v}^{**}_{min} & \text{if} \quad \dot{v}^{**} < \dot{v}^{**}_{min} \end{cases} \tag{8.2.181}$$

The PI control with droop is detailed below:

$$v_e = \left(v^{**} - K_d i_{ld}\right) o_{idcdc} - v_{of} \tag{8.2.182}$$

where k_d is the droop constant and i_{ld} is the load current. The proportional part of the control is obtained as:

$$P_{PI} = K_p v_e \tag{8.2.183}$$

The integral part of the control is obtained from

$$\frac{d}{dt}I_{PI} = \left(K_i v_e\right) o_{idcdc} + \left(-K_i I_{PI}\right) \bar{o}_{idcdc} + I_{AWU} \tag{8.2.184}$$

$$i_{pmax} = \left(P_{PI} + I_{PI}\right) o_{idcdc} \tag{8.2.185}$$

wherein I_{AWU} is anti-windup, which is zero as long as the output of the control, i_{pmax}, is within the prescribed limits. If i_{pmax} is outside the prescribed limits, then the anti-windup can be defined as

$$I_{AWU} = \begin{cases} \dfrac{K_i(i_{pmax\_ul} - i_{pmax})}{\tau_{awu}} & i_{pmax} > i_{pmax\_ul} \\ \dfrac{K_i(i_{pmax\_ll} - i_{pmax})}{\tau_{awu}} & i_{pmax} < i_{pmax\_ll} \end{cases} \tag{8.2.186}$$

The time derivative of the output filter capacitor voltage, v_{of} is obtained as

$$\frac{d}{dt} v_{of} = \frac{i_{of} - i_{ld}}{C_{scm}} \tag{8.2.187}$$

The output filter capacitor voltage, v_{of} is a state and an output. Thus, based on the equations presented above, the only two quantities that need to be derived are i_{of} and i_{if}. These are obtained based on approximating the transformer primary and secondary current waveforms. These are presented in Fig. 8.2.32.

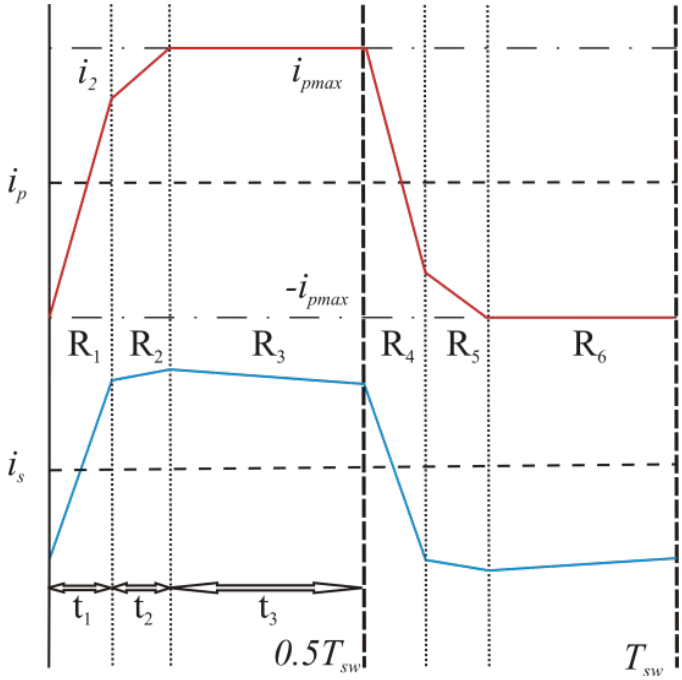

Fig. 8.2.32: Transformer Primary and Secondary Current Waveforms.

The following constants are first described:

$$K = \frac{N_1}{N_2} \tag{8.2.188}$$

$$C_1 = \frac{L_m\left(L_m + L_{ls} + K^2 L_{rec}\right)}{L_m\left(L_{lp} + L_{ls} + K^2 L_{rec}\right) + L_{lp}\left(L_{ls} + K^2 L_{rec}\right)} \tag{8.2.189}$$

$$C_2 = \frac{L_m\left(L_m + L_{lp}\right)}{L_m\left(L_{lp} + L_{ls} + K^2 L_{rec}\right) + L_{lp}\left(L_{ls} + K^2 L_{rec}\right)} \tag{8.2.190}$$

The time in each of the regions: t_1, t_2 and t_3, and i_2 can be obtained as follows:

$$t_1 = \frac{\left(i_2 + i_{pmax}\right)}{v_{if}\dfrac{\left(L_m + L_{ls}\right)}{\left(L_{lp} + L_{ls}\right)L_m + L_{lp}L_{ls}}} \tag{8.2.191}$$

$$t_2 = \frac{\dfrac{v_{of}}{KL_{rec}}\dfrac{Tsw}{2}}{C_2\left(\dfrac{v_{if}}{L_m + L_{lp}} - \dfrac{Kv_{of}}{L_m}\right) + \dfrac{v_{of}}{KL_{rec}}} \tag{8.2.192}$$

$$t_3 = \frac{T_{sw}}{2} - t_1 - t_2 \tag{8.2.193}$$

where

$$i_2 = i_{pmax} - C_1 t_2\left(\frac{v_{if}}{L_m} - \frac{Kv_{of}}{L_m + L_{ls} + K^2 L_{rec}}\right) \tag{8.2.194}$$

Using these expressions, i_{of} and i_{if} are obtained as follows:

$$i_{of} = \frac{1}{2}\frac{Kv_{if}L_m t_1}{\left(L_{lp} + L_{ls}\right)L_m + L_{lp}L_{ls}} \tag{8.2.195}$$

$$i_{if} = \frac{\left(\dfrac{-i_{pmax} + i_2}{2}\right)t_1 + \left(\dfrac{i_2 + i_{pmax}}{2}\right)t_2}{\dfrac{T_{sw}}{2}} \tag{8.2.196}$$

Thus, the complete model has been defined.

Validation:

This model is a highly simplified version of the model set forth in [5.21.1]. Although some studies using the model have been compared to detailed waveform level models, and these comparisons have been generally favorable, the model must be viewed as relatively immature.

References:

[5.21.1] Suryanarayana, H.; Sudhoff, S.D., "Average-value modeling of a peak-current controlled galvanically-isolated DC-DC converter for shipboard power distribution," Electric Ship Technologies Symposium (ESTS), 2013 IEEE , vol., no., pp.152,161, 22-24 April 2013.

8.1.20 DC Fault Detection Unit

The dc fault detection unit consists of a low voltage dc source connected to the DC bus. The unit is depicted in Fig. 8.2.33. This source is used to detect if a fault on the dc bus has been cleared such that the system can be brought back online.

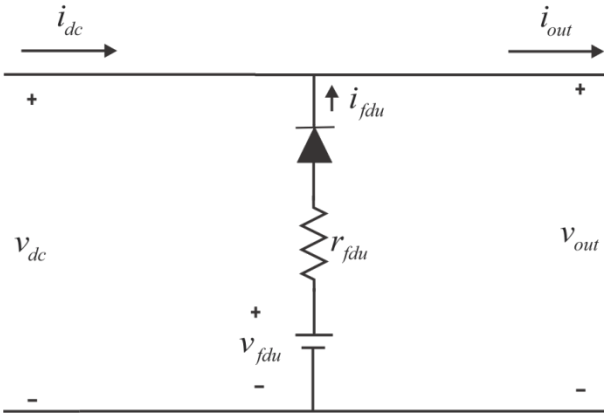

Fig. 8.2.33: DC Fault Detection Unit.

During non-fault operation, there is no current sourced from the fault detection supply due to the series diode. When a fault occurs, the dc voltage of the bus collapses due to fault detection features of the dc bus source. The dc bus will stay at zero as long as the fault is present. Once the fault is cleared, the bus voltage will rise above a threshold defined by the fault detection unit supply voltage. This is an indication to the system that the fault has been cleared and the system can be brought back online. The model structure for the fault detection unit is as follows.

Inputs:

v_{dc} The dc voltage on the bus prior to the unit (V)

i_{out} The dc current on the bus after the unit (A)

Outputs:

v_{out} The dc voltage on the bus after the unit (V)

i_{dc} The dc current in the bus prior to the unit (A)

F The fault status of the system

Parameters:

v_{fdu} The voltage level of the unit (V)

r_{fdu} The resistance of the unit (Ω)

Interface Equations:

$$i_{fdu} = \begin{cases} 0 & v_{dc} \geq v_{fdu} \\ \dfrac{v_{fdu} - v_{dc}}{r_{fdu}} & v_{dc} < v_{fdu} \end{cases} \quad (8.2.197)$$

$$i_{dc} = i_{out} - i_{fdu} \quad (8.2.198)$$

States:
None

Model Equations:

The fault status is determined by the voltage level of the bus. If the bus voltage, v_{out}, is less than the voltage level of the detection unit, then there is a fault on the system as the unit is unable to raise the bus voltage above the threshold. Therefore,

$$F = \begin{cases} 0 & v_{out} >= v_{fdu} \\ 1 & v_{out} < v_{fdu} \end{cases} \quad (8.2.199)$$

Validation:

This component could certainly be used and implemented in a power system, if desired.

References:
None

8.1.21 Non-Isolated Inverter Module

The Non-Isolated Inverter Module model is depicted in Fig. 8.2.34.

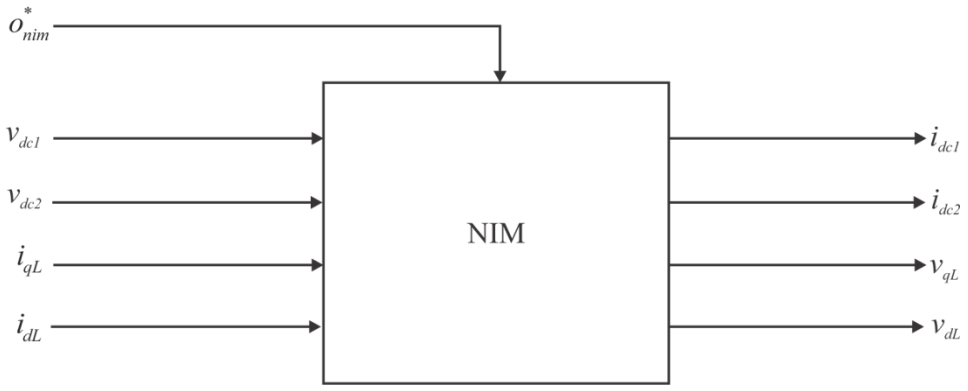

Fig. 8.2.34: Non-Isolated Inverter Module.

The component model structure is as follows.

Inputs:

v_{dc1} The dc voltage of the primary bus (V)

v_{dc2} The dc voltage of the secondary bus (V)

i_{qL} The *q*-axis load current (A)

i_{dL} The *d*-axis load current (A)

o_{nim}^{*} The desired operational status of the component

Outputs:

i_{dc1} The dc current drawn from the primary bus (A)

i_{dc2} The dc current drawn from the secondary bus (A)

v_{qL} The *q*-axis voltage on the load side (V)

i_{dc2} The *d*-axis voltage on the load side (V)

P_{out} The output power of the component (W)

Parameters:

i_{Lt} The threshold level load current (A)

i_{Lf} The fault level load current (A)

C The capacitance of the dc bus (F)

τ The time constant associated with the bus capacitance (s)

v_{q}^{*} The desired *q*-axis output voltage (V)

ω_{e} The electrical speed of the synchronous reference frame (rad/s)

v_{LL}^{*} The desired line-line output voltage (V)

Interface Equations:
None

States:

v_{q} The *q*-axis output voltage (V)

v_{d} The *d*-axis output voltage (V)

Model Equations:

The supervisory control for the NIM is depicted in Fig. 8.2.35. The inputs to the supervisory control are the measured dc voltages on each of the two busses, v_{dc1} and v_{dc2}, and the desired operational status of the load, o_{nim}^{*}.

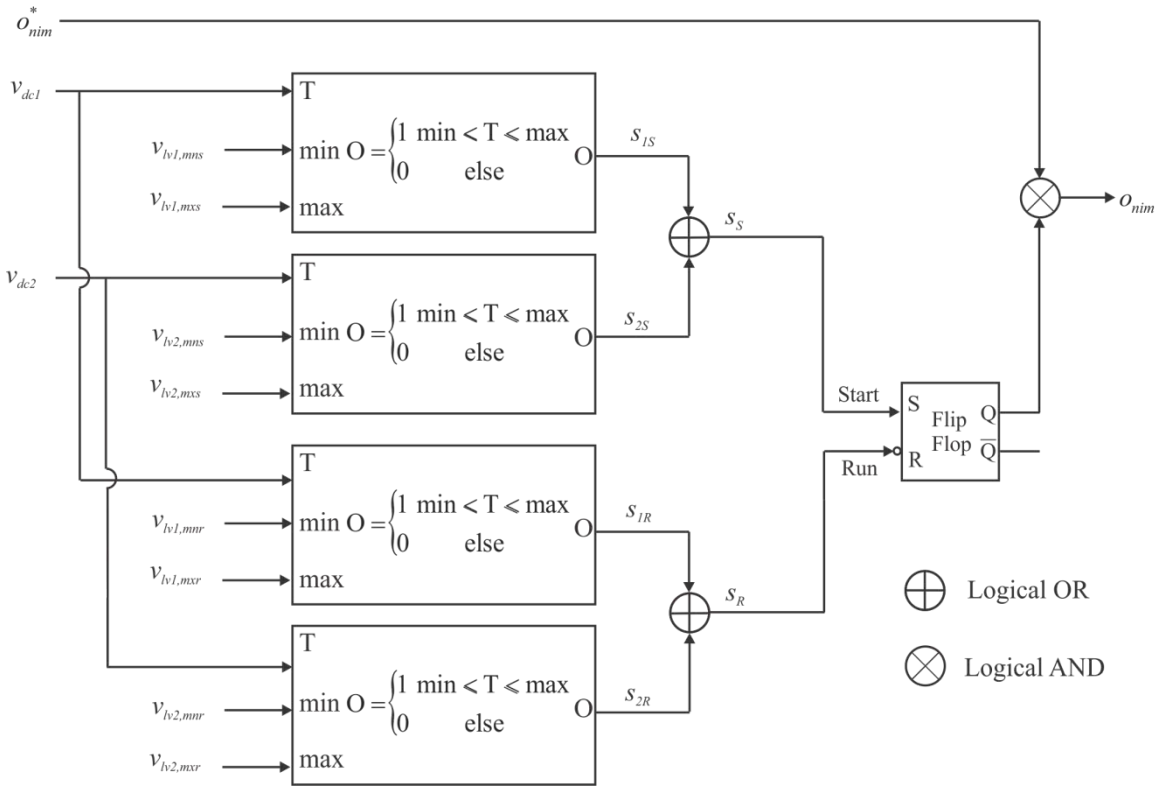

Fig. 8.2.35: NIM Supervisory Control.

The supervisory control categorizes each bus voltage into two categories. The first category relates to being appropriate to start and the second relates to whether the bus voltages are appropriate to continue running. These two conditions have different minimum and maximum voltages level requirements with the startup condition being the more stringent of the two. The output of the control is the operational state of the load, o_{nim}, and is dependent upon the voltage levels for each of the busses being within the limits for either the startup or running condition. The intermediate control variables s_{1S} and s_{2S} are true if the corresponding bus voltages are within their ranges governed by the appropriate min and max voltage levels for component start. One bus being within the required range makes the set input of the flip-flop to true. The intermediate control variables s_{1R} and s_{1R} are true if the corresponding bus voltages are within the range governed by the appropriate min and max voltage levels to run. If either of the two busses is within its required voltage range then the flip-flop is not reset. If they both are out of range then the flip-flop is reset.

The first step in calculating the outputs and states for the NIM is to obtain the rms load ac current. Given that the module is in operation, (o=1), this is done using

$$i_{L\text{rms}} = \frac{1}{\sqrt{2}}\sqrt{i_{qL}^2 + i_{dL}^2} \tag{8.2.200}$$

where i_{qL} is the q-axis load current and i_{dL} is the d-axis load current. The desired q-axis output voltage can then be expressed using the relationship depicted in Fig. 8.2.36.

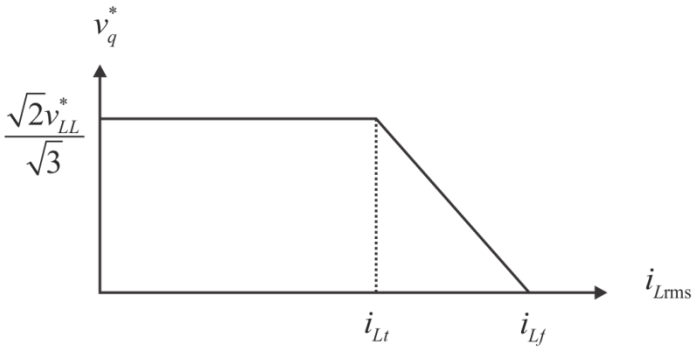

Fig. 8.2.36: NIM *q*-axis Voltage.

In the above figure, the desired *q*-axis voltage is a constant determined by the desired line-line voltage until the rms load current reaches a threshold value where it ramps to zero before the load current can reach the fault threshold. The desired *d*-axis voltage is zero.

Once the desired *q*-axis voltage is determined, the raw *q* and *d* axis currents are calculated using

$$i_{qir} = i_{qL} + \omega_e C v_d + \frac{C}{\tau}\left(v_q^* - v_q\right) \tag{8.2.201}$$

and

$$i_{dir} = i_{dL} - \omega_e C v_q - \frac{C}{\tau}\left(v_d\right) \tag{8.2.202}$$

where v_q and v_d are the states of the NIM. The rms raw inverter current is then calculated as

$$i_{mir} = \frac{1}{\sqrt{2}}\sqrt{i_{qir}^2 + i_{dir}^2} \tag{8.2.203}$$

If the raw rms inverter current, i_{mir}, is less than the threshold load current, i_{Lt}, then

$$i_{qi} = i_{qir} \tag{8.2.204}$$

and

$$i_{di} = i_{dir} \tag{8.2.205}$$

Otherwise,

$$i_{qi} = i_{qir}\left(\frac{i_{mir}}{\sqrt{2}i_{Lf}}\right) \tag{8.2.206}$$

and

$$i_{di} = i_{dir}\left(\frac{i_{mir}}{\sqrt{2}i_{Lf}}\right) \tag{8.2.207}$$

The states of the NIM are obtained from

$$\frac{dv_q}{dt} = \frac{1}{C}\left[i_{qi} - i_{qL} - \omega_e C v_d \right] \tag{8.2.208}$$

and

$$\frac{dv_d}{dt} = \frac{1}{C}\left[i_{di} - i_{dL} + \omega_e C v_q \right] \tag{8.2.209}$$

The output power is obtained from

$$P_{out} = \frac{3}{2}\left(v_q i_{qi} + v_d i_{di} \right) \tag{8.2.210}$$

and the dc current drawn by the NIM from the bus is

$$i_{dc1} = \begin{cases} 0 & o_{nim} = 0 \text{ or } s_{1R} = 0 \\ \dfrac{P_{out}}{v_{dc1}} & o_{nim} = 1 \text{ and } s_{1R} = 1 \end{cases} \tag{8.2.211}$$

$$i_{dc2} = \begin{cases} 0 & o_{nim} = 0 \text{ or } s_{2R} = 0 \\ \dfrac{P_{out}}{v_{dc2}} & o_{nim} = 1 \text{ and } s_{2R} = 1 \end{cases} \tag{8.2.212}$$

Validation:

This is a very simple model of the desired behavior of an inverter module. The degree to which it holds is a function of the specific converter design.

References:
None

9 APPENDIX B: MODEL PARAMETERS

9.1 Main Generator Parameters

Table 9.1.1: Parameters for Notional Single-Shaft Gas Turbine Model

Parameter	Description	Default Value	Source
a	Valve positioner constant.	1	
b	Valve positioner constant.	0.05	
c	Valve positioner constant.	1	
k_{flma}	No-load fuel parameter.	0.2	
k_{flmb}	No-load fuel parameter (1- k_{flma}).	0.8	
. $k_{\alpha\text{-}limit}$	Acceleration limit (pu/s).	0.01	
$k_{i\text{-}\alpha}$	Acceleration control integral gain.	100	
$L_{lower\text{-}Limit1}$	Lower limit for limit block "Limit 1" (fuel limit).	-0.1	
$L_{upper\text{-}Limit1}$	Upper limit for limit block "Limit 1" (fuel limit).	1.5	
T_c	Combustor delay time (s).	0.01	
W	Speed governor constant.	25	
X	Speed governor constant.	0	
Y	Speed governor constant.	0.05	
Z	Speed governor constant.	1	
τ_{FS}	Fuel system time constant (s).	0.4	
τ_{CP}	Compressor discharge volume time constant (s).	0.2	

Table 9.1.2: Parameters for Notional Twin-Shaft Gas Turbine Model

Parameter	Description	Default Value	Source
a	Valve positioner constant.	1	
b	Valve positioner constant.	0.05	
c	Valve positioner constant.	1	
k_{flma}	No-load fuel parameter.	0.2	
k_{flmb}	No-load fuel parameter (1- k_{flma}).	0.8	
k_{EFR1}	Engine speed request function slope.	0.25	
k_{EFR2}	Engine speed request function intercept.	0.75	
$k_{\alpha\text{-}limit}$	Acceleration limit (pu/s).	0.01	
$k_{i\text{-}\alpha}$	Acceleration control integral gain.	100	
$L_{lower\text{-}Limit1}$	Lower limit for limit block "Limit 1" (fuel limit).	-0.1	
$L_{upper\text{-}Limit1}$	Upper limit for limit block "Limit 1" (fuel limit).	1.5	
T_c	Combustor delay time (s).	0.01	
W	Speed governor constant.	25	
W_E	Engine speed governor constant.	30	
X	Speed governor constant.	0	
X_E	Engine speed governor constant.	1	
Y	Speed governor constant.	0.01	
Y_E	Engine speed governor constant.	1	
Z	Speed governor constant.	1	
Z_E	Engine speed governor constant.	0	
τ_{Ig}	Time constant for engine shaft dynamics (s).	8	
τ_{FS}	Fuel system time constant (s).	0.4	
τ_{CP}	Compressor discharge volume time constant (s).	0.2	

Table 9.1.3: Parameters for Notional Round Rotor Synchronous Machine

Parameter	Description	Default Value	Source
S_r	Rated apparent power (MVA).	47	
V_r	Rated voltage (line-line, RMS) (kV).	4.16	
f_r	Rated frequency (Hz).	240	
R_s	Stator resistance (pu).	2.0e-3	
L_l	Stator leakage reactance (pu)	0.15	
L_{md}	D-axis unsaturated magnetizing inductance (pu)	1.5	
L_{mq}	Q-axis unsaturated magnetizing inductance (pu)	1.5	
R_{fd}	Field resistance (pu)	1.0e-3	
L_{lfd}	Field leakage inductance (pu)	0.09	
R_{kd}	D-axis damper resistance (pu)	0.01	
L_{lkd}	D-axis damper leakage inductance (pu)	0.045	
R_{kq1}	Q-axis damper resistance (pu)	0.01	
L_{lkq1}	Q-axis damper leakage inductance (pu)	0.045	
R_{kq2}	Q-axis damper resistance (2^{nd} damper winding) (pu)	0.01	
L_{lkq2}	Q-axis damper leakage inductance (2^{nd} damper winding) (pu)	0.045	
H	Inertia constant (MW*s/MVA)	6	
F	Friction factor (pu).	0	
p	Pole pairs	4	
$V_{sat}(I_{fd})$	Saturation curve.	See Fig. 9.1.1	

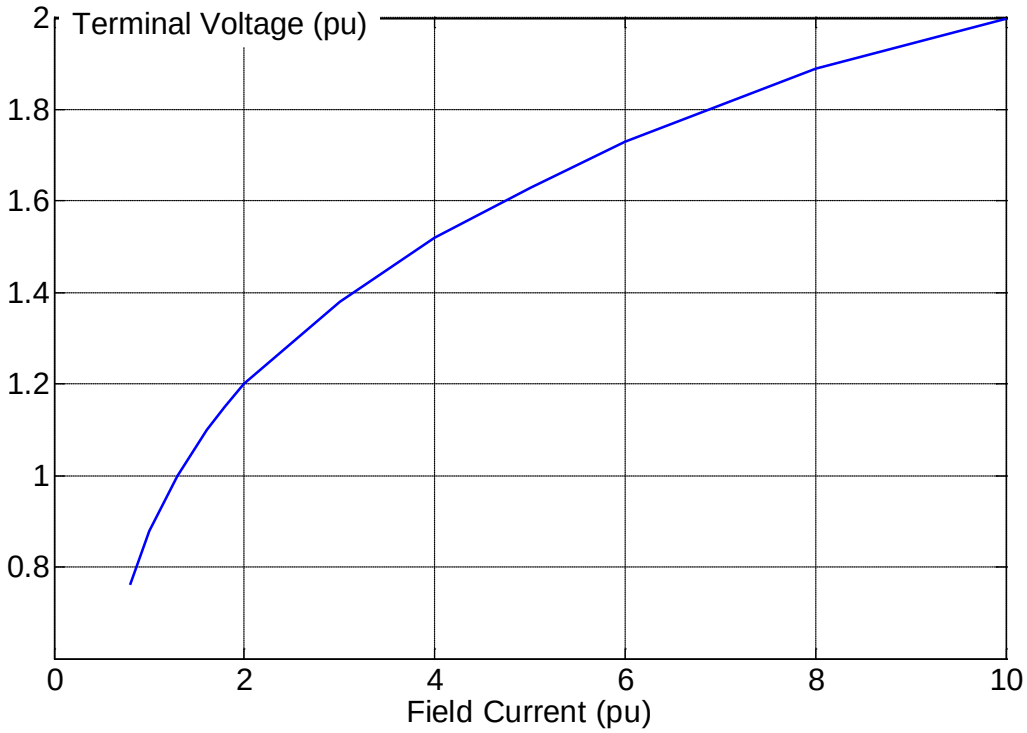

Fig. 9.1.1: Default Saturation Curve for Notional Round Rotor Synchronous Machine.

Table 9.1.4: Parameters for Simplified IEEE Type AC8B Exciter

Parameter	Description	Default Value	Source
k_A	Voltage regulator gain.	1	
k_{DR}	PID controller derivative gain.	0	
k_{IR}	PID controller integral gain.	0.08	
k_E		1	
k_{EF1}	Saturation function coefficient.	1.0119	
k_{EF2}	Saturation function coefficient.	0.0875	
k_{PR}	PID controller proportional gain.	200	
T_A	Voltage regulator time constant (s).	0.0001	
T_e	Integration time constant (s).	1	
T_{DR}	Filter time constant for PID controller derivative branch (s).	0.001	
V_{EMAX}	Field winding excitation voltage upper limit.	∞	
V_{EMIN}	Field winding excitation voltage lower limit.	0	
V_{RMAX}	Voltage regulator upper limit.	5	
V_{RMIN}	Voltage regulator lower limit.	0	

9.1.1 MVAC Specific Parameters

Table 9.1.5: Parameters for Generator Models of MVAC System

		Generators 1 and 2 (main)	Generator 3 and 4 (auxiliary)
Main specifications			
Power (MVA)		47	5
Speed (rpm)		3600	3600
Number of poles		2	2
Frequency (Hz)		60	60
Voltage (kV)		4.16	4.16
Power factor		0.8	0.8
Parameters in (p.u); where p.u.=actual value/base value; Base impedance=base (KV)^2/base MVA			
Stator winding resistance	Rs	0.002	0.005
Stator winding leakage inductance	Ll	0.135	0.09
Stator d-axis mutual inductance	Lmd	1.35	0.9
Stator q-axis mutual inductance	Lmq	1.35	0.9
Field-winding resistance	Rf	0.001	0.001
Field-winding leakage inductance	Llf	0.081	0.045
d-axis damper resistance	Rkd	0.045	0.04
d-axis damper leakage inductance	Llkd	0.0225	0.018
q-axis damper1 resistance	Rkq1	0.01	0.04
q-axis damper1 leakage inductance	Llkq1	0.0405	0.018
q-axis damper2 resistance	Rkq2	0.01	0.04
q-axis damper2 leakage inductance	Llkq2	0.0405	0.018
Inertia Constant	H	4s	5s
Friction factor (N.m.s)	F	0.04	0.04

9.1.2 HFAC Specific Parameters

Table 9.1.6: Parameters for Gas Turbine Models of HFAC System

		Gas turbines 1 and 2 (main)	Gas turbines 3 and 4 (aux)
Main turbine specifications			
Type		Twin-shaft	Single-shaft
Turbine cycle		Simple-cycle	Simple-cycle
Power (MW)		36	4
Speed (rpm)		3600	14400
Engine speed (rpm)		~5000 (assumed)	N/A
Main turbine control parameters			
Speed governor gain		25(4% droop)	25
Speed governor time constant		0.01	0.05
Maximum power limit		1.5	1.5
Minimum power limit		-0.1	-0.1
Valve positioning gain		1	1
Valve positioning time constant		0.05	0.05
Fuel system gain		1	1
Fuel system time constant		0.4	0.4
Combustor time constant		0.01	0.01
Compressor time constant		0.2	0.2
No load fuel (p.u)		0.20	0.20
Engine speed control parameters			
Governor gain		30	N/A
Governor time constant		1	N/A
Governor lag		1	N/A

9.1.3 MVDC Specific Parameters

Table 9.1.7: MTG Parameters for Simscape Notional MVDC System

Parameter	Description	Value	Units
S_b	Rated Apparent Power	47	MVA
rpm	Rated Rotor Speed	3600	rpm
f_b	Rated Electrical Frequency	240	Hz
H	Inertia Constant	6	kW.s/kVA
Poles	Number of Poles	8	n/a
r_s	Stator Winding Resistance	2.0e-3	pu
L_{ls}	Stator Leakage Inductance	0.15	pu
L_{mq}	q-axis Magnetizing Inductance	1.5	pu
L_{md}	d-axis magnetizing Inductance	1.5	pu
r_{kq}	q-Damper Winding Resistance	0.01	pu
L_{lkq}	q-Damper Winding Leakage Inductance	0.045	pu
r_{kd}	d-Damper Winding Resistance	0.045	pu
L_{lkd}	d-Damper Winding Leakage Inductance	0.025	pu
r_{fd}	Field Winding Resistance	1e-3	pu
L_{lfd}	Field Winding Leakage Inductance	0.09	pu
sys_{droop}	Proportional Power Sharing factor	5	n/a
k_p	Exciter Proportional Gain	10	n/a
k_i	Exciter Integral Gain	10	n/a
k_d	Exciter Derivative Gain	0.2	n/a
V_{rmax}	Voltage Regulator Upper Limit	500	pu
V_{rmax}	Voltage Regulator Lower Limit	0	pu

Table 9.1.8: MTG Prime Mover Module Parameters for Simscape Notional MVDC System

Parameter	Description	Value
W_{1q}	Speed governor proportional gain	30
X_{1q}	Speed governor integral gain	1
W_1	Free Turbine speed governor proportional gain	25
X_1	Free Turbine speed governor integral gain	0

Table 9.1.9: MTG Rectifier Module Parameters for Simscape Notional MVDC System

Parameter	Description	Value	Units
Rch	Charging resistor for DC filter capacitance	63	Ω
C_{dc}	DC Capacitance	0.384e-3	mF
R_{dc}	DC Resistance	0	Ω
L_c	AC Inductance	7.65e-5	mH
L_{dc}	DC Inductance	0	H

Table 9.1.10: Parameters for Main Generator Modules of Baseline MVDC System

Parameter	Description	Value	Source
k_{droop}	Power droop factor.	0.05	
k_{scale}	Prime mover scaling factor (prime mover rated power (36 MW) divided by synchronous machine base apparent power (47 MVA).)	0.7660	

Table 9.1.11: Parameters for Prime Mover Model of Main Generator Module of Baseline MVDC System

Parameter	Description	Value	Source
$k_{p\text{-}SG}$	Speed governor proportional gain.	25	
$k_{i\text{-}SG}$	Speed governor integral gain.	8	

Table 9.1.12: Parameters for Rectifier Model of Main Generator Module of Baseline MVDC System

Parameter	Description	Value	Source
Rch	Charging resistor for DC filter capacitance (Ω)	50	
C_{bs}	Bypass Switch Snubber capacitance (F).	1.0e-6	
R_{bs}	Bypass Switch Snubber resistance (Ω).	500	
R_{on}	Bypass Switch on-state resistance (Ω).	1.0e-6	

9.2 Auxiliary Generator Parameters

9.2.1 MVDC Specific Parameters

Table 9.2.1: ATG Parameters for Simscape Notional MVDC System

Parameter	Description	Value	Units
S_b	Rated Apparent Power	5	MVA
rpm	Rated Rotor Speed	14400	rpm
f_b	Rated Electrical Frequency	240	Hz
H	Inertia Constant	10	kW.s/kVA
Poles	Number of Poles	2	n/a
r_s	Stator Winding Resistance	5.0e-3	pu
L_{ls}	Stator Leakage Inductance	0.1	pu
L_{mq}	q-axis Magnetizing Inductance	1	pu
L_{md}	d-axis magnetizing Inductance	1	pu
r_{kq}	q-Damper Winding Resistance	0.01	pu
L_{lkq}	q-Damper Winding Leakage Inductance	0.045	pu
r_{kd}	d-Damper Winding Resistance	0.045	pu
L_{lkd}	d-Damper Winding Leakage Inductance	0.025	pu
r_{fd}	Field Winding Resistance	1e-3	pu
L_{lfd}	Field Winding Leakage Inductance	0.05	pu
sys_{droop}	Proportional Power Sharing factor	5	n/a
k_p	Exciter Proportional Gain	10	n/a
k_i	Exciter Integral Gain	10	n/a
k_d	Exciter Derivative Gain	0.2	n/a
V_{rmax}	Voltage Regulator Upper Limit	5	pu
V_{rmax}	Voltage Regulator Lower Limit	0	pu

Table 9.2.2: ATG Prime Mover Module Parameters for Simscape Notional MVDC System

Parameter	Description	Value
W	Speed governor proportional gain	25
X	Speed governor integral gain	8

Table 9.2.3: ATG Rectifier Module Parameters for Simscape Notional MVDC System

Parameter	Description	Value	Units
Rch	Charging resistor for DC filter capacitance	63	Ω
C_{dc}	DC Capacitance	0.384	mF
R_{dc}	DC Resistance	0	Ω
L_c	AC Inductance	.0765	mH
L_{dc}	DC Inductance	0	H

Table 9.2.4: Parameters for Auxiliary Generator Modules of Baseline MVDC System

Parameter	Description	Value	Source
k_{droop}	Power droop factor.	0.05	
k_{scale}	Prime mover scaling factor (prime mover rated power (4 MW) divided by synchronous machine base apparent power (5 MVA).)	0.8	

Table 9.2.5: Parameters for Prime Mover Model of Auxiliary Generator Module of Baseline MVDC System

Parameter	Description	Value	Source
$k_{p\text{-}SG}$	Speed governor proportional gain.	25	
$k_{i\text{-}SG}$	Speed governor integral gain.	8	

Table 9.2.6: Parameters for Synchronous Machine Model of Auxiliary Generator Module of Baseline MVDC System

Parameter	Description	Value	Source
S_r	Rated apparent power (MVA).	5	
R_s	Stator resistance (pu).	5.0e-3	
L_l	Stator leakage reactance (pu)	0.1	
L_{md}	D-axis unsaturated magnetizing inductance (pu)	1.0	
L_{mq}	Q-axis unsaturated magnetizing inductance (pu)	1.0	
L_{lfd}	Field leakage inductance (pu)	0.05	
H	Inertia constant (MW*s/MVA)	10	
p	Pole pairs	1	

Table 9.2.7: Parameters for Rectifier of Auxiliary Generator Module of Baseline MVDC System

Parameter	Description	Value	Source
C_d	DC side filter capacitance (F).	0.111e-3	
L_s	AC side series inductance (H).	1.1e-3	

9.3 AC/DC Rectifiers

Table 9.3.1: Parameters for Notional Diode Rectifier Model

Parameter	Description	Default Value	Source
C_d	DC side filter capacitance (F).	1e-3	
C_{snub}	Diode snubber capacitance (F).	1e-5	
L_s	AC side series inductance (H).	1.24e-4	
L_d	Diode on-state inductance (H).	0	
R_d	Diode on-state resistance (Ω).	1e-5	
R_s	AC side series resistance (Ω).	7.5e-3	
R_{snub}	Diode snubber resistance (Ω).	100	

9.3.1 MVAC Specific Parameters

Table 9.3.2: Parameters for Uncontrolled Diode Rectifier Models of MVAC System

Parameters	Values
Snubber capacitance, C_s	1e-7 F
Snubber resistance, R_s	10000 Ohm
On-state resistance, R_d	0.001 Ohm
Forward voltage, V_f	0.8 V

9.4 DC/DC Converter Parameters

Table 9.4.1: Parameters for Isolated DC-DC converter

Parameter	Description	Default Value	Source
	High-voltage side circuit		
L_{IF}	Input filter inductance (H)	25e-6	
R_{HV1}	Resistance towards ground (ohm)	5000	
R_{HVC}	Series resistance (ohm)	0.001	
R_{ch}	Charging resistor (ohm)	10	
C_{HVC}	Capacitor (F)	5e-3	
L_{HV}	Inductance (uH)	400e-6	
	Transformer		
V_H	high-side voltage (V)	5000	
V_L	low-side voltage (V)	1050	
f	frequency (Hz)	2500	
S	Nominal power (VA)	5e6	
R_1	Primary side winding resistance (pu)	0	
L_1	Primary side leakage reactance (pu)	0	
R_2	Secondary side winding resistance (pu)	0	
L_2	Secondary side leakage reactance (pu)	0	
R_m	Magnetization resistance (pu)	5000	
L_m	Magnetization reactance (pu)	5000	
	Low-voltage side circuit		
R_{CC}	Clamping capacitor series resistance (ohm)	1e-4	
C_{CC}	Clamping capacitor (mF)	4.86	
L_{CP}	Inductance low-voltage side (H)	1e-3	
R_{LV1}	Resistance towards ground (ohm)	500	
R_{LVC}	Series resistance of capacitor (ohm)	1e-4	
C_{LVC}	Low-voltage capacitor (F)	0.0128	
R_{LV}	Resistance low-voltage side (ohm)	1e-3	
	Switch parameters		
R_{ON}	resistance (ohm)	10e-6	
R_S	snubber resistance (ohm)	500	
C_S	snubber capacitance (F)	250e-9	
f	switching frequency (Hz)	500	

Table 9.4.2: Controller Parameters for Isolated DC-DC converter

Parameter	Description	Default Value	Source
	Buck mode PID-controller with anti-windup		
T_{fbu}	filter time constant (s)	1e-3	
k_P	proportional gain	0.08	
k_I	integral gain	1	
IS_i		0.02	
k_D	derivative gain	0	
N	*derivative filter factor*	50	
max	maximum control signal	0.49	
min	minimum control signal	0.01	
scaleE	Scaling factor on error signal	1e-2	
$TfbuI_C$		1e-3	
actDamp		-0. 2	
droop	Current droop factor	1e-3	
	Converter enable scheme (voltage/time-based)		
VthOff	p.u. voltage level difference from nominal	0.2	
VthOn	p.u. voltage level difference from nominal	0.1	
Tpu	Pick-up time (s) to enable or disable the controller based on under/over-voltage conditions on the MVDC supply bus.	0.01	
Discrete filter	Voltage 1st-order filter with time constant 10 ms		

9.5 Propulsion System Parameters

Table 9.5.1: Parameters for Notional Permanent Magnet Machine

Parameter	Description	Default Value	Source
R_s	Stator resistance (Ω).	0.005	
L_d	D-axis stator inductance (H).	0.8e-3	
L_q	Q-axis stator inductance (H).	0.8e-3	
λ	Flux linkage established by magnets (V·s).	16.58	
J	Moment of inertia (kg·m^2)	1.6e3	
F	Friction (N·m·s)	0.0005	
p	Pole pairs.	12	

Table 9.5.2: Parameters for Two-Level IGBT Bridge Model

Parameter	Description	Default Value	Source
C_s	Snubber capacitance (F).	1.0e-6	
R_{on}	IGBT on-state resistance (Ω).	1.0e-3	
R_s	Snubber resistance (Ω).	1000	
T_f	Fall time for the IGBT (s).	1.0e-6	
T_t	Tail time for the IGBT (s).	2.0e-6	
V_f	IGBT forward voltage drop (V).	0.8	
V_{fd}	Diode forward voltage drop (V).	0.8	

Table 9.5.3: Parameters for Hysteresis Current Control for Two-Level Drive for Permanent Magnet Synchronous Machine

Parameter	Description	Default Value	Source
$I_{d\text{-}r}$	Requested d-axis current (A).	0	
$I_{q\text{-}r\text{-}max}$	PI controller upper limit (A).	∞	
$I_{q\text{-}r\text{-}min}$	PI controller lower limit (A).	-∞	
k_i	PI controller integral gain.	10	
k_p	PI controller proportional gain.	7500	
p	The number of pole pairs of the machine.	12	
ΔI	Hysteresis comparator dead-band width parameter.	0	

Table 9.5.4: Parameters for Notional Fixed-Pitch Propeller Model

Parameter	Description	Default Value	Source
ρ	Density of salt water.	1027 kg/m^3	
D	Propeller diameter.	7.01 m	
η_r	Relative rotative efficiency.	1.0	
$C_Q(v)$	Open water propeller torque coefficient	Used generic data (developed from 2 sets of data)	Ref: [5.12.2] and [5.12.3]
$C_\tau(v)$	Open water propeller thrust coefficient	same as above	same as above
$1\text{-}w_T$	Taylor wake fraction.	same as above	same as above
$1\text{-}t$	Thrust deduction factor.	$\begin{cases} 0.96, & V_{ship} \geq 0 \\ 0.97, & V_{ship} < 0 \end{cases}$	0

Table 9.5.5: Additional Parameters Associated with Notional Fixed-Pitch Propeller Model

Parameter	Description	Default Value	Source
J_1	Moment of inertia of the starboard propeller (not used in the model).	2.0573e5 kg·m^2	0
J_2	Moment of inertia of the port propeller (not used in the model).	2.2767e5 kg·m^2	0

Table 9.5.6: Parameters for Notional Destroyer Hydrodynamic Characteristics Model

Parameter	Description	Default Value	Source
m_{ship}	Mass of the ship.	14.29e6 kg	
$F_{drag}(V_{ship})$	Hydrodynamic resistance.	See Fig. 9.5.1	

Fig. 9.5.1: Hydrodynamic Resistance for Notional Destroyer Model

9.5.1 MVDC Specific Parameters

Table 9.5.7: Propulsion Module Parameters for Simscape Notional MVDC System

Parameter	Description	Value	Units
P_{base}	Rated Real Power	36.5	MW
ω_{base}	Rated Mechanical Speed	12.5664	rad/s
J	Moment of Inertia	1.6e3	kg/m^2
Poles	Number of Poles	24	n/a
r_s	Stator Winding Resistance	5	mΩ
L_{mq}	q-axis Magnetizing Inductance	0.8	H
L_{md}	d-axis Magnetizing Inductance	0.8	H
Λ	Air Gap Flux	16.58	V.s
K_i	Voltage Regulator Integral Gain	4.8e5	n/a
K_p	Voltage Regulator Proportional Gain	7.92e5	n/a
L_{dc}	DC Link Inductance	3.9	mH
C_{dc}	DC Link Capacitance	5	mF
L_{ac}	AC Side Inductance	0.39	mH

Table 9.5.8: Parameters for Propulsion Modules of Baseline MVDC System

Parameter	Description	Value	Source
L_f	Filter inductance (H).	10.0e-6	
R_f	Filter resistance (Ω).	0.001	

Table 9.5.9: Parameters for Permanent Magnet Machine for Propulsion Module of Baseline MVDC System

Parameter	Description	Value	Source
J	Moment of inertia (kg·m^2) (Starboard)	4.3687e5	
J	Moment of inertia (kg·m^2) (Port)	4.5881e5	

Table 9.5.10: Parameters for Motor Drives for Propulsion Module of Baseline MVDC System

Parameter	Description	Value	Source
R_s	Snubber resistance (Ω).	500	
T_f	Fall time for the IGBT (s).	10.0e-6	
T_t	Tail time for the IGBT (s).	20.0e-6	

Table 9.5.11: Parameters for Motor Drive Controls for Propulsion Module of Baseline MVDC System

Parameter	Description	Value	Source
$I_{q\text{-}r\text{-}max}$	PI controller upper limit (A).	8.9550e3	
$I_{q\text{-}r\text{-}min}$	PI controller lower limit (A).	0	

Table 9.5.12: Parameters for Braking Resistor for Propulsion Module of Baseline MVDC System

Parameter	Description	Value	Source
V_{max}	Maximum voltage set point (V).	6500	

9.6 Ship Service Load Parameters

Table 9.6.1: Ship Service Load Data

ID1	Type	ID2	Battle mode (kW)	Cruise mode (kW)	Original Syntek lumped load category	ESRDC Initial baseline implementation
Z1	DC	Z1L1	150	70	DC loads 1	Constant impedance load (resistive load)
Z2	DC	Z1L2	615	0	DC loads 2	Same as Z1
Z3	AC	Z1L3	715	640	Type 1 AC loads	Same as Z1
Z4	AC	Z1L4	400	390	120/208 VAC loads	450 Vac 3-phase (resistive load)
Z5	AC	Z1L5	910	275	Non-vital type 1 AC loads	450 Vac 3-phase constant impedance load (RL)
Z6	AC	Z1L6	0	7	Non-vital single-phase AC loads	120/208 AC load (constant impedance load (RL))
			1460 **1330**	**735** **647**		
			2790	1382		
Z7	DC	Z2L1	1	0	Non-vital DC loads	Lumped DC load (resistive)
Z8	DC	Z2L2	75	20	DC loads	Same as Z2
Z9	AC	Z2L3	1400	930	Type 1 AC loads	Same as Z3
Z10	AC	Z2L4	750	300	120/208 VAC loads	Same as Z4
Z11	AC	Z2L5	975	400	Non-vital type 1 AC loads	Same as Z5
Z12	AC	Z2L6	40	35	Non-vital 120/208 AC loads	Same as Z6
			1726 **1515**	**700** **985**		
			3241	1685		
Z13	DC	Z3L1	40	20	DC loads	Same as Z1
Z14	AC	Z3L2	1200	1200	Type 1 AC loads	Same as Z2
Z15	AC	Z3L3	1900	550	120/208 VAC loads	Same as Z3
Z16	AC	Z3L4	750	375	Non-vital, type 1 AC loads	Same as Z4
Z17	AC	Z3L5	0	4	Non-vital, 120/208 AC loads	Same as Z5
			790 **3100**	**1750** **399**		
			3890	2149		
Z18	DC	Z4L1	60	0	DC loads	Same as Z2
Z19	AC	Z4L2	480	200	Type 1 AC loads	Same as Z3
Z20	AC	Z4L3	1750	415	120/208 VAC loads	Same as Z4
Z21	AC	Z4L4	675	220	Non-vital, 120/208 AC loads	Same as Z5
Z22	AC	Z4L5	0	4	Non-vital, 120/208 AC loads	Same as Z6
			735 **2230**	**224** **615**		
			2965	839		
Z23	DC	Z5L1	3750	2850	HP Radar	DC const. impedance load
			4701 **8175**	**3409** **2646**		
Total Load Power			**12872** (kW)	**6055** (kW)		
	Loads initially connected to upper bus					
	Loads initially connected to lower bus					

9.6.1 MVDC Specific Parameters

Table 9.6.2: Pickup Time Values for Isolated DC/DC Converters

Converter	Time (s)
Zone 1 Port	0.01
Zone 1 Starboard	0.045
Zone 2 Port	0.02
Zone 2 Starboard	0.035
Zone 3 Port	0.03
Zone 3 Starboard	0.025
Zone 4 Port	0.04
Zone 4 Starboard	0.015
Zone 5 Port	0.05
Zone 5 Starboard	0.055

Table 9.6.3: Parameters for simplified zonal load representation (Zone 1S)

Parameter	Description	Default Value	Source
P	Power demand (taken from zonal load data) (W)	[2790e3 1382e3]	
P_r	power ripple, 10% of power demand (W)	[0 0]	
f_r	ripple frequency (Hz)	[1.0e3 1.0e3]	
T_i	current injection time constant (s)	$1/(2\pi 10)$	
Fi	discrete 1st-order filter	c2d(tf(0,[Ti 1]),Ts)	
V_{min}	minimum voltage level (pu)	0.8	
dec	down sampling (decimation)	10e3	

Table 9.6.4: Parameters for simplified zonal load representation (Zone 2)

Parameter	Description	Default Value	Source
P	Power demand (taken from zonal load data)	[3241e3 1685e3]	

Table 9.6.5: Parameters for simplified zonal load representation (Zone 3)

Parameter	Description	Default Value	Source
P	Power demand (taken from zonal load data)	[3890e3 2149e3]	

Table 9.6.6: Parameters for simplified zonal load representation (Zone 4)

Parameter	Description	Default Value	Source
P	Power demand (taken from zonal load data)	[2965e3 839e3]	

Table 9.6.7: Parameters for simplified zonal load representation (Zone 5)

Parameter	Description	Default Value	Source
P	Power demand (taken from zonal load data)	[3750e3 2850e3]	

9.7 Pulsed Load Parameters

Table 9.7.1: Notional Free Electron Laser Data

FEL load definitions					Modes of operation (required power in KW)				
					Pier side	Under way	Operational readiness	Hot standby	Engagement
Z6L1	Filament(1)	10KW	AC	4.16kV\240Hz	10	10	10	10	10
Z6L2	RF	16MW	DC	45 KV	-	-	80	16000	16000
Z6L3	Beam dump	7.7MW	AC	4.16KV\60Hz	-	-	38.5	7700	7700
Z6L4	Cooling	300kW	AC	4.16kV\60Hz	300	300	300	300	300
Z6L5	Cryogenics	1MW	AC	450V\60Hz	100	1000	1000	1000	1000
Z6L6	Beam control	20KW	AC	450V\60Hz	-	-	-	-	20
Z6L7	Vacuum	5kW	AC	450V\60Hz	5	5	5	5	5
Z6L8	Beam optics	1KW	AC	112.5V\60Hz			1	1	1
Z6L9	Computers	5KW	AC	112.5V\60Hz	5	5	5	5	5
Z6L10	Housekeeping	5KW	AC	112.5V\60Hz	5	5	5	5	5
Z6L11	Wiggler(2)	~0(2)	DC	600 V	-	-	-	-	-
Total power during each mode of operation (kW)					**425**	**1325**	**1444.5**	**25026**	**25046**
Transition times					**days**	**hours**	**minutes**	**seconds**	**~ 1 second**

9.7.1 MVAC Specific Parameters

Table 9.7.2: Pulse Load Parameters for Simscape Notional MVAC System

Parameter	Description	Value	Method
$V_{AC,HV}$	AC Type GPL High Voltage Input	4.16 kV	Direct to Port Side Bus
$V_{DC,HV}$	DC Type GPL High Voltage Input	36.55 kV	Step Up Transformer and ZAR
$V_{AC,LV}$	AC Type GPL Low Voltage Input	112.5 V	Transformer
$V_{DC,LV}$	DC Type GPL Low Voltage Input	112.5 V	Transfomer

9.7.2 MVDC Specific Parameters

Table 9.7.3: Pulse Load Parameters for Simscape Notional MVDC System

Parameter	Description	Value	Units
$Pulse_{req}$	Magnitude	3	kA
$Pulse_{t}$	Duration	3.33	S
$Pulse_{slew1}$	Positive Slew Rate	1	kA/s
$Pulse_{slew2}$	Negative Slew Rate	10	kA/s

Table 9.7.4: Parameters for pulse load

Parameter	Description	Default Value	Source
t_{pulse}	pulse timing (s)	[0 1 1.01 3.5 3.51 7 7.01 9.25 9.26 10]	
P_{pulse}	pulse power (kW)	[0 0 400 400 1300 1300 25000 25000 0 0]*1000	
T_i	current injection time constant (s)	$1/(2\pi 700)$	
R_p	parallel resistance (ohm)	5000	
eta	interface efficiency (%)	97	
V_{min}	minimum voltage level (V)	4000	

9.8 Transformer Parameters

Table 9.8.1: Parameters for Three-phase, Two Winding Transformer

Parameter	Description	Default Value	Source
C_1	Configuration of side 1 windings ({Y, Delta})	Delta	
C_2	Configuration of side 2 windings ({Y, Delta})	Delta	
$C_{1\text{-}Y}$	Configuration of side 1 Y (if applicable) ({exposed neutral, unexposed neutral, NA})	NA	
$C_{2\text{-}Y}$	Configuration of side 2 Y (if applicable) ({exposed neutral, unexposed neutral, NA})	NA	
S_b	Rated apparent power (MVA).	5	
f_b	Rated frequency (Hz).	60	
V_1	Winding 1 rated RMS line-line voltage (kV).	4.16	
R_1	Winding 1 resistance (pu).	0.001	
X_1	Winding 1 leakage reactance (pu).	0.01	
V_2	Primary side rated RMS line-line voltage (kV).	4.16	
R_2	Primary side winding resistance (pu).	0.001	
X_2	Primary side leakage reactance (pu).	0.01	
R_m	Magnetization resistance (pu).	500	
X_m	Magnetization reactance (pu).	500	
$\Phi(i)$	Saturation characteristic.	NA (saturation disabled)	

9.9 Energy Storage Parameters

Table 9.9.1: General Parameters for Notional Supercapacitor Energy Storage System

Parameter	Description	Default Value	Source
	Supercapacitor (SC) Power	4.0 MW	Developed parameters based on design study. Supercapacitor data taken from commercial components (General Atomics website)
	Supercapacitor (SC) energy	100 MJ (approximately)	
	Capacitance of Supercapacitor (SC)	850.5 F	
	Supercapacitor (SC) initial voltage	500 V	
eL	Inductance	2×10^{-4} H	
eR	Resistance	0.0001 ohm	
C1	Dc link capacitance	0.2 F	
eL1	Inductance	5×10^{-8} H	
	Transformer Nominal power	5 MVA	
	Transformer Nominal frequency	60 Hz	
	Transformer Winding 1 voltage, V1 Ph-Ph (Vrms)	4.16KV	
	Transformer Winding 1 resistance, R1 (pu)	0.002	
	Transformer Winding 1inductance, L1 (pu)	0.045	
	Transformer Winding 2 voltage, V2 Ph-Ph (Vrms)	0.45KV	
	Transformer Winding 2 resistance, R2 (pu)	0.002	
	Transformer Winding 2 inductance, L2 (pu)	0.045	
	Transformer Magnetization resistance, Rm (pu)	500	
	Transformer Magnetization inductance, Lm (pu)	500	

Table 9.9.2: Parameters for Notional Supercapacitor Energy Storage System Inverter

Parameter	Description	Default Value	Source
ecarrierF	Carrier frequency	2400 Hz	Developed parameters based on design study.
eModIndex	Modulation index	0.84	
Rs	Snubber resistance	1×10^{5} Ohm	
Cs	Snubber capacitance	1×10^{-9} F	

Table 9.9.3: Parameters for Notional Supercapacitor Energy Storage System Buck/boost converter

Parameter	Description	Default Value	Source
eIcharge	Charging current	6000 A	Developed parameters based on design study.
eboostV	Boost voltage	825 V	
eboostF	Boost frequency	1,000 Hz	

9.9.1 MVDC Specific Parameters

Table 9.9.4: MVDC Supercapacitor Parameters

Parameter	Description	Default Value	Source
R_{SC}	Series resistance (ohm)	100e-6	
L_{SC}	Series inductance (H)	200e-6	
C_{SC}	Capacitance (F)	300	
V_{SC0}	Initial capacitor voltage (V)	850	

9.10 Cable Parameters

9.10.1 MVDC Specific Parameters

Table 9.10.1: Cable Parameters in MVDC System

Switchboard 1	Switchboard 2	Resistance	Inductance
Zone 1 Port	Zone 2 Port	1.69e-4 Ω	0 H
Zone 1 Port	Zone 1 Starboard	2.35e-4	0 H
Zone 1 Starboard	Zone 2 Starboard	1.95e-4 Ω	0 H
Zone 2 Port	Zone 3 Port	1.84e-4 Ω	0 H
Zone 2 Starboard	Zone 3 Starboard	1.82e-4 Ω	0 H
Zone 3 Port	Zone 4 Port	2.14e-4 Ω	0 H
Zone 3 Starboard	Zone 4 Starboard	1.66e-4 Ω	0 H
Zone 4 Port	Zone 4 Starboard	2.99e-4 Ω	0 H

9.11 Resistor Brake Parameters

Table 9.11.1: Parameters for Shunt Braking Resistor

Parameter	Description	Default Value	Source
C_{snub}	Snubber capacitance (F).	∞	
L_{on}	On-state inductance of the semiconductor switch (H).	0	
R_{shunt}	Resistance of shunt resistor (Ω).	2.0	
R_{on}	On-state resistance of the semiconductor switch (Ω).	0.001	
R_{snub}	Snubber resistance (Ω).	1.0e5	
T_f	Current 10% fall time of semiconductor switch (s).	1.0e-6	
T_t	Current 10% tail time of semiconductor switch (s).	2.0e-6	
V_f	Forward voltage drop of semiconductor switch (V).	0.8	
V_{max}	Maximum voltage set point (V).	5616	

9.12 Filter Parameters

Table 9.12.1: Parameters for Filter Capacitor with Charging Resistor Circuit

Parameter	Description	Default Value	Source
C_f	Capacitance of filter capacitor (F).	15.0e-3	
R_{ch}	Resistance of charging resistor (Ω).	10.0	

Table 9.12.2: Parameters for Bypass Breaker of Filter Capacitor with Charging Resistor

Parameter	Description	Default Value	Source
C_{bs}	Snubber capacitance (F).	1.0e-6	
R_{bs}	Snubber resistance (Ω).	500	
R_{on}	Breaker on-state resistance (Ω).	1.0e-6	

9.13 Disconnect Switch Parameters

Table 9.13.1: Parameters for Three-phase Circuit Breaker

Parameter	Description	Default Value	Source
C_{bs}	Snubber capacitance (F).	∞	
R_{bs}	Snubber resistance (Ω).	1000	
R_{on}	Breaker on-state resistance (Ω).	0.001	

Table 9.13.2: Parameters for Notional Unidirectional DC Switch Model

Parameter	Description	Default Value	Source
C_{snub}	Snubber capacitance (F).	10e-6	
L_{on}	On-state inductance of the semiconductor switch (H).	0	
R_{on}	On-state resistance of the semiconductor switch (Ω).	0.001	
R_{snub}	Snubber resistance (Ω).	50	
T_f	Current 10% fall time of semiconductor switch (s).	1.0e-6	
T_t	Current 10% tail time of semiconductor switch (s).	2.0e-6	
V_f	Forward voltage drop of semiconductor switch (V).	0.8	

9.13.1 MVAC Specific Parameters

Table 9.13.3: Parameters for DC Disconnect Switches in MVDC System

Parameter	Description	Value	Unit
R_{on}	On State Resistance of Switch	1000	Ω
P_{loss}	Loss due to Resistance	139	kW
$P_{loss,percent}$	Loss due to Resistance (Percent of Total Power)	0.28	(%)

9.13.2 MVDC Specific Parameters

Table 9.13.4: Parameters for DC Disconnect Switches in MVDC System

Parameter	Description	Default Value	Source
C_{bs}	Snubber capacitance (F).	1.0e-6	
R_{bs}	Snubber resistance (Ω).	1.0e5	
R_{on}	Breaker on-state resistance (Ω).	1.0e-4	

10 REFERENCES

[1] Abdelwahed, S.; Asrari, A.; Crider, J.; Dougal, R.A.; Faruque, M.O.; Fu, Y.; Langston, J.; Lee, Y.; Mohammadpour, H.A.; Ouroua, A.; Santi, E.; Shoder, K.; Sudhoff, S.D.; Zhang, Y.; Zheng, H.; Zivi, E., "Reduced order modeling of a shipboard power system," *Electric Ship Technologies Symposium (ESTS), 2013 IEEE* , vol., no., pp.256,263, 22-24 April 2013